Master Thesis

An Analysis of the Impact Forces on a Jack-up Leg During Installation on Stiff Seabed Conditions

European Wind Energy Master

Céline Wolfs

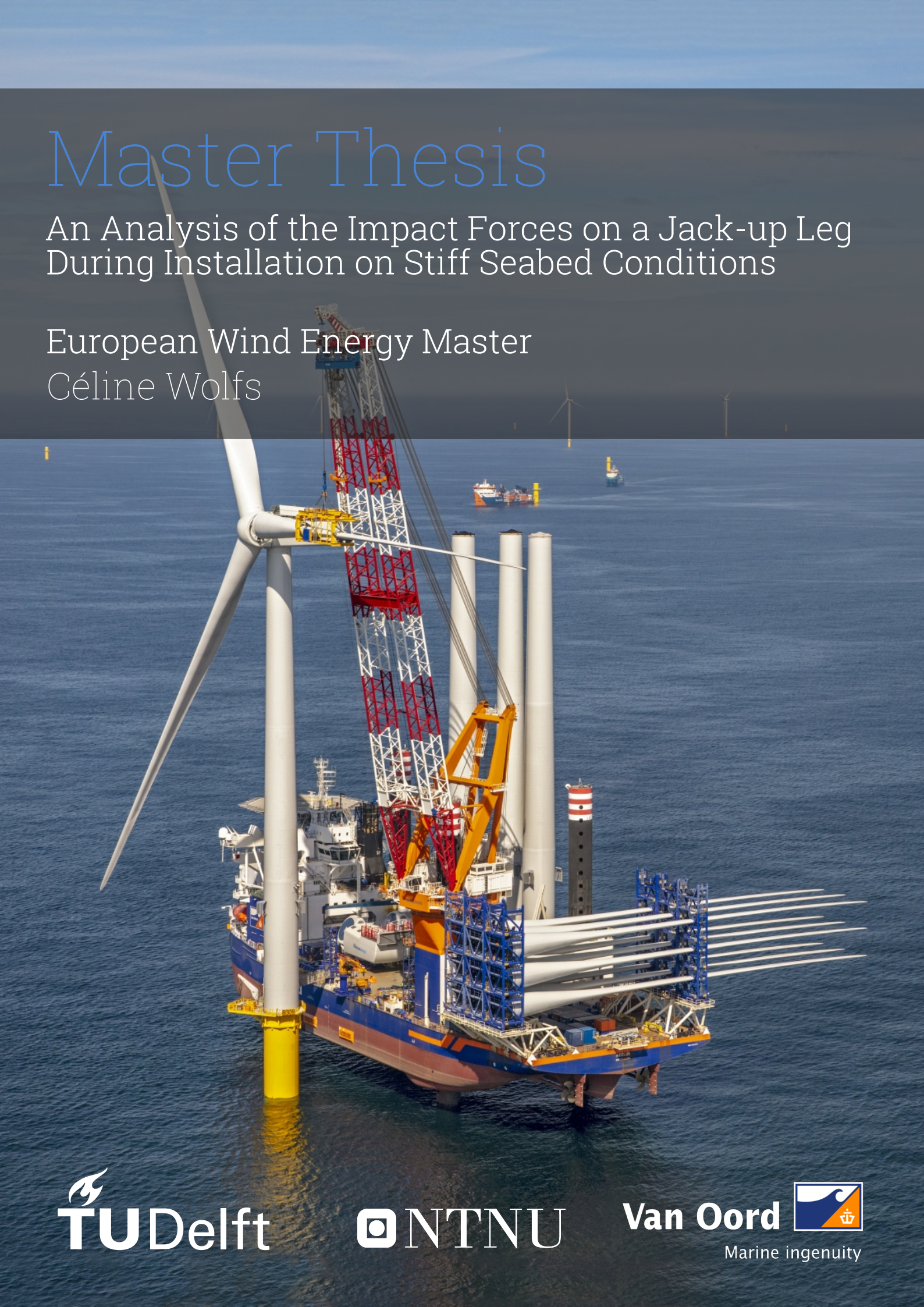

TU Delft NTNU Van Oord Marine ingenuity

Master Thesis

An Analysis of the Impact Forces on a Jack-up Leg During Installation on Stiff Seabed Conditions

by

Céline Wolfs

in fulfillment of the requirements to obtain the degree of
Master of Science
in ”Technology-Wind Energy” at the Norwegian University of Science and Technology
and in ”Offshore and Dredging Engineering” at the Delft University of Technology

Student number:	4563948	TU Delft
	582369	NTNU
Thesis committee:	Prof. dr. A. Metrikine,	TU Delft - chairman
	Ir. J.S. Hoving,	TU Delft - supervisor
	Prof. dr. Z. Gao,	NTNU - supervisor
	Ir. V.A. Wieleman,	Van Oord - supervisor

Cover: The offshore installation vessel Aeolus owned by Van Oord.

TU Delft NTNU Van Oord Marine ingenuity

Abstract

The ongoing global energy transition has led to significant growth in the offshore wind sector. This growth has resulted in a high demand for offshore installation vessels like the 'Aeolus', and the need to push up their limits to meet the rapidly changing market. In the Saint-Brieuc offshore wind project, the Aeolus had to be installed on a stiff seabed, a situation that was expected to induce high impact forces on the jack-up legs. To mitigate these forces, leg modifications were installed to increase the operational limits for jacking operation. However, Van Oord's operational limits for installation on stiff seabed conditions differed from DNV's Joint Industry Project, leading to the need to reassess the necessity of the leg modifications.

The objective of this research was to identify the main physical phenomena that govern the forces in jack-up legs during installation on a stiff seabed, and to understand how these physical factors and a specific leg modification could influence them. This research followed a systematic approach to address the research objective, comprising a literature study on impact mechanics, model development for axial impact forces, model validation, a sensitivity study, and an analysis of the leg modification. Insights from the literature study guided the development of the model to analyse the governing forces. Validation was performed by using field data from the Aeolus, specifically oil pressure readings from the vertical jacking cylinders and vessel motion measurements.

The research found that what governs the forces in jack-up legs during installation on a stiff seabed depends on the energy contained within the system prior to impact and how this energy is absorbed by the soil and structure. Key factors include wave-induced vessel motions, wave height and period, hull characteristics, vessel's inertia, jacking velocity, and the leg length below the hull. The energy absorbed by the soil and structure depends on their stiffness characteristics and behaviour, which primarily concluded that axial forces dominate over lateral forces during impacts on a stiff seabed. However, lateral forces should be considered in deeper waters or where seabed protrusions are anticipated.

The sensitivity analysis indicated that the vessel mass, initial velocity, and normal soil stiffness significantly influence the impact force, with the initial velocity predominantly influencing the impact force, and the overall system stiffness dictating the impact duration. By introducing the leg modification, the impact force was reduced by approximately 70-75%, along with an increased impact duration of 320-370%. Moreover, it was found that the impact force and duration are interconnected rather than separate occurrences. The leg modification also reduced the influence of soil stiffness variability. Furthermore, for a more realistic representation, incorporating the nonlinear behaviour of soil load-deformation and leg modification characteristics is needed, but this would increase the computational demand. Consequently, this suggests the need for advanced solutions and an engineering assessment to balance desired accuracy against computational complexity.

Preface

This master's thesis is submitted to fulfil the requirements for obtaining the master's degree in Offshore and Dredging Engineering at the Delft University of Technology (TU Delft), as well as the master's degree in Technology-Wind Energy at the Norwegian University of Science and Technology (NTNU) under the European Wind Energy Master (EWEM) programme. This study has been conducted in collaboration with Van Oord, a leading international marine contractor that provides dredging, offshore, and marine engineering solutions.

Firstly, I would like to express my sincere gratitude to my university supervisors. I want to thank Jeroen Hoving for his guidance and effort throughout the project. You pointed me in directions to learn a lot from this process and helped me during times when I got stuck. I always felt your door was open and you took the time to help me. Our meetings were not only useful, they were also a lot of fun, thank you for that.

Additionally, I also want to extend my gratitude to Zhen Gao for the enlightening discussions we had during my literature study in Trondheim. You have been my supervisor for a significant part of my master's program, and your dedication to this work is truly appreciated. I am delighted that we had the opportunity to meet in person and continued our meetings despite the geographical distance, with me in the Netherlands and you in China. The time difference never mattered in your guidance, I thank you for everything.

Last but certainly not least, I would like to offer my profound gratitude to Andrei Metrikine for his input during this project. I admire your knowledge and expertise in this field and your comments were very much appreciated. With just a few words, you were able to explain the relevant issue to me, thereby providing a lot of clarification. Thank you for that.

Secondly, I would like to convey my sincere thanks to Vera Wieleman and the entire hydrodynamic team at Van Oord. Specifically, Vera, who has guided and supported me throughout this entire process. You often offered a different perspective from the company's point of view, from which I have learned so much. You introduced me to Van Oord and your wonderful colleagues, with whom I have greatly enjoyed working. Thank you for your support and honesty. I am looking forward to officially joining the Van Oord team.

Finally, I would like to thank my family, friends, and everyone who has aided and encouraged me throughout these years. The past two years of being a European Wind Energy Master student have been unforgettable. Studying at three different universities in three different countries has truly enriched my life. I am grateful for my fellow EWEM students. The new friends I have made across different countries and the experiences we have shared are invaluable.

As a final note, I wish to express my deep sense of privilege with this graduation committee that I have had the opportunity to work with. I have gained immense knowledge from all of you in the past few months. Your extraordinary expertise has been incredibly instructive, and I have felt truly guided throughout the entire process. I would like to take this opportunity to express my deepest gratitude one last time.

Céline Wolfs
Delft, August 2023

Nomenclature

Abbreviations

Abbreviation	Description
CAGR	Compound Annual Growth Rate
CEL	Coupled Euleerian-Lagrangian
COP26	26th UN Climate Conference of the Parties
DOF	Degrees of Freedom
DP	Dynamic Positioning
DSV	Downward Spudcan Velocity
FDM	Finite Difference Method
FE	Finite Element
JIP	Joint Industry Project
MRU	Motion Reference Unit
NZE	Net Zero Emission
OAT	One-at-a-Time
ODE	Ordinary Differential Equation
PDE	Partial Differential Equation
PSF	Portside Fore
SBA	Starboard Aft
SDOF	Single-Degree-of-Freedom

Latin Symbols

Symbol	Definition
A	Cross-sectional area
c	Damping coefficient
c	Wave velocity
c_c	Critical damping coefficient
c_{eq}	Equivalent damping coefficient
c_s	Soil damping coefficient
d	Horizontal distance between jack-up leg and centre of flotation
e	Coefficient of restitution
E	Modulus of elasticity
F	Force
F_H	Horizontal impact force
F_V	Vertical impact force
$F(t)$	Time-dependent force
h	Water depth
H_s	Significant wave height
I	Moment of inertia
I_m	Mass moment of inertia
J_{angular}	Angular impulse
J_{linear}	Linear impulse
k	Spring stiffness
k_{eq}	Equivalent spring constant
k_H	Lateral stiffness of the jack-up leg

Symbol	Definition
k_{hyd}	Hydrostatic restoring stiffness vessel
k_s	Soil stiffness
k_V	Overall stiffness of the jack-up leg
M	Moment
m_1, m_2	Body mass
M_b	Bending moment
M_{sp}	Spudcan mass
M_{tot}	Total mass of vessel, leg and spudcan
M_v	Vessel mass
L	Leg length
P_H	Horizontal impact force
P_V	Vertical Impact force
q	Force per unit volume
$Q_V(z)$	Vertical resistance of seabed as a function of spudcan penetration
$S1$	First-order sensitivity index
$S2$	Second-order sensitivity index
ST	Total-order sensitivity index
t	Time
T	Period of motion
t_c	Impact duration
T_p	Peak period
u	Displacement
v_1, v_2	Body velocity before collision
v_1', v_2'	Body velocity after collision
v_i	Initial velocity
V_s	Shear force
x_r	Relative distance from MRU to spudcan in the x-direction
y_r	Relative distance from MRU to spudcan in the y-direction
z_1	Maximum spudcan penetration during impact
z_2	Maximum leg system shortening during impact
$\dot{z}$	Vertical velocity vessel
$\dot{z}_s$	Vertical velocity spudcan

Greek Symbols

Symbol	Definition
δ	Spring elongation
ε	Strain
η	Material viscosity
η_c	Critical viscosity
θ	Amplitude of rotational motion
$\dot{\theta}$	Angular velocity of rotational motion
$\dot{\theta}$	Rotational pitch translation
ξ	Structural damping ratio
ξ_s	Soil damping ratio
ρ	Density
σ	Stress
ϕ	Maximum rotation about point O during impact
$\dot{\phi}$	Rotational roll translation
ω	Angular velocity
ω	Frequency

Contents

List of Tables

List of Figures

1

Introduction

The need for renewable energy in the world due to the ongoing energy transition has led to significant growth in the offshore wind energy sector. Wind energy is a dominant renewable energy source of which offshore wind is cost-competitive, reduces rising energy prices, and supports energy security. Offshore wind projects, in particular, have the potential to scale up power generation and take advantage of higher and more consistent wind speeds, larger turbine sizes, and large-scale offshore sites, resulting in higher capacity factors compared to onshore wind [1]. Consequently, it is not surprising that the 26th UN Climate Conference of the Parties (COP26) in Glasgow has set new targets for offshore wind energy to meet the Net Zero Emission (NZE) targets for 2030 and 2050. These goals are reflected in the promising outlook for the global offshore wind market, as shown in Figure 1.1, which indicates a significant increase in the global installation of new offshore wind turbines. The expected Compound Annual Growth Rate (CAGR) is 6.3% until 2026 and 13.9% up to the beginning of the next decade [2]. This growth in the industry will inevitably lead to a high demand for offshore installation vessels.

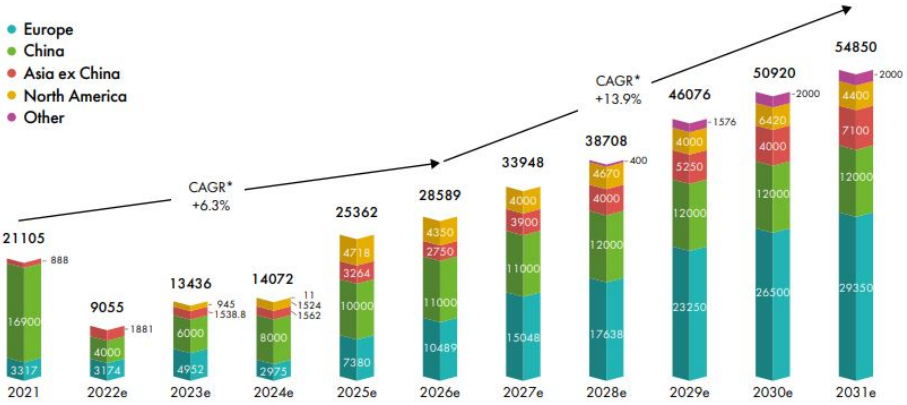

Figure 1.1: New global offshore wind installations (MW) [2].

To keep up with the increasing installation demand, new offshore wind installation vessels are needed. But in addition, current state-of-the-art installation vessels need to push up their limits to meet the rapidly changing market. A well-known challenge in the industry is that the market is changing faster than the capacity of the installation vessels. The three main trends driving this change are the increasing turbine sizes, greater distances to ports, and the increasing depths at the installation sites [3]. These trends have reduced the more sustainable lifetime of vessels from 25 years to 10 years [4], which is detrimental for the industry as well for the owners and investors.

The above highlights the importance of improving the workability of installation vessels. Such improvements may include upgrading vessels to handle more advanced projects or implementing modifications

to enable operations in more challenging environmental conditions. Both apply to Van Oord, a leading international marine contractor that provides dredging, offshore, and marine engineering solutions, with whom this research is conducted. Van Oord owns a jack-up vessel called the 'Aeolus', which is specifically designed for the installation of offshore wind farms (see Figure 1.2). The vessel entered the market in 2014, but has already experienced two crane upgrades to remain competitive in the rapidly changing market. The first upgrade in 2018 involved increasing the crane's loading capacity to more than 1,600 tons, and the second upgrade in early 2023, involved the installation of a new longer boom on the existing crane. These upgrades have enabled the Aeolus to transport and install the new generation of offshore wind turbines of 12-15 MW. Additionally, the vessel can operate in water depths up to 45 meters, features a Dynamic Positioning (DP) system, and has an advanced jacking system to control its four cylindrical jack-up legs [5–7].

Figure 1.2: The offshore jack-up installation vessel Aeolus with the old crane boom [8].

Despite its capabilities, the workability of the Aeolus continues to be pushed by running projects that have more challenging environmental conditions. One such project is the construction of the offshore wind farm in the bay of Saint-Brieuc, where strong currents, high waves, and severe swell waves can be expected. During this project, the Aeolus is responsible for drilling and installing the pin-piles of the jacket foundations [9, 10]. These foundation types are chosen due to the present rocky seabed, which marks the difficulties for the Aeolus. Installation on stiff seabeds causes higher forces in the jack-up legs than with softer seabeds. Therefore, the focus of this research is to analyse the impact forces on jack-up legs during installation on stiff seabed conditions.

1.1. Jacking Operation of Jack-up Vessel

In order to analyse the forces in jack-up legs, it is essential to understand the different phases of the jacking operation and to identify when maximum impact forces occur. According to DNV-RP-C104 [11], these phases can be described as follows:

- Transit phase: the vessel moves from one location to another.
- Installation phase: the vessel transitions from a floating state to an elevated state, where the four cylindrical jack-up legs contact the seabed and transfer the vessel's weight onto the legs. This gradual process elevates the vessel out of the water and significantly reduces the wave-induced

motions. After jacking up to its working height, an air gap is created to prevent wave excitation. Before the vessel is put into operation, a preloading procedure is performed to ensure its ability to withstand operational loads and potential storm conditions [12–14].

- Operation phase: the vessel is elevated above the wave zone, providing a stable platform for drilling, heavy lift operations, and wind turbine installation. This positioning minimizes the impact of wave loads on the vessel, reducing sensitivity to sea conditions [15, 16].
- Retrieval phase: the vessel retracts its legs from the seabed and moves to another location by jacking down the hull, creating an upward buoyancy force that allows the legs to be lifted from the seabed.

The installation and retrieval phases of a jack-up vessel are critical operating phases, as they involve placing and lifting the legs of the vessel from the seabed. These phases are particularly vulnerable to high impact forces caused by wave-induced vessel motions [17]. In this regard, the maximum impact force is most likely to occur during these phases. Since the initial kinetic energy of the vessel is higher during installation than during the retrieval phase, the scope of this study exclusively focuses on the installation phase.

1.1.1. Installation and Operational Limits

The installation phase starts by lowering the jack-up legs onto the designated location on the seabed. During this critical phase, the vessel is subjected to environmental loads such as wind, current, and waves that significantly affect its stability and positioning. Based on findings from a previously conducted literature study [18], it is concluded that compared to wave loads, the wind and current loads are constant and mainly cause the vessel to drift away. Therefore, the DP system is employed to maintain the vessel's position, while the vessel motions are predominately caused by the wave loads. However, it should be noted that the wind and current cause changes in the wave height and period according to DNV-RP-C205 [19].

The tip of the jack-up legs are fitted with special footings, called 'spudcans' shown in Figure 1.3 [11]. When these spudcans are close to the seabed, the probability of impact increases. The interval from initial spudcan contact until all spudcans are positioned on the seabed is of particular interest, as it is expected to contain the peak impact force on the legs. This force is anticipated to occur at the first moment of contact when the vessel has the highest kinetic energy. Once the vessel motions are significantly reduced and the vertical spudcan motions become negligible, severe impact forces are no longer expected. At this point, the legs only respond to wave loads when the spudcans are in continuous contact with the seabed [20].

Figure 1.3: Spudcan design of the Aeolus [21].

During the jacking operation, it is essential to ensure that the structural limits, including the maximum allowable axial loading and bending moment, are not exceeded. Van Oord utilises these criteria to determine the operational limits of the jacking operation [14]. These operational limits are defined in terms of the critical significant wave height (H_s) and peak period (T_p), assuming no consideration for wind and current effects. A combination of these wave parameters, H_s and T_p, defines a sea state. Sea states resulting in leg forces below the structural limits are referred to as 'allowable sea states'.

To determine the operational limits, multiple analyses are typically performed prior to the operation. Motion analyses of the vessel are conducted and compared with various sea states. The objective is to identify a limiting sea state that ensures an acceptable probability of not exceeding the structural limits [14, 22, 23]. It should be noted that safety factors are taken into account when establishing the operational limits, although their detailed consideration falls outside the scope of this thesis.

As previously indicated, the maximum impact forces are anticipated during the initial contact of the jack-up leg with the seabed, a phase referred to as 'stand-on' [24]. The permissible limit for this impact force is determined by the predefined structural limits, expressed in maximum allowable axial loading and bending moment. These structural limits are related to the maximum allowable forces and moments of the jacking system. The Aeolus is equipped with a hydraulic jacking system comprising an upper and lower jacking frame, each fitted with six cylinders and three locking pins, as illustrated in Figure 1.4. The function of the jacking system will be elaborated in Section 1.1.2. The six hydraulic cylinders have a maximum allowable pressure, which must not be exceeded by the impact force. Furthermore, the lateral force acting on the spudcan generates a bending moment in the leg, with the maximum moment occurring at the lower guide of the jacking system. Hence, the maximum lateral force is related to the position of the spudcan below the lower guide of the leg. It should be noted that the jacking system also has a maximum allowable torsional moment, which is determined by the strength of the guiding pins and the bearing capacity of the sliding blocks into which the guiding pins are inserted [24].

1.1.2. Hydraulic Jacking System

The hydraulic jacking system can operate in two modes, single and double ring jacking. Single ring jacking is employed during the stand-on phase as it is a faster jacking process, which minimises the duration from initial spudcan contact until all spudcans are positioned on the seabed. Each jacking frame is connected to the vessel by the vertical oriented cylinders, enabling the frames to slide along the leg. The frames are alternately connected to the leg by three locking pins, which are responsible for load transfer. During the jacking up process, the jacking system undergoes multiple operation cycles, detailed in Appendix A.

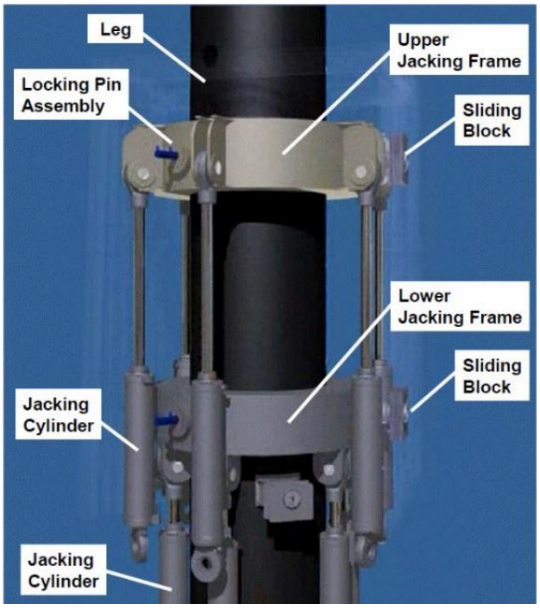

Figure 1.4: Schematic drawing of hydraulic jacking system [14].

Each operation cycle begins and ends with both frames in the same position. For instance, the upper frame is locked in top position and the lower frame is unlocked in bottom position. The frames then move in opposite direction until the upper frame is in the bottom position and the lower frame in the top position, ready to lock the pins into the holes of the leg. The lower frame extends the pins, the load transfers from frames, and the upper frame retracts the pins. The frames then move again in opposite directions until the top and bottom positions are reached, the pins are extended, the load is transferred, the pins are retracted, and the starting position is reached.

1.2. Research Motivation and Objectives

For the Saint-Brieuc offshore wind farm, Van Oord is responsible for the transport and installation of 62 jacket foundations, as well as the foundation piles of the substation. The Aeolus is assigned to drill and install all the pin-piles at this challenging installation site, characterised by strong currents, high waves, severe swell waves, and rocky seabeds. Due to these adverse conditions, the legs of the Aeolus were modified for this project to mitigate the leg impact forces. These leg modifications were implemented for safety purposes and based on earlier analysis and calculations that did not yield the desired operability [24]. Operability denotes the duration available to safely execute an operation within a specified reference period. Usually, it is assessed by using the operational limits and scatter diagrams of the specific offshore site [23].

In addition, Van Oord participated in DNV's Joint Industry Project (JIP), which documented the main results and conclusions on leg forces during jacking operation [20]. The analyses within this project were performed for a vessel with similar characteristics to the Aeolus, which is shown in Figure 1.5. This figure illustrates the wave-induced vessel motions and the leg lowering process during installation, a phase where the probability of impact increases, ultimately leading to its occurrence. However, the results for the operational limits, H_s and T_p, for installation on stiff seabed conditions differed from Van Oord's in-house model results. Specifically, the critical H_s and T_p values determined by the JIP exceeded those determined by Van Oord. Due to confidence in their own analyses and to minimise risks, Van Oord applied the leg modifications to the Aeolus to increase the operational limits of the jacking operation. However, it led to the need of reassessing the necessity of the leg modifications, which indicates the motivation for this research.

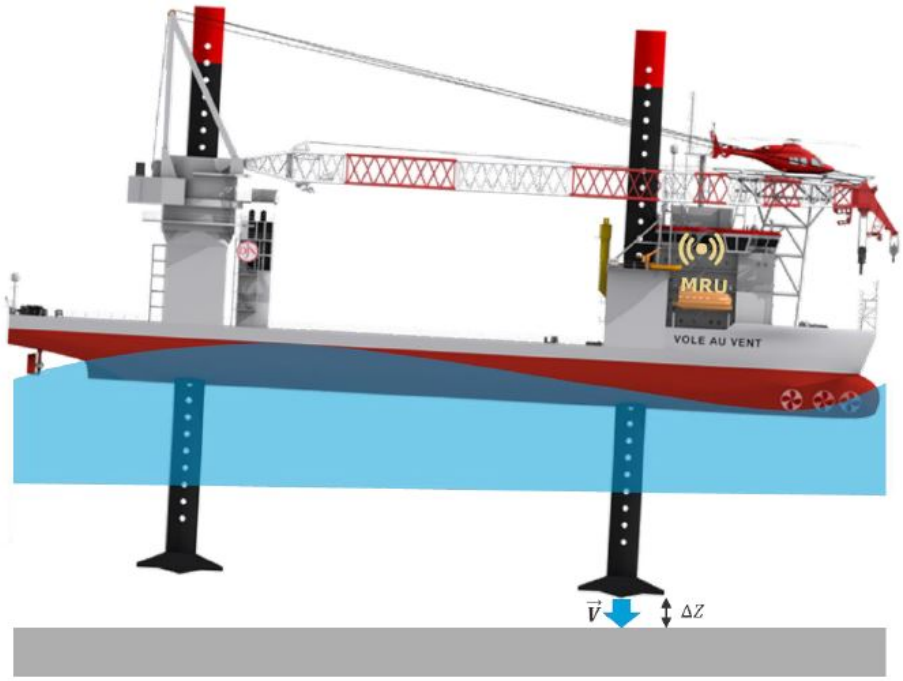

Figure 1.5: Wave-induced vessel motions and leg lowering during installation: Similar vessel to the Aeolus [20].

The objective of this thesis is to identify and elucidate the main physical phenomena that govern the forces in jack-up legs during installation on a stiff seabed. This research aims to enhance understanding of the influence of these physical factors on the governing forces and how specific leg modifications can potentially influence them. This insight will enable the evaluation of the effects that conservative assumptions, commonly found in the offshore industry, have on these factors. Moreover, it could enable a comparison between the distinct assumptions made by Van Oord and DNV that result in different operational limits. Nonetheless, a direct comparison of these assumptions falls outside the scope of this study.

In addition, determining the influence of various factors on jack-up leg forces could be of interest to numerous vessel operators. This is substantiated by literature, indicating the lack of knowledge about the stand-on phase as compared to other phases of the jacking operation, especially on stiff seabeds [18].

From these objectives, the main research question arises:

> *What governs the forces in jack-up legs during installation on stiff seabed, and what influence do specific leg modifications have?*

To structure the research and systematically address the main question, the following subquestions are defined:

1. What factors govern the forces in jack-up legs during installation on stiff seabed?
2. How do these factors influence the governing forces?
3. How well does the specific leg modification perform?

1.3. Research Methodology and Thesis Outline

This thesis will follow a systematic approach, comprising five main steps to address the research objectives and answer the research questions: a literature study, model development, model validation, a sensitivity study, and an analysis of the leg modification.

Chapter 2 presents a literature study on impact mechanics, focused on the relevance regarding jacking operations on stiff seabed conditions. The aim of this review is to identify the key physical factors that govern the forces in jack-up legs during installation. By understanding these physical phenomena, the forces involved during this phase can be better analysed. By the end of this chapter, the first research question will be addressed by identifying the factors governing the forces in jack-up legs during installation on stiff seabeds.

Based on the insights drawn from the literature study, a model is developed in Chapter 3 to analyse the governing forces. This model incorporates the identified key factors that influence these forces in jack-up legs during installation on stiff seabeds. Additionally, this chapter introduces the specific leg modification and includes model verification to ensure that the model operates as intended.

Chapter 4 presents the validation of the model, using data from the Aeolus provided by Van Oord. This data includes oil pressure readings from the vertical jacking cylinders and vessel motion measurements from the Motion Reference Unit (MRU). The purpose of this step is to ascertain if the model is a valid representation of the actual scenario being simulated.

Chapter 5 performs a sensitivity study to analyse the influence of the identified factors on the governing forces. This analysis entails adjusting the variables and assessing their impact on the forces in the jack-up leg. This step aims to answer the second subquestion: How do these factors influence the governing forces?

Subsequently, the specific leg modification is incorporated into the model, and the sensitivity study is repeated. By comparing the results of this study with the previous one, the influence of the leg modification on the governing forces and its overall performance can be assessed. This final step allows for addressing the last subquestion: How well does the specific leg modification perform?

Chapter 6 discusses the results, providing an in-depth understanding of the research findings, interpreting them in the context of the overall study. Chapter 7 draws conclusions based on the results

and discussions from the previous chapters, including recommendations for future research. These recommendations are based on the identified limitations of the current study and emerging questions that warrant additional investigation.

2

Impact Mechanics

In general, an impact is described as a short-duration, collision-like event that involves high forces. Impact scenarios are of interest for predicting the behaviour of colliding objects and anticipating possible elastic and plastic deformations of these objects [25]. In this study, the term 'impact' is defined as the interval during which the leg is in contact with the seabed. It is expected that this impact exerts the highest loads during the stand-on phase, as previously mentioned. The leg impact forces during this phase are mainly caused by the wave-induced vessel motions. These vessel motions are confined to six Degrees of Freedom (DOF), consisting of three mutually perpendicular translations and three rotational translations, detailed in the previously conducted literature research [18]. Consequently, these translations result both in horizontal and vertical velocities of the spudcans just before impact, leading to axial and lateral forces on the jack-up legs. The magnitude of these impact forces depends on the energy contained within the system just before impact and how this energy is absorbed by the colliding bodies.

According to Chakrabarti [26], the vessel motions and its spudcan velocities depend on several factors. These factors include wave height, wave period, hull characteristics, jacking velocity, and the length of the legs below the hull, which is determined by the water depth. These factors, along with the inertia of the vessel, influence the vessel's energy prior to impact. The vertical and horizontal impact forces on the spudcan are further influenced by the soil stiffness characteristics, which vary depending on the soil type. Additionally, what makes the problem even more complex is that the soil load-deformation behaviour is nonlinear.

When the spudcan contacts the seabed, vibrations are induced, dependent on the leg's mass and its length below the hull [26]. To comprehend the resulting behaviour from axial and lateral forces, it is necessary to consider the mechanics of one-dimensional impacts in deformable bodies, detailed in Section 2.3. Preceding this, Section 2.1 and 2.2 delve into different types of collisions and rigid body impact mechanics, respectively. The complex soil-structure interaction is then examined in Section 2.4. Following the exploration of impact mechanics, Section 2.5 presents existing methodologies for calculating the impact forces, including relevant research and common practices. These insights result in identifying the factors that govern the forces in jack-up legs during installation on stiff seabeds, and conclusions can be drawn in Section 2.6.

2.1. Different Types of Collision

The impact scenario analysed in this thesis can be considered as a collision between two bodies: the jack-up leg and the seabed. In this context, the term 'impact' refers to any abrupt change in force, position, velocity, or acceleration that influences the involved bodies [27]. To provide a comprehensive understanding of distinct collision behaviours and to serve as an introduction to existing impact methodologies, different collision types are described [28]:

- Perfectly elastic collisions are collisions where all kinetic energy is conserved, with no dissipation into other forms of energy. Here, both momentum and kinetic energy remain conserved through-

out the collision.

- Inelastic collisions involve energy dissipation into other forms, such as thermal energy, sound energy, and material deformation. Although the momentum of the system is conserved, the kinetic energy is not.
- Perfectly plastic collisions occur when the colliding bodies stick together after the collision. In this case, the momentum is conserved, but the kinetic energy is maximally reduced.

The conservation of momentum in a closed system is represented by

$$m_1 v_1' + m_2 v_2' = m_1 v_1 + m_2 v_2 \tag{2.1}$$

where, m_1 and m_2 are the masses of the two bodies, v_1 and v_2 represent their velocities before collision, and v_1' and v_2' the velocities direct after collision. This equation implies a consistent linear momentum before and after impact, assuming all external forces during the short impact interval are small compared to the impact force. The conservation of energy, depicted in Equation 2.2, implies that for a perfectly elastic impact, the kinetic energy before and after impact is equal [29]. However, in the case of an inelastic collision, an additional term is required in the equation to account for the energy loss.

$$\frac{1}{2} m_1 v_1'^2 + \frac{1}{2} m_2 v_2'^2 = \frac{1}{2} m_1 v_1^2 + \frac{1}{2} m_2 v_2^2 \tag{2.2}$$

It is important to note that the mentioned collision types can be classified by the change of the total kinetic energy of the system before and after collision. The coefficient of restitution, as defined in Equation 2.3, represents the variation in kinetic energy conservation by parameterising the decrease in rebound velocity. The coefficient of restitution is a positive real number ranging between 0 and 1. A value of 0 indicates a perfectly plastic collision and a value of 1 represents a perfectly elastic collision. Although this approach seems functional, it cannot predict the forces exerted on the objects during collisions or determine the stresses developed within the bodies [25].

$$e = \frac{|v_2' - v_1'|}{|v_1 - v_2|} \tag{2.3}$$

Collisions can be further classified based on the orientation of the velocities of the colliding bodies and their centres of mass relative to the impact line. Specifically, direct impacts involve velocities that align with the impact line, while oblique impacts show misalignment. Furthermore, if the centres of mass of the colliding bodies align with the impact line, it is characterised as central impact, while misalignment denotes eccentric impact.

2.2. Rigid Body Impact Mechanics

In addition to classifying collision types, it is crucial to characterise the properties of the colliding bodies to fully understand the physics of impact. In rigid body impact mechanics, it is assumed that the bodies are undistortable masses where the interparticle distances remain constant, even when the body undergoes some motion. Furthermore, this perspective assumes that the body's entire mass is concentrated in the centre of mass, implying that the impact force, even though generated at the contact surface, is transferred to the centre of mass [27].

Impact analysis of a rigid body typically assumes a small contact area that undergoes negligible deformation during the impact process. When two bodies collide, a mutual exchange of momentum occurs, generating forces at the contact surface. However, the forces can not propagate into the bodies unless there are small deformations leading to stress development. Within the framework of rigid body mechanics, such stress development is considered insignificant relative to the overall dimensions of the colliding bodies. This perspective is most applicable when impact velocities are small and the involved materials are considerably stiff [27].

Contrastingly, in scenarios with higher impact velocities or relatively flexible structures, stresses develop and propagate across the structures as stress waves. These stresses, along with their associated strains, can reach a critical threshold, leading to failure or permanent deformations, such as yielding or brittle fracture. These phenomena can only be captured in a broad sense through the restitution coefficient, which is incapable of describing the mechanics of failure resulting from inelastic deformations in the material [27].

2.3. One-Dimensional Impact Mechanics of Deformable Bodies

In contrast to rigid bodies, elastic or viscoelastic bodies undergo deformations when subjected to external forces, resulting in the development and propagation of stress waves within the structure. These stress waves in solids can be in the form of compression, shear, or surface waves, and understanding their behaviour is essential in the study of impact mechanics [27]. This section focuses on one-dimensional systems to provide insights into the physics of impact and compression waves.

2.3.1. Mass-Spring-Damper System

Several mechanical and structural systems can be idealised as Single-Degree-of-Freedom (SDOF) systems. In practice, the mass is distributed but can, for simplicity, be analysed as a single point mass. Similarly, the elasticity of the system can be idealised by a single spring (k), and the energy dissipation by a damper (c), as shown in Figure 2.1. The dynamic behaviour of such a system can be mathematically described by the following equation of motion:

$$m\ddot{x} + c\dot{x} + kx = F(t) \tag{2.4}$$

where, $F(t)$ is a time-dependent force exciting the system [25].

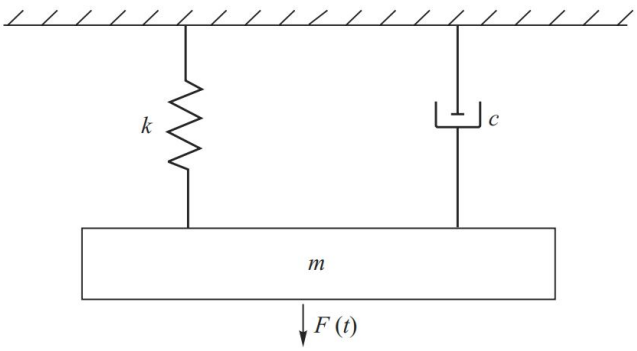

Figure 2.1: A schematic drawing of a SDOF spring-damper system [27].

An elastic body has the ability to deform and return to its original shape once the force is removed. Consequently, during an impact, the body experiences deformation, thereby storing energy within the material as potential energy. Furthermore, viscoelastic bodies exhibit both elastic and viscous characteristics when subjected to impact forces, implying that the energy within the structure is transformed into other forms of energy [30].

For the purposes of this research, it is assumed that no plastic deformations occur during impact, taking into account the stiffness of the system and the need for repeated jacking operations during the vessel's lifetime without causing excessive damage. Therefore, a spring-damper system is believed to be sufficiently accurate description of the structural deformation during impact [31]. Additionally, several SDOF spring-damper systems can be combined in order to form a higher order DOF system that represents reality more accurately. However, a prerequisite is that the system's properties should be well known, which is typically the case for materials such as steel, but difficult to define for various soil types [25].

2.3.2. The One-Dimensional Wave Equation

Horizontal and vertical impact forces on a jack-up leg induce longitudinal and transverse motions within the leg. These motions are essentially propagating stress waves within the material and along the surface. Although wave propagation typically occurs in three dimensions relative to the global axes, this study narrows the focus to one-dimensional wave propagation, which can already offer valuable insights into the system's behaviour. These waves can be in the form of longitudinal waves in rods or shear waves in beams, discussed in Sections 2.3.3 and 2.3.4, respectively [27].

Wave propagation can be mathematically modelled using the wave equation, a partial differential equation representing processes varying across time and space. The classical wave equation for one-

dimensional wave propagation through an elastic body is as follows:

$$\frac{\partial^2 u(x,t)}{\partial t^2} = c^2 \frac{\partial^2 u(x,t)}{\partial x^2} \tag{2.5}$$

Here, $u(x,t)$ is the displacement in the x-direction, and c represents the wave velocity.

2.3.3. Longitudinal Waves in Thin Rods

A longitudinal wave produced by an impact force, propagates along the length of the elastic rod, as depicted in Figure 2.2. The rod has an uniform cross-sectional area A, a density ρ, and a modulus of elasticity E. Furthermore, the longitudinal displacement is denoted by $u(x,t)$, the dynamically varying stress field by $\sigma(x,t)$, and the forces per unit volume are given by $q(x,t)$, resulting in the following equation of motion [29]:

$$\rho \frac{\partial^2 u}{\partial t^2} = \frac{\partial \sigma}{\partial x} + q \tag{2.6}$$

According to Hooke's law [32], the stress σ and the strain ε have the linear relation:

$$\sigma = E\varepsilon = E\frac{\partial u}{\partial x} \tag{2.7}$$

In the absence of forces, the differential equation of longitudinal vibrations in the rod is:

$$\rho \frac{\partial^2 u}{\partial t^2} = E\frac{\partial^2 u}{\partial x^2} \tag{2.8}$$

This yields the wave equation for $c = \sqrt{E/\rho}$, which represent the longitudinal wave velocity.

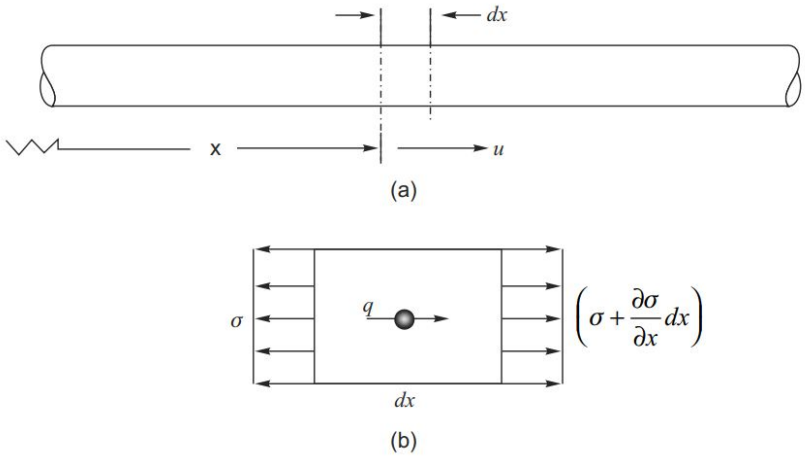

Figure 2.2: A rod (a) with displacement u in the x-direction, and (b) depicting the stresses subjected to a rod element [27].

Finally, the axial force in the rod can be expressed in terms of longitudinal displacement as follows:

$$F = A\sigma = EA\frac{\partial u}{\partial x} \tag{2.9}$$

Propagation Characteristics of Longitudinal Waves

The differential equation describing the longitudinal wave propagation can be solved using D'Alembert's solution, represented by Equation 2.10. This commonly used method provides a clear understanding of the wave behaviour within the rod. The waves propagate without distortion at a velocity c, moving both away from and towards the impulse source due to reflection [33].

$$u(x,t) = f\left(x - ct\right) + g\left(x + ct\right) \tag{2.10}$$

The system's boundary conditions govern wave reflection and transmission, also determining the nature of the reflected wave. Reflection of an incident wave from a fixed boundary is the simplest case, but all wave reflections can be mathematically described, as detailed in Graff [33]. To illustrate this phenomenon, the simplest case of displacement and stress pulse propagation and reflection is shown in Figure 2.3 via the method of images. It should be noted that the stress waves superimpose, leading to a double peak value at steps (b) and (c). Post interaction, the reflected stress pulse is identical to the incident pulse, meaning that compression reflects as compression and tension as tension. However, since this phenomenon depends on the system's boundary conditions, it is essential to acknowledge this behaviour in the analysis of resultant forces in a rod, given that the reflected stress pulse can be the inverse of the incident pulse [33].

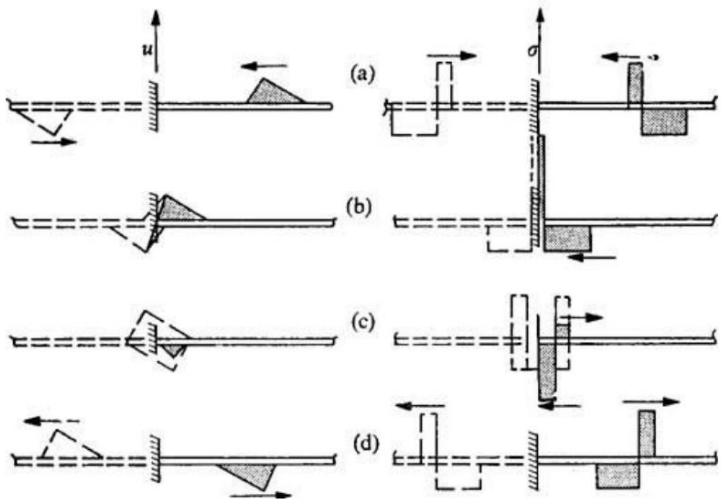

Figure 2.3: The displacement and stress pulse propagation and reflection of a fixed boundary condition by the method of images [33].

2.3.4. Flexural Waves in Thin Beams

Transverse motions within the leg result from transverse forces or bending action. The Euler-Bernoulli and the Timoshenko beam theory are the two main theories used to model these motions. The Euler-Bernoulli theory accounts only for axial and bending deformation, whereas Timoshenko includes shear deformation [34]. The Timoshenko beam theory is typically used for relatively thick structures, while the Euler-Bernoulli beam theory is used for slender structures. Given that the length of the jack-up leg is at least ten times larger than its diameter, the Euler-Bernoulli beam theory is an appropriate choice for analysis [35].

The Euler-Bernoulli beam theory implies that cross-sections initially perpendicular to the beam's axis maintain their planarity and perpendicularity to the neutral axis during bending. Assuming that the deflections of the beam are small, the bending moment (M_b) and curvature relation can be given by

$$\frac{d^2y}{dx^2} = -\frac{M_b}{EI} \tag{2.11}$$

where, I represents the moment of inertia, and y denotes the coordinate perpendicular to the beam's neutral surface, as depicted in Figure 2.4 [33].

The considered beam has the same properties as the rod defined in Section 2.3.3, resulting in the following equation of motion:

$$\rho\frac{\partial^2y}{\partial t^2} = \frac{\partial V_s}{\partial x} + q \tag{2.12}$$

Here, V_s represents the shear force. In the absence of forces, substituting Equation 2.11 and the relation $V_s = \partial M_b/\partial x$ into Equation 2.12 gives

$$\frac{\partial^4y}{\partial x^4} + \frac{1}{a^2}\frac{\partial^2y}{\partial t^2} = 0, \quad a^2 = \frac{EI}{\rho A} \tag{2.13}$$

It should be noted that this expression is not in the form of the wave equation, and the operator a does not have the dimension of velocity.

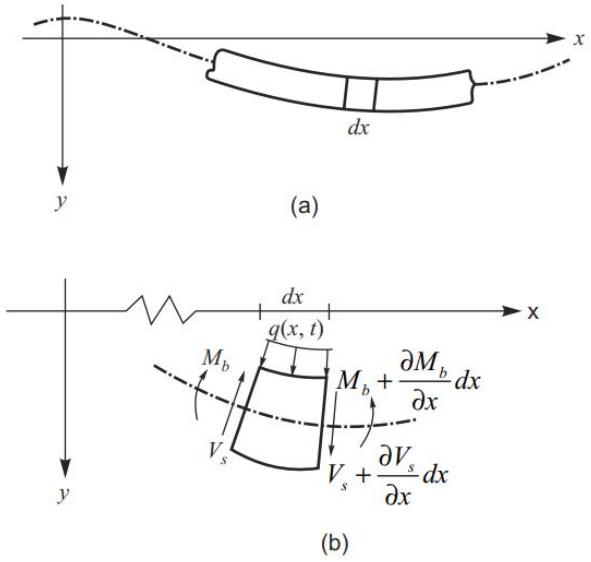

Figure 2.4: A beam (a) undergoing transverse motion, and (b) depicting an element subjected to various loads [27].

Beams in Compression

A more realistic representation of the jack-up leg is a beam subjected to axial and transverse loading. This can be mathematically modelled as a beam under compression by the following equation of motion:

$$\rho A \frac{\partial^2 y}{\partial t^2} + EI \frac{\partial^4 y}{\partial x^4} + P \frac{\partial^2 y}{\partial x^2} = 0 \tag{2.14}$$

In this equation, the first term symbolises inertia, the second represents bending stiffness, and the third denotes compression stiffness. Essentially, P corresponds to the axial force, $EAu'(t)$, in the rod theory, indicating that both problems can be solved independently but are in principle not completely independent [36].

2.4. Soil-Structure Interaction

The previous sections mainly govern the structural processes during impact, while soil behaviour is another crucial factor that significantly influences the system's responses during impact. The soil-spudcan interaction is a complex phenomenon of which its behaviour depends on the soil type and deformation characteristics, classified as either elastic or plastic soil deformations. As earlier mentioned, elastic deformations revert to their original shape, while plastic deformations result in permanent changes. In reality, soil behaviour contains both aspects which indicates the complexity and nonlinearity. In the context of this study, a rocky seabed with a high bearing capacity is considered, justifying the assumption that no plastic deformations occur. Furthermore, assuming that the elastic deformations are minimal, the soil behaviour can be modelled by a spring-damper system [26, 37].

The above indicates that the soil is assumed to behave as a viscoelastic material that has a small indentation. Therefore, the maximum force is quickly reached, supported by the fact the the leg is also a stiff system. The contact area of the soil-structure interaction depends on the vertical penetration depth, which is known to be small. As a result, the spudcan's horizontal displacement is also small, given its direct relation with the vertical penetration depth. In other words, a reduced contact area yields a smaller lateral resistance and thus a diminished horizontal force, assuming a constant bottom friction. In essence, stiffer systems have shorter impact durations, which lead to higher peak forces for similar impact energies [22, 24, 38].

Moreover, the relatively smaller vertical displacements on stiff seabeds lead to axial forces that tent to be more impactful than lateral forces. This contrasts with softer soils, where greater vertical penetration often occurs. Despite axial forces are typically larger than lateral ones, it is essential to acknowledge that lateral forces can produce a significant moment at the lower guide of the jacking system, potentially exceeding structural limitations. Even though it is expected that axial forces are governing on stiff seabeds, care must be taken at greater water depths where an increased moment arm amplifies the influence of lateral forces.

In conclusion, it is important to note that this study assumes a uniform soil layer with perfectly horizontal bathymetry. Although this characterisation of soil behaviour significantly simplifies the actual complexities involved, it is less conservative than assuming the soil as a rigid body, which would suggest a complete transmission of the impact energy into the leg.

2.5. Existing Methodologies for Determining the Impact Force

The study of impact mechanics offers a variety of methodologies for determining the impact force. This section delves into the most relevant methods for calculating impact forces on jack-up legs.

2.5.1. Impulse-Momentum Theory

The impulse-momentum theory is an application of Newton's second law of motion, and it states that the impulse applied to a body equals the change in its momentum. The principle is shown in Equation 2.15 for linear impulse and in Equation 2.16 for angular impulse.

$$J_{\text{linear}} = \int_0^{t_c} F dt = m\Delta v = m\left(v' - v\right) \tag{2.15}$$

$$J_{\text{angular}} = \int_0^{t_c} M dt = I\Delta\omega = I\left(\omega' - \omega\right) \tag{2.16}$$

Where, F represents the force, M the moment, t_c the impact duration, I the mass moment of inertia, and ω denotes the angular velocity [39].

Both linear and angular impulses hold significance as both central and eccentric impacts are probable scenarios. In the latter scenario, a moment is created with respect to the body's centre of mass and a part of the initial translational energy transitions into rotational energy. Consequently, the impact energy is distributed across multiple DOF, reducing the overall impact force.

Furthermore, the impulse-momentum theory is applicable when the initial collision duration is significantly smaller than the natural period of the considered motion. This method allows the decoupling of the impact kinematics and energy transfer during the impact from the analysis of strain energy dissipation within the colliding bodies [39]. However, applying this method effectively requires a precise understanding of the impact duration and post-impact velocity to draw accurate conclusions about the impact force, which is often not the case in real-world scenarios.

2.5.2. Method Based on Principle of Energy Conservation

Early methodologies for impact analysis during jacking operations are based on the principle of energy conservation, such as the one described by DNV-RP-C104 [11]. The method assumes that the relative velocity between the spudcan and seabed is governed by pitch and roll motions. Additionally, it assumes that all energy present in the impact is absorbed by one single leg, the spudcan immediately stops when touching the seabed, and the seabed is indefinitely rigid.

The total impact energy is assumed to be absorbed by the spudcan, the leg, and the jacking house. Consequently, the intensity of these forces are dependent on the wave conditions, the water depth, the structural variables, and the position of the leg relative to the centre of flotation. The components of the impact force, both horizontal and vertical, can subsequently be expressed as follows:

$$F_H = \frac{2\pi}{T}\theta\sqrt{\frac{I_m k_H}{\left[1 + \frac{k_V}{k_H}\left(\frac{d}{h}\right)^2\right]}} \tag{2.17}$$

$$F_V = \frac{2\pi}{T}\theta\sqrt{\frac{I_m k_V}{\left[1+\frac{k_H}{k_V}\left(\frac{h}{d}\right)^2\right]}} \tag{2.18}$$

Where, k_H represents the lateral stiffness of the leg, k_V the overall stiffness of the leg, I_m the mass moment of inertia with respect to roll and pitch motion, T the period of roll and pitch, and θ the amplitude of roll and pitch [11]. Additionally, d is the horizontal distance between the leg and the centre of flotation, and h is the water depth, as can be seen in Figure 2.5.

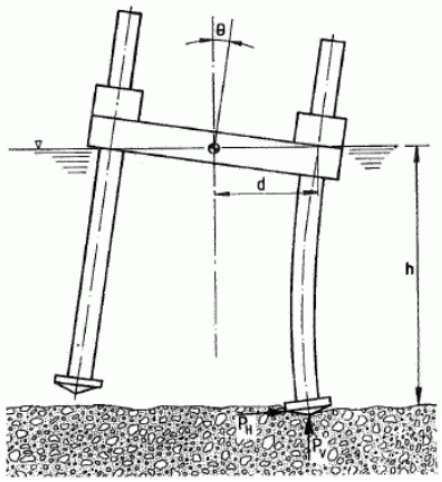

Figure 2.5: The leg impact forces on a jack-up [11].

The methodology proposed by DNV restricts the analysis by ignoring the contribution of heave, considering only the structural members of the leg, and presuming an infinitely rigid seabed. This means that it does not account for energy dissipation through the soil, leading to potentially large estimates of the impact force. However, according to Vazquez et al. [40], this method is a valid prediction of the linear relation between the leg velocity and impact force.

2.5.3. Improved Energy Method

The JIP presented a revised version of DNV's energy method, detailed in DNV-RP-C104 and explained in Section 2.5.2. This 'improved energy method' for leg impact incorporates heave motion, arbitrary spudcan load penetration curves, and hydrostatic restoring action. It integrates heave and rotational motion by introducing a lateral offset for the centre of rotation for the impact motion, as shown in Figure 2.6. Evaluation of mass moment of inertia, leg deformation, and hydrostatic restoring action is based on this modified centre of rotation [20].

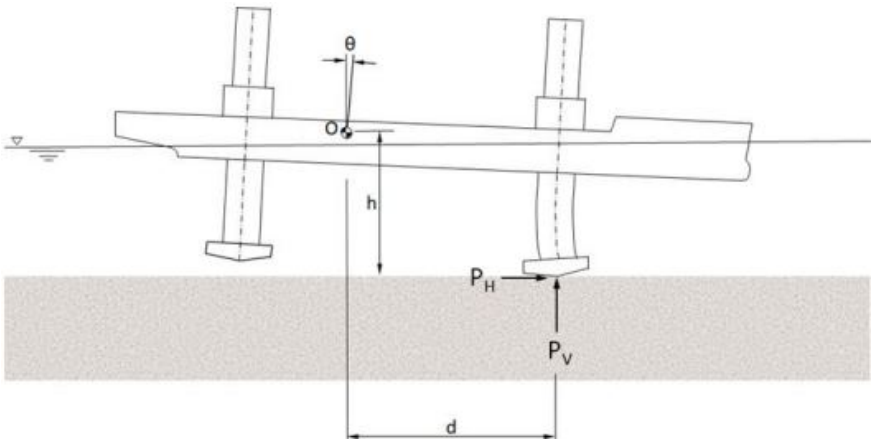

Figure 2.6: The centre of rotation for the impact motion [20].

With the assumption that the kinetic energy of the vessel is absorbed by the seabed, leg system, and hydrostatic restoring action, the following equation is obtained:

$$\frac{1}{2}I_m\dot{\theta}^2 = \int_0^{z_1} Q_V(z)dz + \frac{1}{2}k_V z_2^2 + \frac{1}{2}k_H[\phi h]^2 + \frac{1}{2}k_{hyd}\phi^2 \tag{2.19}$$

Here, $\dot{\theta} = \frac{2\pi}{T}\theta$ denotes the angular velocity of rotational motion with T as the period and θ as the amplitude. Additionally, k_{hyd} represents the vessel's hydrostatic restoring stiffness, $Q_V(z)$ is the seabed's vertical resistance as a function of spudcan penetration, z_1 is the maximum penetration during impact, $z_2 = Q_V\left(z_1\right)/k_V$ the maximum leg system shortening during impact, and $\phi = \left[z_1 + z_2\right]/d$ signifies the maximum rotation about point O during impact [20].

The maximum spudcan penetration z_1, can be calculated by iteratively solving the above equation, while the vertical and horizontal impact forces can be expressed as follows:

$$P_H = k_H\phi h \tag{2.20}$$

$$P_V = Q_V\left(z_1\right) \tag{2.21}$$

Assuming a linear relation for the spudcan load-penetration simplifies the method and the vertical and horizontal impact forces are represented as:

$$P_H = \frac{2\pi}{T}\theta\sqrt{\frac{I_M k_H}{\left[1 + \frac{k_V}{k_H}\left(\frac{d}{h}\right)^2 + \frac{k_{hyd}}{k_H h^2}\right]}} \tag{2.22}$$

$$P_V = \frac{2\pi}{T}\theta\sqrt{\frac{I_M k_V}{\left[1 + \frac{k_H}{k_V}\left(\frac{h}{d}\right)^2 + \frac{k_{hyd}}{k_V d^2}\right]}} \tag{2.23}$$

The method can be modified for scenarios where two legs impact the seabed simultaneously. Nevertheless, the JIP concluded that the method should be conservative as it determines the operational limits and is therefore based on a single leg impact [20].

2.5.4. Previous Research and Common Practices

Beyond the methodologies presented in the previous sections, several work has been published on the impact forces on jack-up legs during installation. Frequently, the studies were focused on analysis of softer soil types such as sand and clay, incorporating nonlinear properties and plastic deformations. Therefore, advanced software or numerical solutions are often utilised. Specifically, the early work by Smith et al. (1994, 1996) [22, 41], used a 2D Finite Element (FE) model to simulate soil-structure interaction, revealing that impact forces vary significantly with soil types. Additionally, it was found that the highest forces and moments occur at the lower guide, predominantly by heave compared to surge. In other early research by Chakrabarti et al. (1995, 2007) [42, 43], the leg's structural analyses and models were established by the beam theory.

Later research by Chakrabarti [26], performed a nonlinear dynamic impact analysis for different water depths and soil conditions and compared the results with the classical DNV approach [11]. This study confirmed the conservative nature of DNV's estimates for softer soils, yet observed that for stiff seabeds, the computed impact forces were either equal or exceeded the DNV calculations. According to the author, this is primarily due to that DNV neglects soil plastic deformations and leg dynamics. Moreover, the study implemented a FE model for the structural analysis, and elucidated the key factors influencing the vessel's energy prior to impact.

Recent contributions, such as Kreuzer et al. [44], proposed a simpler mechanical rheological model for soil-structure interaction, to reduce the computational demand compared to FE methods. This work also introduced a numerical model implementing the Coupled Euleerian-Lagrangian (CEL) method in ABAQUS, which is used for soil-structure interaction analysis.

Further, Daun and Olsson [25] and Ringberg et al. [31] suggested splitting the impact scenario into separate elements for structural and soil deformation behaviour, given their different response to impact.

The soil model is based on the bearing capacity theory and the structural model is based on contact mechanics, specifically a spring-damper system. Which is believed to be an accurate representation of the structural deformation when only elastic deformations are considered. Furthermore, this study indicates that an analytical beam theory gives a reliable estimate on the structural capacity of the leg, while the FE analysis introduces numerical uncertainties and increases the complexity of the analyses.

A different approach was adopted by Vazquez et al. (2016) [40], where leg impact forces were determined by the Downward Spudcan Velocity (DSV). An extension of this research by Vazquez et al. (2017) [45], compared the forces generated in elastic soils modeled in OrcaFlex with those in non-linear soils represented in ABAQUS. The study concluded that a simplified linear methodology could offer conservative yet reasonable results, considering stiff seabeds.

2.6. Concluding Remarks

The aim of this literature study on impact mechanics, with a focus on its relevance to jacking operations on stiff seabed conditions, is to identify the key physical factors that govern the forces in jack-up legs during installation. This is to answer the first subquestion of this study: What factors govern the forces in jack-up legs during installation on stiff seabed?

This study revealed that wave-induced vessel motions are the primary drivers of the impact forces on jack-up legs, leading to horizontal and vertical spudcan velocities that generate axial and lateral forces in the leg. The magnitude of these forces during the stand-on phase depends on the energy contained within the system prior to impact and how this energy is absorbed by the soil and structure. Firstly, factors that contribute to the amount of energy contained in the system are the wave height, wave period, hull characteristics, vessel's inertia, jacking velocity, and the length of the legs below the hull, which is determined by the water depth. The environmental loads and dynamic responses that act on the system prior to impact are detailed in previously conducted literature research [18]. Secondly, the energy absorbed by the soil and structure depends on their stiffness characteristics and behaviour. This is often a challenging aspect to determine, underlining the importance of formulating accurate assumptions that reflect reality.

The above indicates that it is important to include all elements that influence the soil and structure stiffness characteristics and behaviour. However, the dynamic soil-spudcan interaction process is a complex phenomenon that is not extensively covered in existing standards or detailed in literature. The impulse-momentum theory requires a precise understanding of the impact duration and post-impact velocity, often not the case in real-world scenarios. The classical DNV approach restricts the analysis by ignoring the contribution of heave, assumes that the seabed is indefinitely rigid, and that all energy prior to impact is absorbed by one single leg. This implies that energy dissipation through the soil is not accounted for, while the soil characteristics and behavior are identified as important factors regarding impact forces.

An improvement to the classical DNV approach is the 'improved energy method' introduced by the JIP, incorporating heave motion, arbitrary spudcan load penetration curves, and hydrostatic restoring action. However, this analysis yielded operational limits different from Van Oord's in-house model results. Therefore, instead of replicating the exact method that led to these differences, the decision was made to consider only those elements from the impact analyses that are relevant. Furthermore, it is important to note that when using existing methodologies, it is essential to be familiar with the assumptions made and to consider the method most appropriate for the problem being analysed. Additionally, employing a conservative method can be an informed decision when using impact forces to determine operational limits.

Although the colliding system is considered to be stiff, it is relevant to obtain the stress waves within the leg. Since it is assumed that no plastic deformations occur, both the structural analysis and soil behaviour can be modeled using a spring-damper system. Insights from prior research suggest that the impact scenario can be divided into separate elements for structural and soil deformation behaviour, given their different response to impact. Additionally, the beam and rod theory provides a reliable estimate of the leg's structural capacity. As such, it can serve as a simplified representation of the leg, while FE models, despite their usefulness, increase the computational demand and complexity of the calculations.

The minimal soil-penetration depth results in a small contact area, leading to relatively more impactful axial forces than lateral forces. Therefore, it can be concluded that axial forces predominate over lateral forces during impacts on stiff seabeds. Moreover, this stiff system yields relatively high peak forces due to the short impact duration characteristic of such systems. Consequently, assuming that all energy prior to impact is converted into a single dimension results in a higher total impact force than when the energy is distributed across multiple DOF. Additionally, it was observed that for stiff seabeds, a simpler linear methodology can yield reasonable results compared to more complex nonlinear soil representations.

This literature study elucidated the key physical factors that govern the forces in jack-up legs during installation on stiff seabeds. The primary conclusion is that axial forces dominate over lateral forces during impacts, due to the minimal soil-penetration depth that results in a small contact area. This insight justifies the simplification of the system to a one-dimensional model, as this approach yields the largest impact forces, which are crucial for determining the operational limits. Consequently, the next chapter will develop a one-dimensional rod model that is specifically designed to analyse the axial forces, and to determine how the identified key factors influence these governing forces.

3

Rod Model for Axial Impact Forces

In order to answer the research question, a model is created that can determine the influence of the identified factors that govern the forces in jack-up legs during installation on stiff seabeds. As concluded in the previous chapter, axial forces dominate over lateral forces during impact, thus a one-dimensional rod model is designed to analyse the axial forces. The model aims to provide insights into the main physics during impact, and the different processes need to be understood. To perform this properly, the problem needs to be described as well as the assumptions that have been made. To simplify the analysis, the model only considers one leg, enabling the inclusion of the maximum possible impact force. For instance, in this scenario, the weight of the vessel could potentially act on one leg upon impact with the seabed. With these simplifications in place, the problem is described and the model is introduced in Section 3.1. The model's solution methodology and verification are discussed in Section 3.2. Afterwards, Section 3.3 elucidates the careful selection of variables, and Section 3.4 introduces the specific leg modification.

3.1. Problem Description and Model Introduction

Initially, the jack-up vessel possesses a certain kinetic energy resulting from the wave-induced vessel motions and jacking velocity. The jack-up leg, connected to the hull via the jacking system, can be modelled as a vertical rod in the z-direction. Since the primary focus is on the axial forces, only the vertical velocity of the rod is considered. This means that the rod has an initial velocity in the z-direction that represents the mentioned physical phenomena, which is an essential input for the model.

In other words, when the spudcan approaches the seabed and the probability of impact increases, the rod possess a certain amount of kinetic energy. Upon contact with the seabed, the kinetic energy is converted into potential energy within the soil and initiates a compression wave in the rod. The rod stops when the kinetic energy is fully transferred to potential energy, at which point the forces within the rod are expected to reach their maximum. However, this should also emerge in the model, but which is yet to be proven. Subsequently, the rod's kinetic energy will increase again due to the impact with the stiff seabed or also by the vessel's motions. Eventually, the contact force becomes zero and the rod disconnects from the seabed. Since the maximum force is expected between the first contact moment until disconnection, the model is simulated until the contact force is zero [36].

In this study, the leg-hull connection is assumed to be rigid. However, it is crucial to acknowledge that it is a complex interaction mechanism influenced by the relative stiffness of the components and the leg-hull clearance. A detailed evaluation of the load distribution on the pins can be performed by a nonlinear FE model. Nevertheless, the simplest and most prevalent method treats the leg-hull connection as either a linear spring or a rigid connection [46–48]. For simplicity and to obtain the highest peak forces, the leg-hull connection is assumed to be modeled as rigid. Moreover, It should be noted that the impact of this assumption is negligible when conducting a sensitivity study with the aim to determine the influence of the identified factors on the governing forces.

An schematic drawing of the simplified rod model is presented in Figure 3.1. This visualisation aids in comprehending the simplified problem and facilitates further mathematical exploration. The entire weight of the vessel is represented by a point mass, M_v, connected to the rod at $z = 0$. The properties of the rod are defined by the length L, uniform cross-sectional area A, density ρ, and modulus of elasticity E. Furthermore, the initial velocity v_i, and the displacement of the rod $u(z,t)$, are pointed into the positive z-direction. Another important component that must be included in the system is the spudcan. Accounting for a significant part of the total leg weight, the spudcan is added to the tip of the rod as a mass denoted by M_{sp}. Since the interval of interest spans from the first contact moment until disconnection, the tip of the rod is defined to be connected to the seabed. This connection is modeled as a spring-damper system, with the spring storing the potential energy transferred from the rod's kinetic energy to the soil. However, energy can also be converted into heat or other forms of energy, such as friction. Therefore, the system includes a damper to dissipate energy through interaction with the seabed.

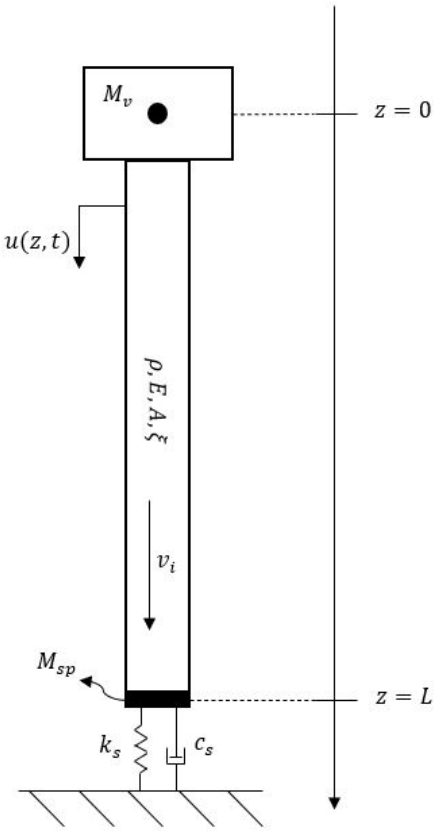

Figure 3.1: Schematic rod model for axial impact force.

The potential energy stored by the rod through a compression wave is related to stress, which is expressed by Hooke's law:

$$\sigma_z = E\varepsilon_z = E\frac{\partial u(z,t)}{\partial z} \tag{3.1}$$

Here, σ_z represents the stress and ε_z denotes the strain in the z-direction [49]. The equation demonstrates that the potential energy absorbed by the rod is essentially the strain energy caused by elastic deformation. In addition, the rod experiences a form of energy dissipation due to material damping, which can have a significantly effect on the total stress. The material damping can be included in the equation of motion of a classical rod, which is based on the Kelvin-Voigt rheological model [50]. The model is based on the axial stress-strain relation and can be given by

$$\sigma_z = E\varepsilon_z + \eta\frac{\partial \varepsilon_z}{\partial t} \tag{3.2}$$

where, η is the material viscosity. According to Trubat and Molins [50], the material viscosity of a rod can be expressed as follows

$$\eta = \xi\eta_c = \xi\frac{4L}{\pi}\sqrt{\rho E} \tag{3.3}$$

where, ξ represents the damping ratio of steel, and η_c denotes the critical viscosity, the expression of which is given. This expression is derived by assuming that the rod is only subjected to a pure axial load and describes the critical damping specifically for the first longitudinal mode of vibration. The modified Young's modulus of a viscoelastic rod can now be defined as

$$\hat{E} = E(1 + \xi\frac{4L}{\pi c}\frac{\partial}{\partial t}) = E(1 + \xi_c\frac{\partial}{\partial t}) \tag{3.4}$$

where, ξ_c is an operator that includes the damping ratio and $c = \sqrt{E/\rho}$ is the longitudinal wave velocity.

To achieve the model's aim of determining the influence of the identified factors on the axial impact force, it is essential to ascertain the maximum impact force at a specific location along the length of the rod. More specific and most important to this research, the position where the jacking system is located, in the model's case the rod-vessel connection at $z = 0$. The described propagating stress waves are directly related to the axial forces, which can be defined by

$$F = A\sigma \tag{3.5}$$

This highlights the significance of obtaining the time-dependent stress distribution along the rod, as it is a crucial output for the model in determining the maximum impact force.

Based on the assumptions and relations given above, the system's equation of motion can be defined as:

$$\rho A\frac{\partial^2 u(z,t)}{\partial t^2} - \hat{E}A\frac{\partial^2 u(z,t)}{\partial z^2} = 0 \tag{3.6}$$

Here, the first term represents inertia, and the second term corresponds to the axial stiffness of the system. Further elaboration of the equation of motion gives the following:

$$\frac{\partial^2 u(z,t)}{\partial t^2} - c^2\frac{\partial^2 u(z,t)}{\partial z^2} - c^2\xi_c\frac{\partial^3 u(z,t)}{\partial z^2 \partial t} = 0 \tag{3.7}$$

The external forces acting on the system due to the vessel mass and the seabed contact are described by the boundary conditions at $z = 0$ and $z = L$, respectively. These boundary conditions are expressed as follows:

$$EA\frac{\partial u(0,t)}{\partial z} + EA\xi_c\frac{\partial^2 u(0,t)}{\partial z \partial t} = M_v\frac{\partial^2 u(0,t)}{\partial t^2} \tag{3.8}$$

$$EA\frac{\partial u(L,t)}{\partial z} + EA\xi_c\frac{\partial^2 u(L,t)}{\partial z \partial t} = -M_{sp}\frac{\partial^2 u(L,t)}{\partial t^2} - c_s\frac{\partial u(L,t)}{\partial t} - k_s u(L,t) \tag{3.9}$$

Furthermore, the initial conditions are given as:

$$u(z,0) = 0 \tag{3.10}$$

$$\frac{\partial u(z,0)}{\partial t} = v_i \tag{3.11}$$

3.2. Model Solution Methodology

The equation of motion can be solved in either the time or frequency domain. Therefore, according to Yang [51], it is essential to differentiate between individual problems and unified final problems while determining the desired solution. A given problem can be solved in time domain using methods such as the separation of variables, d'Alembert's solution, and Green's function. These methods are typically used to solve individual problems and elucidate the solving process instead of the final solution. Importantly, the presence of nonlinear behaviour in a system necessitates the use of time domain calculations.

On the other hand, a unified solution encompasses the formulation that incorporates all contributions from external excitation, nonzero initial conditions, and inhomogeneous boundary conditions. This

unified solution is particularly useful for addressing complex engineering problems, such as the problem defined in this study. Therefore, to obtain the final solution and to directly solve the problem, the Fourier transform or the Laplace transform can be used, which operate in the frequency domain or s-domain, respectively. Given that the system's behaviour is assumed to be linear, calculations in the frequency domain are not only viable but also faster [52].

The equation of motion is a Partial Differential Equation (PDE) that is generally difficult to solve. Therefore, the mentioned integral transforms can be applied to reduce the initial problem to a simpler Ordinary Differential Equation (ODE) [53]. However, the methods are slightly different and the choice of method depends on the system's characteristics. Considering this particular rod model, the initial velocity is specifically important and therefore Laplace should be used instead of Fourier. In addition, it is an impact problem of which the transient behaviour can be captured by the Laplace transform.

3.2.1. Laplace Transform

The Laplace transform of a function $f(t)$, denoted as $\mathcal{L}[f(t)]$, is defined as

$$\mathcal{L}[f(t)] = f(s) = \int_0^{+\infty} e^{-st} f(t) dt \tag{3.12}$$

where, s is the complex Laplace parameter. This parameter is expressed as $s = i\omega + \sigma$, where σ is a small positive real value, and ω is the frequency [53].

When using the Laplace transform to solve PDEs, it is essential to use the Laplace transform of different-order derivatives. The Laplace transform for the first and second order derivative are given in Equation 3.13 and 3.14, respectively.

$$\mathcal{L}\left[\frac{\partial f(t)}{\partial t}\right] = sf(s) - f_0 \tag{3.13}$$

$$\mathcal{L}\left[\frac{\partial^2 f(t)}{\partial t^2}\right] = s^2 f(s) - sf_0 - \dot{f}_0 \tag{3.14}$$

Here, f_0 and $\dot{f}_0$ represents the nonzero initial conditions. This indicates that the Laplace transform of the time domain derivatives of a function accounts for the initial conditions, which is of significant interest for solving the defined problem. Importantly, if the Fourier transform were to be applied in this context, these initial conditions would be disregarded [52].

Applying the Laplace transform to the defined system and fulfilling the initial conditions yields the following expression for the equation of motion:

$$s^2 \tilde{u}(z,s) - c^2 \left(1 + \xi_c s\right) \tilde{u}''(z,s) = v_i \tag{3.15}$$

Furthermore, implementing the Laplace transform to the boundary condition at $z = 0$ results in:

$$EA \left(1 + \xi_c s\right) \tilde{u}'(0,s) - M_v s^2 \tilde{u}(0,s) = -M_v v_i \tag{3.16}$$

And applying it to the boundary condition at $z = L$ generates:

$$EA \left(1 + \xi_c s\right) \tilde{u}'(L,s) + \left(M_{sp} s^2 + c_s s + k_s\right) \tilde{u}(L,s) = M_{sp} v_i \tag{3.17}$$

A more detailed presentation of the analytical derivations can be found in Appendix B.

The initial problem is now defined as an ODE in the Laplace domain and still depends on the $z-$position along the rod. Eventually, it is of interest to find the strain, which leads into the stress distribution along the rod and the axial impact force. Therefore, an expression of $\tilde{u}(z,s)$ must be found which can later be numerically converted to the time domain by the inverse Laplace transform. The solution for $\tilde{u}(z,s)$ can be obtained either analytically or numerically.

3.2.2. Analytical and Numerical Solution

The analytical solution is obtained by considering the problem as continuous, thereby assuming uniformity and constant structural characteristics along the rod. Although this study simplifies the problem by assuming the rod to be homogeneous, minor variations in axial stiffness exist along the length of the leg in reality. However, these minor differences are assumed to have negligible effects on the impact forces. Therefore, an analytical solution can be derived, which is detailed in Appendix B.1.1.

Since the equation of motion is nonhomogeneous, the general solution $\tilde{u}_g(z,s)$ consists of the sum of the homogeneous solution $\tilde{u}_h(z,s)$ and the particular solution $\tilde{u}_p(z,s)$. This can be expressed as follows:

$$\bar{u}_g(z,s) = \bar{u}_h(z,s) + \bar{u}_p(z,s) \tag{3.18}$$

Importantly, the homogeneous part reduces over time due to structural damping, while the particular solution exists as long as the forcing function is present [49]. The derived expression for the general solution is given by:

$$\bar{u}_g(z,s) = C_1 e^{-\beta z} + C_2 e^{\beta z} + \frac{v_i}{s^2} \tag{3.19}$$

Here, the parameter β is derived as:

$$\beta = \frac{s}{c\sqrt{1+\xi_c s}} \tag{3.20}$$

The constants C_1 and C_2 are calculated by substituting the solution of the homogeneous equation into the boundary conditions.

One advantage of the continuous solution is that it simplifies the system to a single equation of motion when considering a single DOF. Moreover, it provides a reliable representation of the system under the assumption of uniformity. Conversely, the discrete or numerical solution separates the rod into multiple segments, each with its own equation of motion. This solution is more advanced and can be extended to a more realistic representation of reality by accounting for different axial stiffnesses. As for future expansions to a beam model, this approach holds potential to simulate various lateral forces along the leg length. Essentially, it can incorporate the nonuniform properties of the system. Therefore, the Finite Difference Method (FDM), which will be defined in the next section, is used. This method allows for future complexity improvements of the system. The validity of the model is confirmed by comparison with the analytical solution.

3.2.3. Finite Difference Method

Three commonly used formulas in FDM are forward, backward, and central differences. These formulas estimate the derivatives of a function by utilising the values of two neighboring points. Among these methods, the central difference method is preferred due to its accuracy, as it incorporates information from both forward and backward points in space or time. This is in contrast to the one-sided forward and backward differences [54].

Solving an ODE with the FDM consists of the following steps [54, 55]:

1. Discretise the spatial domain into $N+1$ points
2. Fulfilling the equation at a finite set of discrete points
3. Substituting derivatives with finite differences
4. Formulate a recursive algorithm

The different steps are detailed in Appendix B.1.2, and result in the following recursive algorithm:

For $n = 0$:

$$s^2\tilde{u}^0 - c^2\left(1+\xi_c s\right)\frac{2\tilde{u}^1 - 2\tilde{u}^0}{\Delta z^2} + \frac{2c^2}{EA\Delta z}M_v s^2\tilde{u}^0 = v_i\left(1 + \frac{2c^2}{EA\Delta z}M_v\right) \tag{3.21}$$

For $n = 1, \ldots, N-1$:

$$s^2\tilde{u}^n - c^2\left(1+\xi_c s\right)\frac{\tilde{u}^{n+1} - 2\tilde{u}^n + \tilde{u}^{n-1}}{\Delta z^2} = v_i \tag{3.22}$$

For $n = N$:

$$s^2\tilde{u}^N - c^2\left(1+\xi_c s\right)\frac{2\tilde{u}^{N-1}-2\tilde{u}^N}{\Delta z^2} + \frac{2c^2}{EA\Delta z}\left(M_{sp}s^2 + c_s s + k_s\right)\tilde{u}^N = v_i\left(1+\frac{2c^2}{EA\Delta z}M_{sp}\right) \tag{3.23}$$

The ODE is converted into a system with $N+1$ algebraic equations and $N+1$ unknowns, meaning that the system can be solved and the values for $\tilde{u}(z^n, s)$ can be determined. This coupled system of algebraic equations can be written in matrix form, which is essential for the numerical solving process [55]. The matrix is fully detailed in Appendix B.1.2 and is presented in the following form:

$$\boldsymbol{Au} = \boldsymbol{B} \tag{3.24}$$

Where, $\boldsymbol{u} = [\tilde{u}^0, ..., \tilde{u}^N]$, and matrix $\boldsymbol{A}$ depends on the complex parameter s.

The system is numerically solved for various frequencies, with a small chosen value of σ to ensure the convergence of the Laplace integral. Displacements determined by both solution methods are plotted against these frequencies to ascertain the system's response and verify the FDM with a simpler calculation. These plots, shown in Appendix B.2, are similar despite the higher sensitivity of the analytical solution to lower frequencies. This is due to the particular solution which increases significantly for small values of s, due to the small chosen value of σ. Nevertheless, the results of the stress distribution in the rod are similar, as will be discussed in Section 3.2.4.

The absolute value of $\tilde{u}(z, s)$, depicted in Figure 3.2, determines the frequency range within which a solution can be found. In the frequency domain identified from this plot, the solution must converge to zero to ensure no parts of the solution are omitted. A value of $\omega = 100$ is sufficient for obtaining a complete solution and is therefore used for the integration back to the time domain using the inverse Laplace transform, explained in the subsequent section.

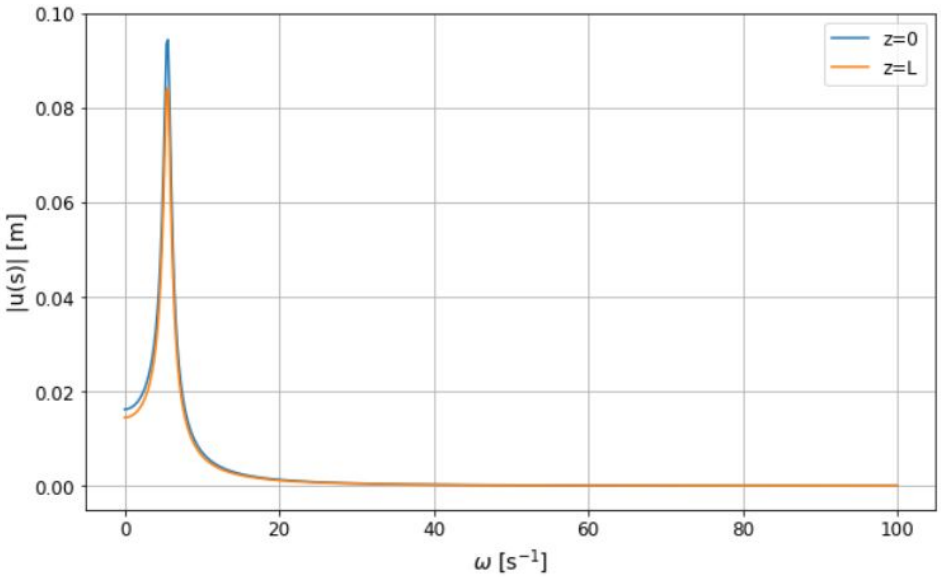

Figure 3.2: The absolute value of $\tilde{u}(z, s)$ at $z = 0$ and $z = L$ using the FDM.

3.2.4. Inverse Laplace Transform

The inverse Laplace transform is employed to determine the solution of the original problem in the time domain. A typical representation of the inverse Laplace transform is given by

$$f(t) = \mathcal{L}^{-1}[\tilde{f}(s)] = \frac{1}{2\pi i}\int_{\sigma-i\infty}^{\sigma+i\infty}\tilde{f}(s)e^{st}ds \tag{3.25}$$

which is also referred to as the Bromwich integral. According to Hoving and Metrikine [52], the inverse Laplace transform can be expressed in the frequency domain as follows:

$$f(t) = \mathcal{L}^{-1}\{\tilde{f}(s)\} = \frac{e^{\sigma t}}{\pi} \int_0^{+\infty} \text{Re}\left\{\tilde{f}(s)e^{\mathrm{i}\omega t}\right\} d\omega \tag{3.26}$$

As a result, the inverse Laplace transform is no longer expressed in terms of the complex Laplace operator s. The displacements in the time domain are determined numerically, in addition to the fact that the inverse Laplace transform can not be performed analytically. Moreover, the previous found truncation frequency, $\omega = 100$, is implemented in the integral to be able to find a numerical solution.

The inverse Laplace transform is numerically performed for both the FDM and the analytical solution in the frequency domain. The computed displacements are used to determine the strain and subsequently the stress distribution along the rod. The stress at the top ($z = 0$) and bottom ($z = L$) positions of the rod are illustrated in Figure 3.3, with further details provided in Appendix B.2.

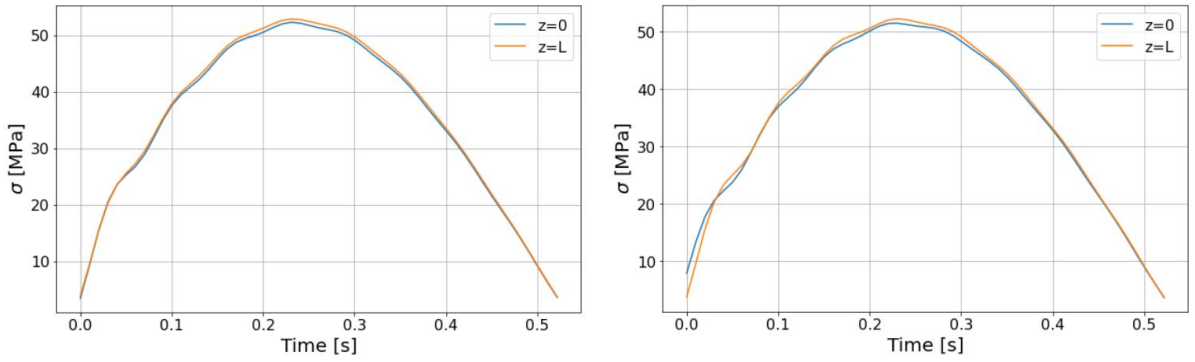

Figure 3.3: The stress distribution σ at $z = 0$ and $z = L$: Comparison of results from the FDM (a) and the analytical solution (b).

As can be observed, the figures yield approximately the same results. The minor differences primarily exist in the initial part of the simulation. As earlier mentioned, the simulation starts from the first contact moment until the contact force becomes zero and the rod disconnects from the seabed. It is also noticeable that the rod's maximum force coincides with the complete conversion of its kinetic energy into potential energy, as anticipated. This observation is consistent with Equation 3.5, which establishes the stress-force relation and confirms that the maximum force corresponds to the highest stress value.

Furthermore, the stress waves can be noticed in the graph by the observed wave patterns. As referenced in Section 2.3.3, stress waves propagate in both directions, away from and towards the impulse source, due to wave reflection. These wave reflections cause stress waves from opposing directions to converge, leading to their mutual reinforcement or attenuation and ultimately resulting in a wave pattern. Additionally, the observed difference in force magnitude between the top and bottom positions of the rod can be attributed to the structural damping of the rod.

To gain deeper insight into the stress development within the rod and enhance understanding of the system's physics, the displacement in the time domain is depicted in Figure 3.4. A comparison with Figure 3.3 indicates a correlation: larger displacement differences between the two positions on the rod result in increased stress development. This correlation is observable throughout the simulation. At the beginning, both stress and displacement differences are minimal. At their peak, the maximum stress aligns with the largest displacement differences. As the simulation progresses towards the end and the rod nears disconnection, these values decrease. Upon reaching zero displacement difference and stress, disconnection occurs, marking the end of the simulation.

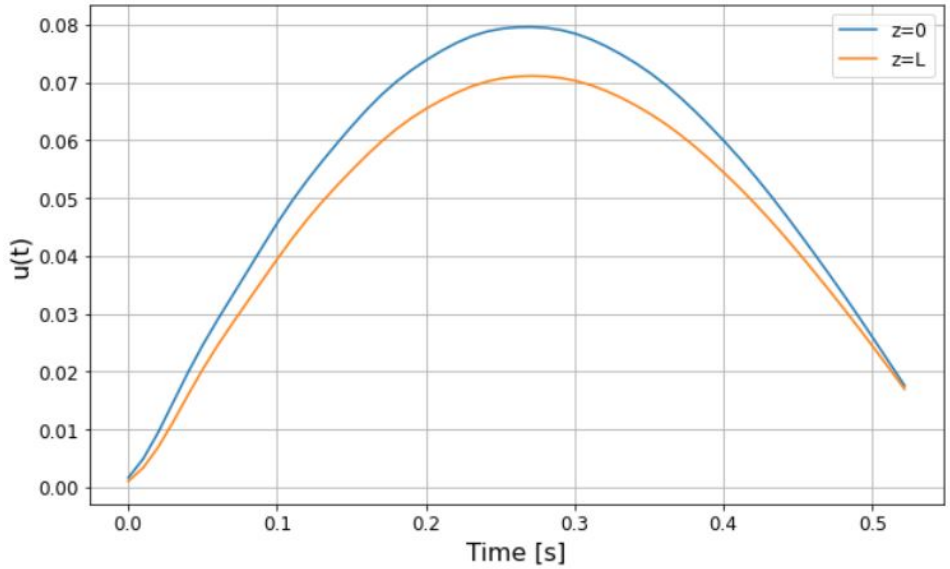

Figure 3.4: The displacement in the time domain at $z = 0$ and $z = L$ using the FDM.

3.3. Model Input Variables

In order to generate a simulation that is as representative as possible to reality, careful consideration must be given to the selection of variables. Furthermore, it is important to provide a clear starting position description before conducting the sensitivity study. The various initial variables used are presented in Table 3.1, with the values marked as X being confidential. All initial variables will be further explained in this section.

Table 3.1: The initial variables used in the rod model for axial impact forces (values marked with X are confidential).

Parameter	Symbol	Value	Unit
Submerged leg length	L	35	[m]
Area cross-section leg	A	X	[m^2]
Young's Modulus	E	210	[GPa]
Density steel	ρ	8000	[kg/m^3]
Structural damping ratio	ξ	0.01	$[-]$
Mass single spudcan	M_{sp}	X	[mT]
Mass vessel	M_v	X	[mT]
Initial velocity	v_i	0.5	[m/s]
Seabed normal stiffness	k_s	X	[kN/m/m^2]

The vessel's and jack-up leg properties are taken from Van Oord's own stand-on analysis [14]. Moreover, the soil stiffness has been estimated using geotechnical site survey data and an impact analysis was performed, resulting in a normal seabed stiffness [38]. Additionally, a realistic initial velocity is chosen just as a starting point.

According to DNV-RP-C104 [11], the structural damping is expected to be between 1-3%, depending on the leg design. Additionally, Ou et al. [56] and Zhang et al [57] suggest that a damping ratio in the longitudinal direction of 1-5% is reasonable. Considering that an increased stiffness reduces the damping ratio, and given that the studied system contains a high stiffness, a structural damping ratio of 1% is selected to determine the highest forces.

Furthermore, the damping coefficient of the soil is determined by the critical damping coefficient and the damping ratio as follows:

$$c_s = c_c \xi_s = 2\xi_s \sqrt{k_s m_{\text{tot}}} \tag{3.27}$$

Here, c_c represents the critical damping coefficient, m_{tot} the total mass of the vessel, leg and spudcan, and the damping ratio is assumed to have a value of $\xi_s \approx 0.1$ [36, 49]. This damping ratio, $\xi_s \approx 0.1$, indicates the rate at which oscillations in a system decay after a disturbance and is a measure of the level of damping relative to the critical damping. For $0 < \xi < 1$, the system is underdamped and exhibits oscillations, while $\xi > 1$ implies an overdamped system without oscillations. A critically damped system, which provides the fastest return to equilibrium without oscillation, corresponds to $\xi = 1$. Given the expected oscillatory behaviour of the modeled system, a damping ratio of $\xi_s \approx 0.1$ is assumed in this study [29].

3.4. Specific Leg Modification

This section introduces the specific leg modification detailed in this study. This introduction is essential to address the final subquestion: How well does the specific leg modification perform? Due to confidentiality, the detailed leg modification design will not be illustrated. Instead, the focus will be on its simplified working principle. Essentially, applying the leg modification to the spudcan introduces an additional spring-damper system, capable of storing potential energy and allowing for extra energy dissipation. Therefore, this function is anticipated to reduce the stress distribution along the leg, consequently decreasing the overall maximum impact force.

In the context of the rod model, incorporating the leg modification involves transforming the spring-damper system of the boundary condition at $z = L$ into a double spring-damper system in series. To effectively implement this modification in the model, it is necessary to examine how a double spring-damper system in series can be converted into a single spring-damper system. According to Rao [49], an expression can be derived for an equivalent spring constant of two springs that are connected in series. Considering the springs depicted in Figure 3.5, the total elongation of both springs under a load W, is given by

$$\delta_{\text{st}} = \delta_1 + \delta_2 \tag{3.28}$$

Since both springs are subjected to the same force, an equilibrium is reached, resulting in the following expression:

$$W = k_1\delta_1 = k_2\delta_2 = k_{\text{eq}}\delta_{\text{st}} \tag{3.29}$$

Here, k_{eq} denotes the equivalent spring constant of the two springs connected in series. Substituting this expression into Equation 3.28 yields the following equation:

$$\frac{1}{k_{\text{eq}}} = \frac{1}{k_1} + \frac{1}{k_2} \tag{3.30}$$

Additionally, the same applies to two dampers in series:

$$\frac{1}{c_{\text{eq}}} = \frac{1}{c_1} + \frac{1}{c_2} \tag{3.31}$$

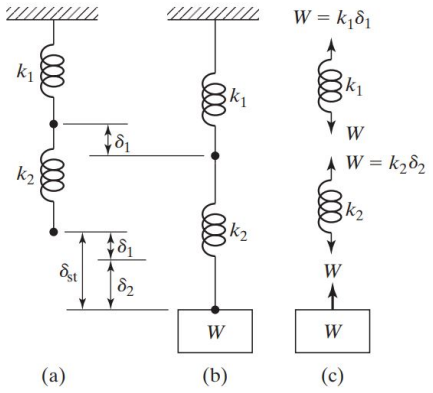

Figure 3.5: Two springs in series [49]

The properties of the specific leg modification are specified by Van Oord's stand-on analysis [14]. The modification exhibits nonlinear characteristics; however, the current model cannot capture this nonlinearity due to its frequency domain solving process. Nevertheless, for simplicity, the modification's behaviour is assumed to be linear, with best and worst-case scenarios estimated. Here, the best-case scenario corresponds to the lowest stiffness, and the worst-case scenario corresponds to the highest stiffness. Consequently, the sensitivity study outlined in Chapter 5 is repeated for these two differently defined stiffnesses of the leg modification. It should be underscored that these assumptions could lead to results that deviate from reality. However, in general, they still allow for an assessment of the leg modification's overall performance.

The impact force on the rod, determined with and without leg modification, is depicted in Figure 3.6. These graphs are normalised due to data protection and to enable a fair comparison with the data presented in the next chapter. Normalised values are denoted by (*).

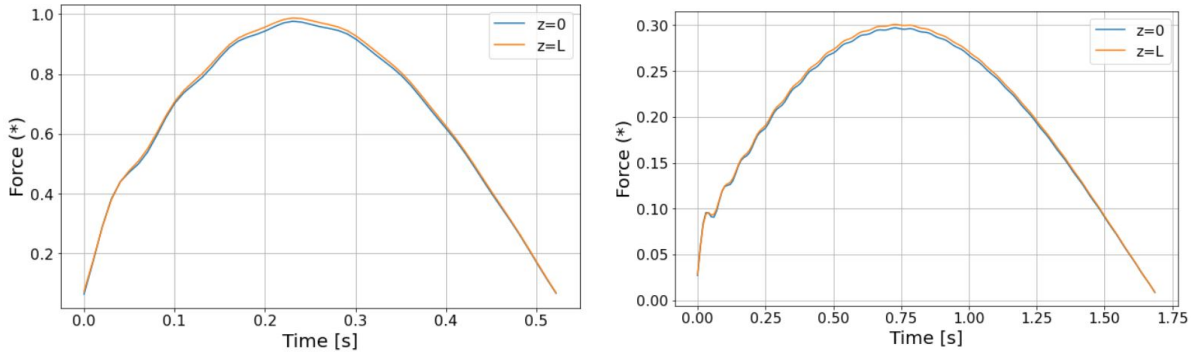

(a) (b)

Figure 3.6: Normalised impact force at $z = 0$ and $z = L$, without (a) and with (b) leg modification.

What is immediately noticeable is that the implementation of the leg modification results in a reduction in maximum impact force, while simultaneously increasing the duration of the impact. Additionally, a vibration at the beginning of the simulation is observed when the leg modification is in place.

4

Validation of Rod Model for Axial Impact Forces

The developed model is validated using data from the Aeolus, provided by Van Oord. This data comprises oil pressure readings from the vertical jacking cylinders and vessel motions measured by the Motion Reference Unit (MRU). Firstly, the source of the examined data is addressed in Section 4.1, including its generation process and associated measurement techniques. Subsequently, Section 4.2 continues the analysis with the identification of impact within the data and discusses the methods of observation. Once the moment of impact is extracted, it is compared with the developed rod model for validation purposes in Section 4.3. This validation process is important as it determines the alignment of the model with reality. A concise discussion and conclusion subsequently ensue.

4.1. Data Collection and Characterisation

The Saint-Brieuc wind farm project comprises 62 wind turbines and one substation, resulting in 63 distinct jacking up locations where the Aeolus operates. The geographic layout of the wind farm and the locations of the wind turbines are depicted in Figure 4.1. Data was available from sites where the drilling and installation of the pin-piles were completed in 2022. These sites are situated in areas with the stiffest seabeds. Therefore, at these locations the leg modifications were mounted on the spudcans, which is crucial to consider when examining the data from these sites.

Additionally, two different data types were present due to changes in the vessel's measurement methods over time. The older measurement method involved data points collected at larger time intervals. Moreover, these data points did not align with different measurements, such as the oil pressures in the vertical cylinders with the MRU readings. This discrepancy complicated the impact analysis, leading to the conclusion that the impact was unidentifiable from these data points. Consequently, multiple locations were not suitable for impact analysis due to these data constraints. Unfortunately, most of the stiffest seabed locations contained this data type. These locations featured unweathered bedrock, indicating the presence of a bedrock overlaid by a superficial deposit of 1.0m or less.

Subsequently, a new device was installed that aligned all measurements, standardising the time steps. This improvement in measurement precision facilitated the identification of impact forces on a jack-up leg. However, only one location contained unweathered bedrock and the new signal, making it the location that is mainly studied. Additionally, for this study, it is of interest to examine the stiffest possible seabed, as it is expected to result in the highest impact forces. Consistently, the model presumes a highly stiff seabed, which further substantiates the selected location as the most suitable for validation purposes. Importantly, the impact was easiest to identify at the location with unweathered bedrock. While other locations were also examined, detecting the impact became increasingly difficult. This difficulty is likely due to the reduced stiffness of the seabed, regardless of the sea state at the time of measurements.

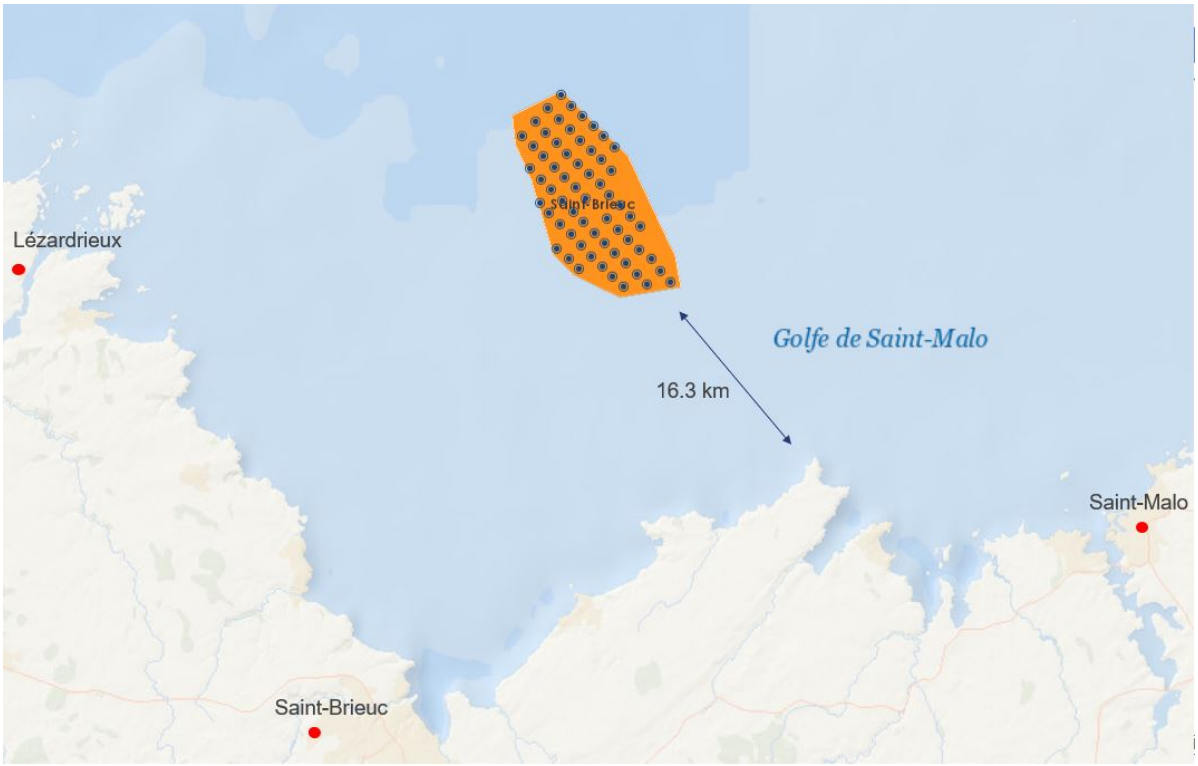

Figure 4.1: Geographic layout of the Saint-Brieuc offshore wind farm [58].

4.2. Identification of Impact Forces

The key measurements of interest that were available include the oil pressures in the vertical cylinders of the jacking system, the vessel's motions by the MRU, and the leg height. The MRU measurements encompasses the vessel's displacement, velocity, and acceleration. Furthermore, the oil pressure is measured separately for each cylinder, indicating that there are six individual oil pressure measurements for each jacking frame. Notably, these signals also incorporate pre-calculated force values. For analysing impact, it is essential to identify instances when the vessel motions significantly decrease while oil pressures peak. Equally important is to differentiate between oil pressure peaks caused by the jacking system and those due to the impact force. Therefore the following criteria are considered when identifying the impact force:

1. Coinciding with the oil pressure peak, a severe change in the vessel's motions occurs, particularly in the heave direction.
2. The six oil pressures individually exhibit similar behaviour and are of comparable magnitude during a peak load.

The last criterion can be further explained by the conclusion that peaks arising from the jacking system display discernible patterns, often occurring just before the cylinders switch from pushing to pulling and vice versa, as depicted in Figure 4.2. Each colour in the graph represents a single cylinder, and it can be observed that both the peak behaviour and magnitude vary. Typically, a consistent group of three cylinders often exhibit opposing behaviours, moving in opposite directions. This is exemplified by the vertical cylinder group consisting of 'cyan', 'red', and 'purple', and the group comprising 'green', 'yellow', and 'blue'. These events can be observed at approximately 13:45:30 and 13:48:30 in Figure 4.2.

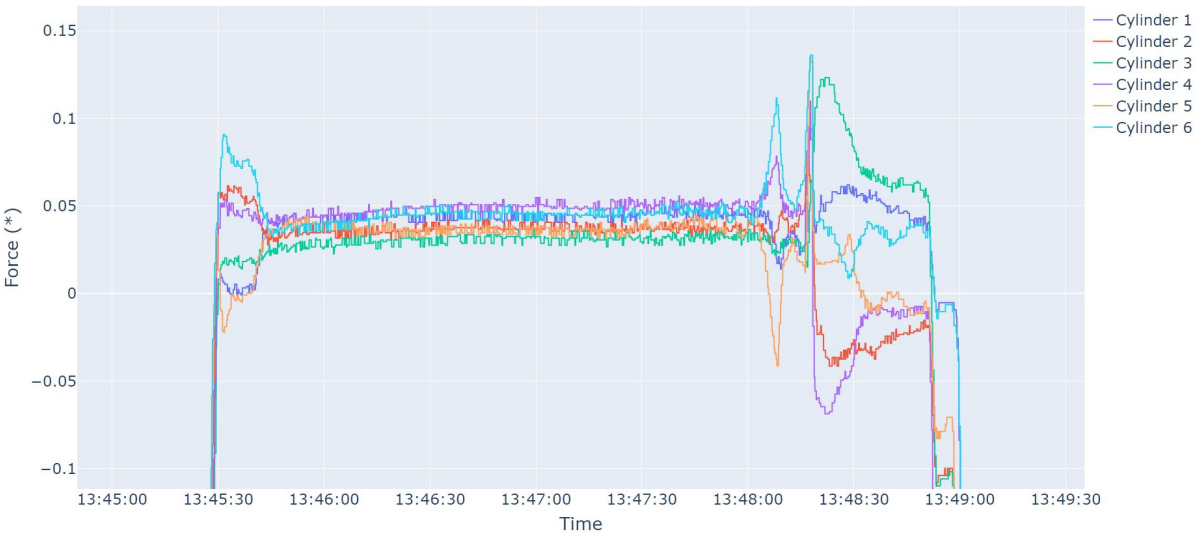

Figure 4.2: Normalised peak load in jacking cylinders due to jacking system.

Consequently, when the six oil pressures individually exhibit similar behaviour and are of comparable magnitude during a peak load, it can be concluded that it is impact. This is illustrated in Figure 4.3, where it can be observed that the oil pressure in all cylinders rapidly increases, followed by a release of forces, and subsequently, a sinusoidal variation in the oil pressure. Notably, the start of impact is denoted by a black dotted line in the figure. It is hypothesised that these force fluctuations are attributable to the wave loads on the leg, though this remains to be confirmed. Furthermore, the duration of impact is observed to be sufficiently long for stress waves to distribute along the leg, indicating that the stresses change over time.

Figure 4.3: Normalised peak load in jacking cylinders due to impact.

The magnitude of the maximum impact force can be determined by adding up all the six cylinders for each leg, as depicted in Figure 4.4. This figure presents the total force measured in the jacking frame of the Portside Fore (PSF) leg in 'blue', and the Starboard Aft (SBA) in 'red', with the leg heights of PSF and SBA shown in 'green' and 'orange', respectively. The obtained impact of PSF is measured to have a maximum force of around 1.0 (*), which is far below the maximum allowable axial loading. Moreover, the SBA leg is depicted for comparison of the oil pressure behaviour and to be able to draw conclusions. Since the oil pressure fluctuations after impact are similar across both legs, indicating that they are in

contact with the seabed, it can be inferred that these fluctuations result from wave loads. Moreover, during the jacking up process, as the vessel is progressively lifted out of the water, buoyancy decreases. This suggests that the opposing force to the impact force, attributed to the vessel's mass, gradually increases throughout the process. This trend is clearly visible towards the end of the simulation, where a significant increase in leg height indicates the vessel's emergence from the water. This observation directly clarifies why the sign of the force reverses over time.

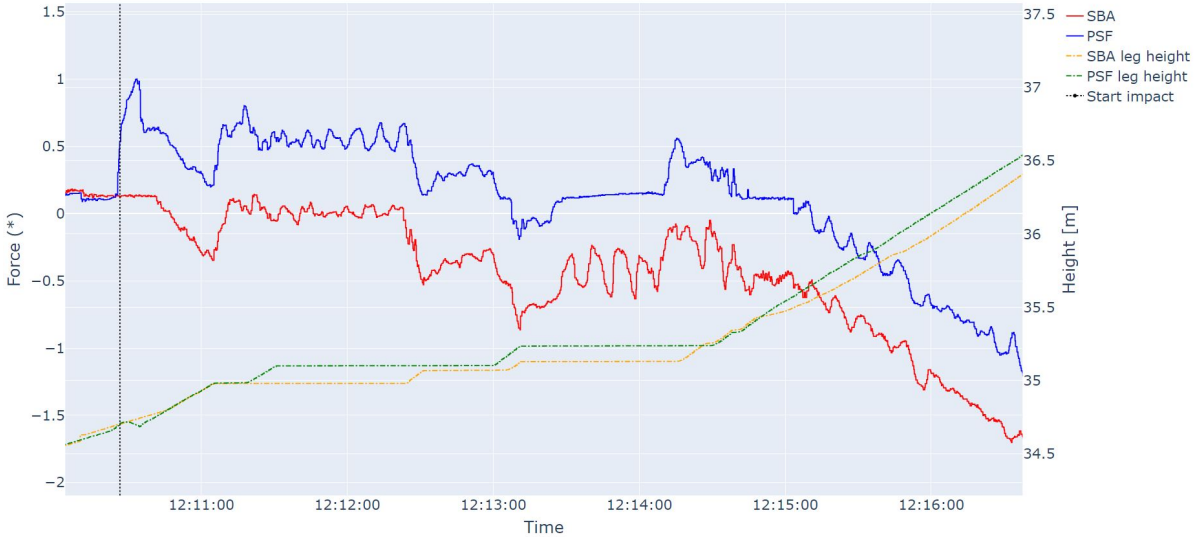

Figure 4.4: The normalised maximum force measured on a single jacking frame: Comparison of SBA (red) and PSF (blue), with corresponding leg heights for SBA (orange) and PSF (green).

4.3. Rod Model Comparison and Validation

To validate the developed model, it is essential to determine the initial velocity before impact. Therefore, the vessel's vertical velocity and the maximum force measured in the PSF leg are depicted in Figure 4.5. It can be inferred from the figure that the vertical velocity of the vessel was minimal prior to impact, indicating the presence of a low sea state. This is corroborated by site-specific buoy data, which reveals values of $H_s = 0.56$m and $T_p = 5.1$s [59]. It is important to note that the obtained velocity is measured at the location where the MRU is installed, meaning that it is not the initial velocity of the spudcan. Therefore, under the assumption that the vessel is one rigid body and no relative deformations occur, the velocity of the spudcan is calculated by the following formula [60]:

$$\dot{z}_s = \dot{z} - x_r \cdot \dot{\theta} + y_r \cdot \dot{\phi} \tag{4.1}$$

Here, $\dot{z}_s$ represents the vertical velocity of the spudcan, while x_r and y_r denote the relative distances from the MRU to the spudcan. Furthermore, $\dot{z}$ signifies the vertical velocity of the vessel, $\dot{\theta}$ the rotational pitch translation, and $\dot{\phi}$ the rotational roll translation, all of which are measured by the MRU.

The vessel's velocity prior to impact can be inferred from Figure 4.5 by the abrupt velocity change to zero and subsequent velocity reversal, indicating impact. This moment approximately coincides with the maximum oil peak, although a slight delay appears to be present. The moment at which the vessel's vertical velocity is measured as zero is denoted by a green dotted line. Given the vessel's size and mass, and the fact that these events are measured at two distinct locations, such delay is not unexpected. Specifically, there exists an inevitable time interval between the spudcan's moment of impact and when the effects of this impact become discernible in the vessel's motions. This delay refers to the necessary period for the system to respond to alterations in external forces and reach a new equilibrium or state of motion. However, this complicates defining the exact initial spudcan velocity just before impact using data from the MRU.

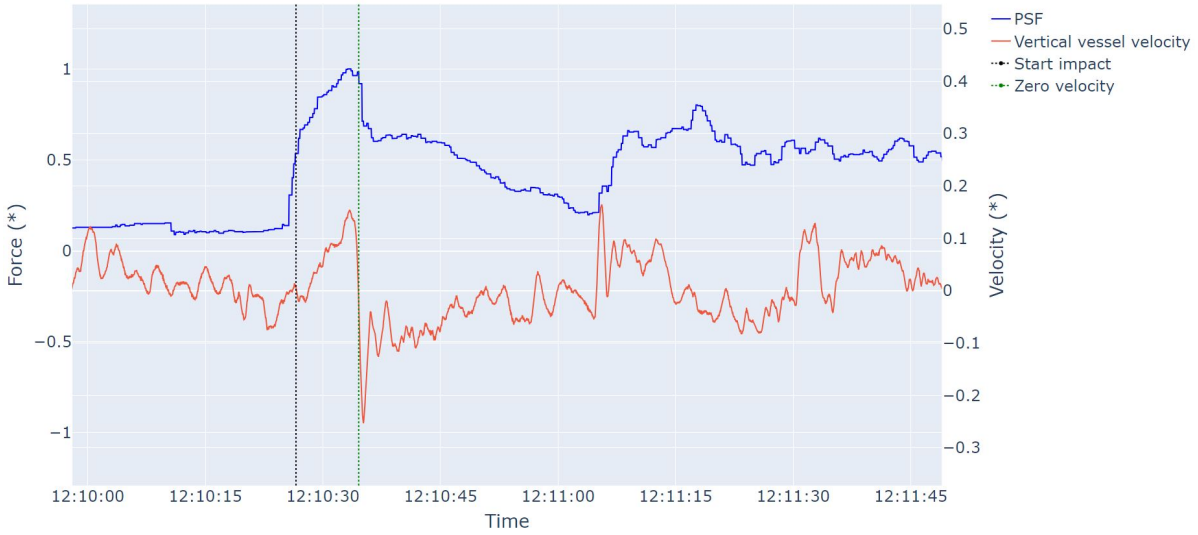

Figure 4.5: The normalised maximum force in the PSF leg and the normalised vertical vessel velocity measured by the MRU.

The vertical spudcan velocity, determined by Equation 4.1, is depicted in Figure 4.6. This figure features the black dotted line, signifying the start of impact, and the green dotted line, indicating the moment of zero vertical velocity. These are consistent with the same dotted lines presented in Figure 4.5. The figure indicates that the initial velocity prior to impact ranges between -1.0 (*) and 1.0 (*). However, determining the exact initial velocity of the spudcan from this graph is challenging. This difficulty is partly due to the delay between the spudcan's moment of impact and the motions measured by the MRU. Moreover, the rapid fluctuations in the graph compound this difficulty by obscuring the exact moment of impact. The spudcan's velocity, determined concurrent with the vessel's abrupt velocity shift, is approximately 0.5 (*). Additionally, the computation method used to calculate the spudcan velocity can introduce computational errors, as the entire structure is assumed to be one rigid body. For these reasons, is it decided to consider multiple initial velocities, including one that represents the maximum possible initial velocity. Crucially, these inferred initial velocities, ascertained from the vessel motions, should incorporate the single ring jacking velocity of 0.25 (*). This integration results in effective initial velocities of 1.25 (*) and 0.75 (*). The forces calculated by the developed rod model based on these effective initial velocities are presented in Figures 4.7 and 4.8.

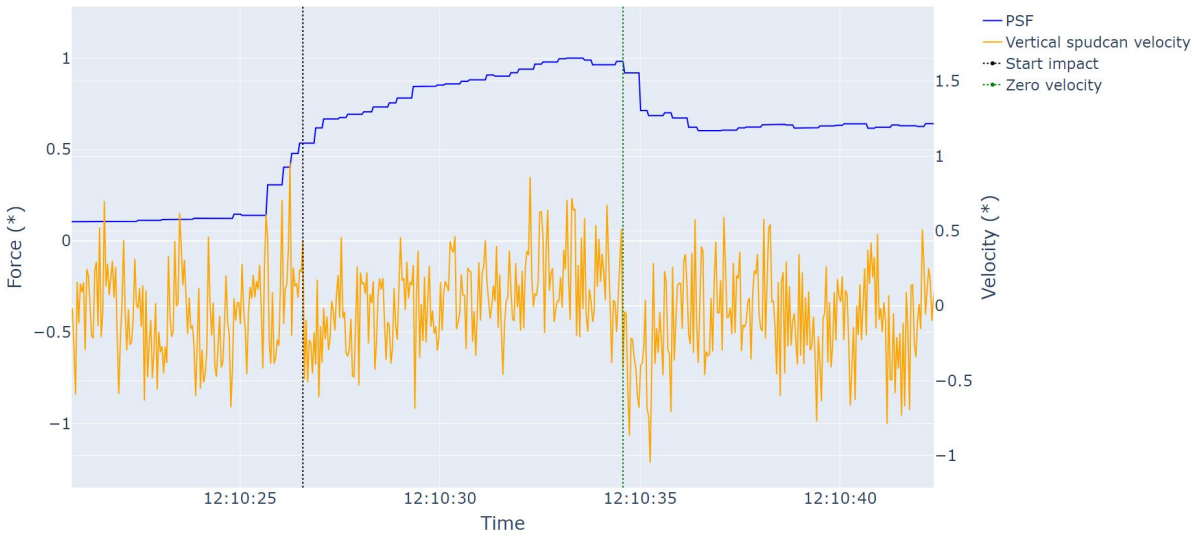

Figure 4.6: The normalised maximum force in the PSF leg and the normalised vertical spudcan velocity.

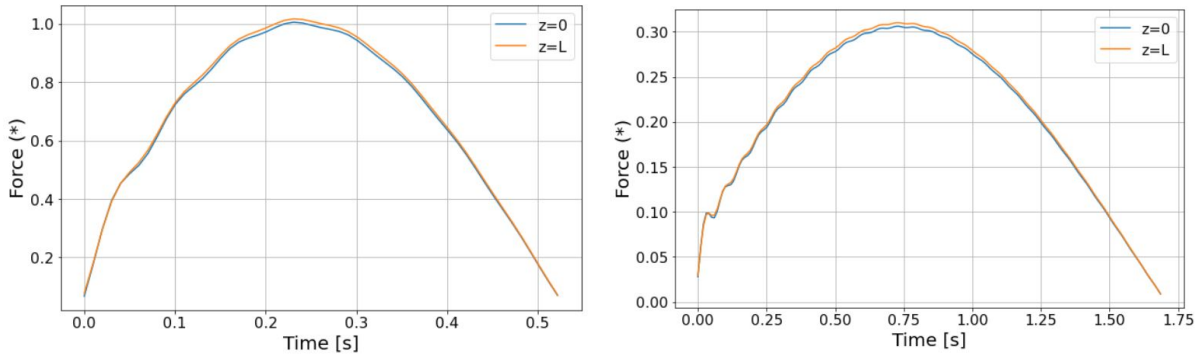

Figure 4.7: Normalised calculated force using rod model for $v_i = 1.25$ (*) without (a) and with (b) leg modification.

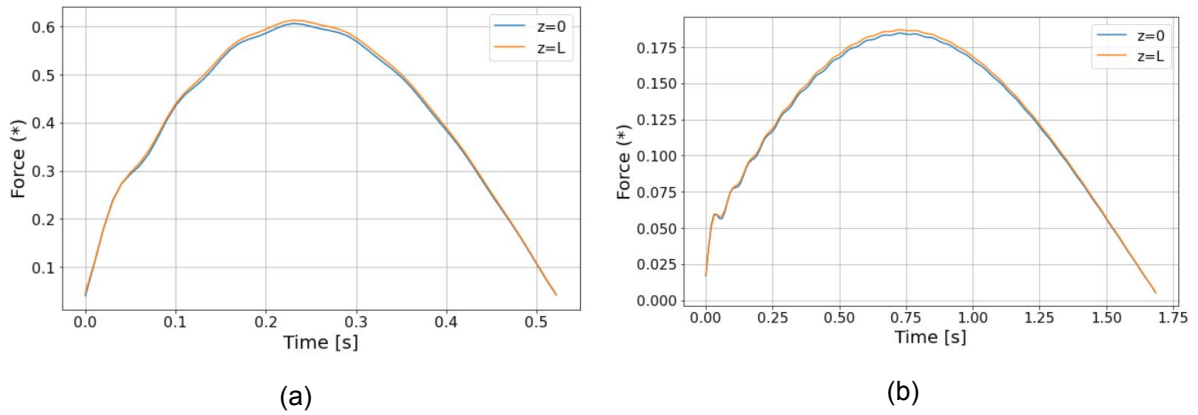

Figure 4.8: Normalised calculated force using rod model for $v_i = 0.75$ (*) without (a) and with (b) leg modification.

Figures 4.6 and 4.7 illustrate a close correspondence between the determined force without leg modification and the force measured from the data, both of which are approximately equal to 1.0 (*). However, there is a notable disparity between the determined impact duration by the model and the duration derived from the data. This discrepancy in impact duration is expected to influence the magnitude of the impact force, suggesting the presence of variations in the results. It is more plausible that a shorter impact duration under the same initial conditions results in a higher peak load. Which indicates that it would be more consistent with the obtained data if the determined forces by the model were estimated higher or the impact duration longer. Since this is not the case, it can be inferred that the determined force by the model is underestimated, different initial conditions are used, or this discrepancy is attributed to limitations within the model.

Considering the potential variability in initial conditions, the vessel mass and soil properties used in the model were estimated, given that the exact values at the specific jacking up location were unknown. This may have contributed to the observed differences in impact force. Moreover, a comparison of Figures 4.7 and 4.8 reveals that even minor differences in initial velocity can lead to significant variation in impact forces. This implies that a deviation in determining the initial conditions can result in considerable discrepancies.

Additionally, despite taking into account the initial underestimation of the impact force, the calculations that incorporate the leg modifications still appear to underestimate the impact force. Alternatively, the effect of the leg modifications may have been overestimated. Therefore, the established leg modification stiffnesses are re-evaluated, taking into account the nonlinear behaviour of the modifications. Notably, the data under consideration was collected during the period when the leg modifications were mounted, suggesting that the calculations incorporating these modifications should align more closely with the actual data.

The inclusion of the maximum and minimum stiffnesses of the modifications was initially conducted by excluding significantly high outliers for very small displacements. However, in this scenario, where the initial velocity is markedly low, it becomes crucial to accommodate these minimal displacements. Given the nonlinear behaviour of the modification, there is a likelihood of underestimating the stiffness at these low velocities. Therefore, the model calculations with leg modifications were re-executed, incorporating the assumption that smaller displacements occur at such velocities. This reconsideration leads to a significant increase in the stiffness of the modifications. The resulting forces using the rod model with leg modification, for both velocities, are illustrated in Figure 4.9.

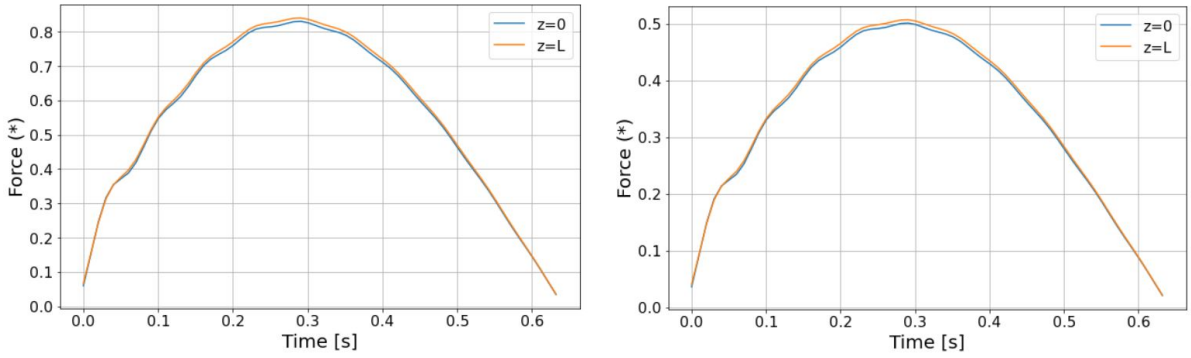

Figure 4.9: Normalised calculated force using rod model with leg modification for $v_i = 1.25$ (*) (a) and $v_i = 0.75$ (*) (b).

The figures underscore the necessity of accounting for minimal displacements at markedly low initial velocities, as this has a substantial influence on the calculated impact force. This revision of the stiffness of the leg modification elucidates that for small initial velocities, the model's estimate of the influence of the leg modification can deviate significantly from reality, due to its heightened sensitivity to these input parameters. Nevertheless, it should be noted that potential discrepancies between the model and actual scenarios may still exist. For instance, the model still seems to underestimate the impact force, despite having made conservative assumptions. This discrepancy could be attributed to the calculations not being performed with the exact vessel mass and soil conditions. Although these parameters were thought to be chosen conservatively, the model's underestimation could also be due to omission of any prevailing nonlinear behaviour of the system, in addition to other limitations of the model.

As previously mentioned, the impact duration determined by the model does not align with the measured data, a discrepancy that could be attributed to various factors or limitations within the model. One such factor could be the exclusion of waves and their associated wave periods, which may extend the impact interval due to vessel motions. Additionally, the actual soil stiffness could be lower than the value used in the model, which would explain the longer measured impact duration. However, this is in contradiction with the model's already underestimated impact force. Underestimation of the initial velocity is another possible factor, although the results suggest that this has a minor effect on the impact duration. Further inconsistencies could arise from potential inaccuracies in assumptions or calculations regarding the leg modifications, which appear to significantly affect the impact duration. The model's inability to account for the nonlinear behaviour of the modifications likely contributes to these issues. Moreover, the model's simplification of the vessel's mass as a point mass deviates from reality, and variations in the actual vessel mass could exert further influence. Finally, inherent model limitations, potentially from oversimplifications or numerical errors, could also contribute to the differences in impact duration.

4.4. Concluding Remarks

This chapter detailed the validation process of the developed rod model, using data collected from the Aeolus provided by Van Oord. The key stages in this process, including data collection, impact identification, and model validation, were discussed in detail.

From the data analysed, one location was of particular interest due to the presence of unweathered

bedrock and an improved signal quality. These attributes made it the most suitable location for identifying impact and validating the developed rod model. The data set incorporated leg modifications, oil pressures in the vertical cylinders of the jacking system, vessel motions from the MRU, and the leg height. Distinguishing between oil pressure peaks caused by the jacking system and those due to impact was key to identifying impact. This differentiation was based on two criteria: a substantial change in the vessel's motions, and similarity in behaviour and magnitude of the six oil pressures during a peak load.

The rod model's validation was executed through a comparison between model predictions and real-world measurements. An essential and challenging aspect was ascertaining the initial spudcan velocity from MRU measurements, partly due to an observed delay between the spudcan's moment of impact and the vessel motions measured. Therefore, two different initial velocities were compared, which revealed an underestimation of the impact force by the model, despite conservative assumptions. Additionally, minor alterations in initial velocity led to significant differences in calculated impact force, which easily creates potential discrepancies with reality. Moreover, the calculated impact duration diverged from measurements, which can be attributed to the exclusions of waves and related wave periods, model limitations, variations in vessel mass and soil properties, and difficulties in incorporating nonlinear behaviour associated with the leg modifications.

Considering the nonlinear behaviour of the leg modification, there is a likelihood of underestimating the stiffness at low initial spudcan velocities. Given the notably low initial velocity in the obtained scenario, it is crucial to account for minimal leg modification displacements, as they significantly influence the calculated impact force. The model's sensitivity to these parameters can lead to significant deviations from reality in estimates of the leg modification's influence at low velocities. These conclusions, based on a single jacking location, should be solidified with data from additional locations, when available. Moreover, future research could benefit from incorporating the nonlinearity of the leg modification into the model.

5

Sensitivity Study

In order to answer the research question, a sensitivity study is performed to analyse the influence of the identified factors on the governing forces. This analysis entails adjusting the variables and assessing their impact on the forces in the jack-up leg. Subsequently, the specific leg modification is incorporated into the model, and the sensitivity study is repeated for two differently defined stiffnesses. By comparing the results of this study with the previous one, the influence of the leg modification on the governing forces and its overall performance can be assessed. Firstly, Section 5.1 outlines the methodology of a local sensitivity analysis and establishes the range of the considered variables, followed by the conduction of the analysis and a discussion of its results. In Section 5.2, the methodology for the global sensitivity analysis is detailed, the results are subsequently discussed, and some concluding remarks are presented.

5.1. One-at-a-Time Sensitivity Analysis

The One-at-a-Time sensitivity analysis (OAT), also known as local sensitivity analysis, is a common approach that is used to investigate the effect of individual input parameters on the output of the model. It is performed by choosing a baseline for the input variables, and then changing one variable at each time while keeping the other variables constant [61]. This analysis is executed to have a first approximation of the influence of the identified factors on the governing forces.

The baseline for the input variables is specified in Section 3.3. The ranges for adjusting these variables, as detailed in Table 5.1, have been carefully selected. The ranges for the vessel's properties, specifically the vessel mass and leg length, extend beyond the minimum and maximum values [62]. This approach not only ensures comprehensive coverage, but also provides insights into the potential influence of these properties related to considering a different vessel. The normal stiffness of the seabed, derived from geotechnical site survey data, is selected between the stiffest measured value and a significantly lower value, which still classifies as a stiff seabed [38]. The initial velocity range is based on velocities used in evaluating the translational damping of the leg modifications [14]. Lower velocities are excluded, as Chapter 4 elucidated that the influence of leg modifications at these velocities can significantly deviate from reality. This discrepancy arises from the nonlinear behaviour of the modifications and the specific maximum and minimum equivalent spring stiffnesses defined for the analyses. The damping ratio is established in line with the modelled system's expected oscillatory behaviour.

Table 5.1: The ranges of variables used in the sensitivity analysis.

Parameter	Symbol	Value range	Unit
Mass vessel	M_v	$0.57 - 1$	[(*)]
Submerged leg length	L	$20 - 50$	[m]
Initial velocity	v_i	$0.3 - 1.0$	[m/s]
Seabed normal stiffness	k_s	$0.3 - 1$	[(*)]
Damping ratio	ξ_s	$0.1 - 0.2$	[–]

The analysis started by generating a model output using all baseline values. Then the analysis continued by varying a single parameter while keeping the others at their baseline values. Once the variation was assessed, the parameter was returned to its nominal value, and the process was iteratively repeated for all other parameters. The primary outputs of interest from the model are the calculated impact force and the impact duration. The sensitivity to these outputs is quantified by determining the percentage change from the initial analysis conducted with only baseline values.

The initial analysis is performed under three conditions: without leg modification, with leg modification at minimum equivalent stiffness (k_{eq} min), and at maximum equivalent stiffness (k_{eq} max). Subsequently, each analysis performed within the defined variable range was individually compared with the initial analysis of the corresponding condition, a process referred to as the 'OAT analysis for individual comparison'. Furthermore, all analyses were compared with the initial analysis performed without leg modification, denoted as the 'OAT analysis for global comparison'. The 'OAT analysis for individual comparison' offers insight into the influence of individual variables on the condition under observation, while the 'OAT analysis for global comparison' properly reflects the effect of the leg modifications on the impact force. Both are relevant to this study and are presented in Appendix C.

5.1.1. Results and Discussion

The conducted sensitivity analysis indicates that the vessel mass, initial velocity, and normal soil stiffness have the most significant influence on the impact force. It should be noted, however, that the range of variables under observation also influences the interval of force change. Notably, the variation of the vessel mass and initial velocity on the impact force shows a linear relation, while a slight nonlinearity can be observed in the change of the soil stiffness . The affect of the vessel mass and initial velocity on the impact force is similar across all conditions. Interestingly, the variability in soil stiffness has less influence on the conditions with leg modifications, which is partly due to the significant reduction in the overall impact force through these modifications. To illustrate, the graphs of the soil stiffness variation from the 'OAT analysis for individual comparison' are depicted in Figure 5.1.

Furthermore, the leg length exerts a relatively minor influence on the total impact force, of which the variance can primarily attributed to the structural damping within the material. For the condition without modification, the influence of the leg length is linear, while for conditions with modifications, it becomes nonlinear and exerts even less influence on the overall impact force. Additionally, the damping ratio also has relative little influence on the impact force and the effect on the different conditions is comparable.

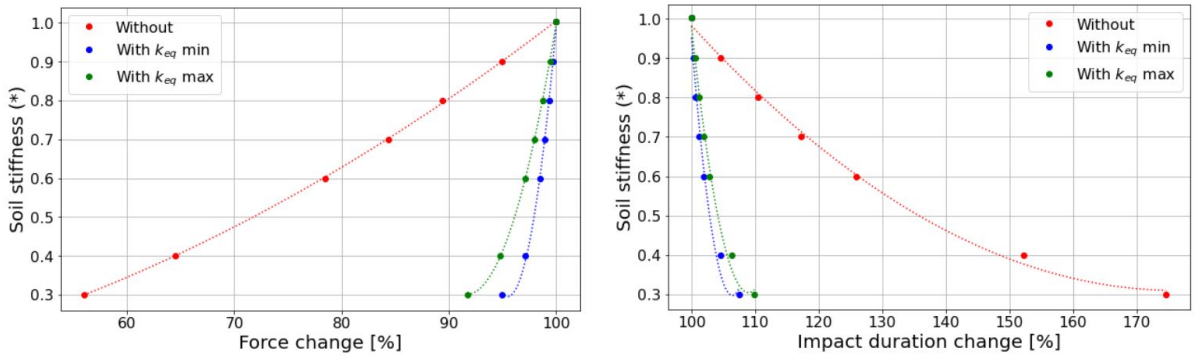

Figure 5.1: Change in impact force (a) and impact duration (b) resulting from soil normal stiffness variation: An OAT analysis for individual comparison.

The plots for the soil stiffness in Figure 5.1 and the leg length accurately depict the relationship between the impact force and impact duration. As the impact duration increases, the total impact force decreases, and vice versa. Furthermore, the vessel mass and damping ratio have similar influence on the impact duration as the impact force, given that the percentage ranges on both output variables are similar. Importantly, the initial velocity does not influence the impact duration, while the soil stiffness significantly affects it. In conclusion, the impact duration mainly depends on the overall stiffness of the

system, which in this scenario primarily arises from the soil stiffness, but also significantly from the axial stiffness of the leg.

The overall performance of the leg modification is primarily derived from the 'OAT analysis for global comparison'. These plots suggest that the inclusion of leg modifications results in an approximate 70-75% reduction of the impact force. Although it may be debated whether this exact percentage holds in reality, it undeniably signals a significant reduction in the impact force. Furthermore, the analysis concludes that the impact duration increases by 320-370% with the inclusion of leg modifications. These percentages are consistently reflected across all plots presented in Appendix C. The graphs that depict the soil stiffness variation from the 'OAT analysis for global comparison' are displayed in Figure 5.2.

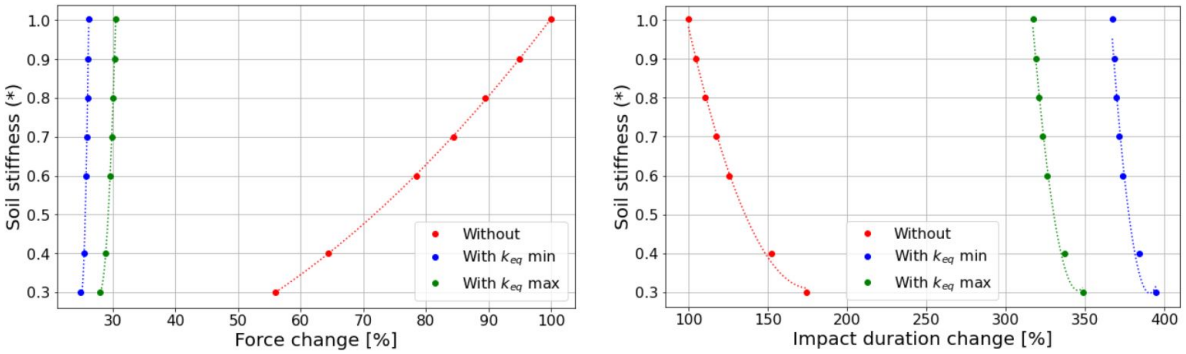

(a) (b)

Figure 5.2: Change in impact force (a) and impact duration (b) resulting from soil normal stiffness variation: An OAT analysis for global comparison.

The OAT analysis provides a first approximation of the influence of the identified factors on the governing forces and the performance of the leg modifications. However, its limitations include the inability to reveal interactions between input parameters [61]. Therefore, a global sensitivity analysis is conducted in the next section to provide a more detailed and complete picture of the importance of different input parameters and their interactions [63].

5.2. Global Sensitivity Analysis

Global Sensitivity Analysis is a quantitative technique employed to ascertain the influence of input parameters variation on a model's output. In contrast to the OAT sensitivity analysis, this method identifies the most impactful parameters on the model's output by varying all selected variables across their complete range through repeated sampling. This approach provides a more comprehensive analysis, including interaction effects, but is computationally more intensive. A widely used method for global sensitivity analysis is the Sobol method, as incorporated in the Python library, SALib, employed in this study [63, 64].

The Sobol sensitivity analysis is a variance-based sensitivity analysis that evaluates both the individual and interactive effects of input parameters. This is achieved through variance decomposition, yielding three sensitivity indices: the first-order (S1), total-order (ST), and second-order sensitivity index (S2). The computation of these indices involves evaluating the model over a Sobol sequence, a quasi-random sequence that uniformly samples the parameter space [65].

The first-order sensitivity index (S1) quantifies the influence of an input parameter on the output variance, assuming all other parameters are kept constant. Contrary to the OAT analysis, which provides insight based on local changes around a fixed baseline, the S1 index offers a global perspective by decomposing the total output variance across the entire parameter space. Here, an S1 value of 1 indicates a significant impact of the specific parameter on the model's output, while a value near 0 suggests minimal influence [61, 65].

The total-order sensitivity index (ST) measures the influence of a parameter on the output variance, accounting for both its individual and interactive effects. An ST value close to 1 signifies that the

parameter and its interactions have a substantial effect on the model's output, while a value close to 0 indicates minimal influence. The second-order sensitivity index (S2), provides insight into the interactive effects of pairs of parameters, capturing the outcome of their simultaneous variation. The S2 index is valuable in identifying non-additive interactions between parameters [61, 65].

The Sobol sensitivity analysis, while being more computationally intensive than the OAT method, provides a more comprehensive understanding of the effects and interactions of model parameters. It is particularly useful when necessary to deal with nonlinear models [63]. Moreover, the addition of more variables not only increases the computational demand but also tends to reduce the accuracy of the results. To mitigate this, the global sensitivity analysis is performed for three different sets of variables, depicted in Appendix C.2.

Specifically, 'Analysis 1: Most Influential Parameters' (Appendix C.2.1) includes the variables that according to the OAT analysis have the most significant influence on the impact force: the vessel mass, the initial velocity, and the normal soil stiffness. 'Analysis 2: Parameters with the Most Uncertainty' (Appendix C.2.2) encompasses the initial velocity and the variables associated with the highest uncertainty, such as the normal soil stiffness and damping ratio. Finally, 'Analysis 3: Vessel-Related Parameters' (Appendix C.2.3) considers the initial velocity and the variables pertaining to the vessel's properties and the site-specific conditions, including the vessel mass and leg length. This analysis elucidates the potential influence of these vessel-related variables, offering valuable insights for considerations of different vessel usage.

5.2.1. Results and Discussion

The results of the global sensitivity analysis are presented in Appendix C.2. Generally, the S1 and ST sensitivity indices yield higher values than the S2 sensitivity index. This implies that variables exert more influence individually than in pairs simultaneously. However, such information can be utilised to evaluate the model's performance and its ability to produce logical results. The results of the S1 and ST sensitivity analysis for the impact force and impact duration, as derived from Analysis 1, considering both conditions without and with leg modification at maximum k_{eq}, are depicted in Figures 5.3 and 5.4, respectively.

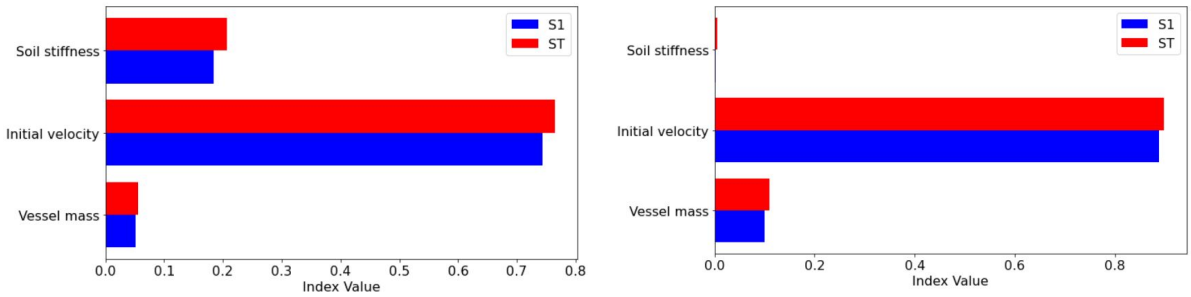

Figure 5.3: S1 and ST Sobol sensitivity analysis 1: Impact force without (a) and with (b) leg modification at maximum k_{eq}.

What can be observed is that the impact force significantly depends on the initial velocity, which is not entirely unexpected, given that the initial velocity directly influences the system's energy just before impact. However, the considerable disparity with the other two variables is noteworthy and can be attributed to the fact that the kinetic energy is proportional to the velocity squared. Another notable observation is that the introduction of the leg modification substantially diminishes the influence of the soil stiffness. Conversely, the relative influence of the vessel mass and initial velocity on the impact force slightly increases by the implementation of the leg modification.

Compared to the other two global analyses, it also becomes clear that the initial velocity substantially influences the impact force. Moreover, the analysis indicates that the inclusion of the leg modification reduces the influence of the soil stiffness. While the vessel's mass exerts a noticeable influence, its relative change remains minor upon introduction of the leg modification. As previously concluded, the

overall impact of the damping ratio and leg length is minimal.

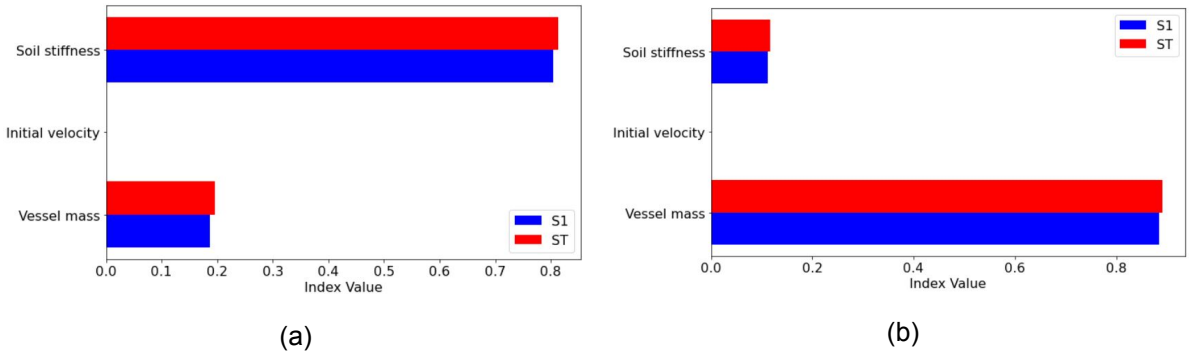

Figure 5.4: S1 and ST Sobol sensitivity analysis 1: Impact duration without (a) and with (b) leg modification at maximum k_{eq}.

When examining the impact duration, it is notable that the influence of vessel mass and soil stiffness are significantly different in the conditions with and without leg modification. The soil stiffness is of great influence for the condition without modification, and significantly less for the condition with modification, while for the vessel mass this is exactly the opposite. Again the impact duration mainly depends on the overall stiffness of the system, whereas in reducing this by the modification, the vessel mass becomes relatively more important. Additionally, the initial velocity appears to exert no influence on the impact duration in either condition.

Compared to the other two global analyses, it also becomes apparent that the soil stiffness holds the most substantial influence on the impact duration. When the influence of the soil stiffness reduces due to the introduction of the leg modification or remains constant, the vessel mass primarily affects the impact duration. Additionally, the damping ratio gains more influence upon introducing the leg modification, which is not surprising given its relation with the equivalent stiffness and the system's oscillatory behaviour. Similarly, the initial velocity has no effect on the impact duration, and the influence of the leg length is minimal.

5.3. Concluding Remarks

The sensitivity study conducted to assess the influence of the identified factors on the governing forces on a jack-up leg yielded significant insights. The analysis exposed that the most critical factors influencing the impact force were the vessel mass, initial velocity, and normal soil stiffness. Variations in these factors had linear or slight nonlinear effects on the impact force. The leg length and damping ratio, however, had less influence on the impact force.

Interestingly, introducing the specific leg modification into the system changed the influence of the variables on the impact force and duration. The modifications significantly reduced the affect of soil stiffness variability on the system, contributing to a significant reduction of the overall impact force. Notably, the introduction of leg modifications resulted in a 70-75% reduction in the impact force, signaling the significant performance of the leg modifications. Concurrently, the analysis marked a substantial increase in the impact duration by 320-370% following these modifications. Additionally, the impact force and duration are interconnected rather than separate occurrences: a shorter impact duration leads to higher peak loads, while a longer impact duration results in a lower peak load. This relationship illustrates that the reduction in impact force and the increase in duration are not entirely independent phenomena.

The global sensitivity analysis further emphasised these results, demonstrating that individual variables often exert a stronger influence than simultaneous variation of variable pairs. It specifically highlighted the strong dependence of the impact force on the initial velocity. Furthermore, the analysis underscored the effect of the leg modification on the impact force, indicating a substantial decrease in the influence of the soil stiffness, while slightly amplifying the relative effect of vessel mass and initial velocity on the impact force. Additionally, by introducing the leg modification and thereby decreasing the overall stiffness of the system, the duration of impact increases, resulting in a consequent reduction of the impact force.

In conclusion, the study provides a deeper understanding of how specific factors influence the governing forces in a jack-up leg and evaluates the performance of a specific leg modification. It highlights the significant role of the vessel mass, initial velocity, and soil stiffness in determining the impact force and the essential performance of leg modifications.

6

Discussion

This chapter discusses the results and provides an in-depth interpretation of the findings in the context of the overall study. The objective of this research was to identify and elucidate the main physical phenomena that govern the forces in jack-up legs during installation on a stiff seabed. It further aimed to understand the influence of these physical factors on the governing forces and how a specific leg modification could influence them. This objective has led to the following research question:

What governs the forces in jack-up legs during installation on stiff seabed, and what influence do specific leg modifications have?

This research followed a systematic approach to answer this research question, incorporating a literature study on impact mechanics, model development for axial impact forces, model validation, a sensitivity study, and an analysis of the leg modification.

6.1. Factors that Govern the Forces in Jack-up Legs during Installation on Stiff Seabed

The key findings suggest that what governs the forces in jack-up legs during installation on a stiff seabed depends on the energy contained within the system prior to impact and how this energy is absorbed by the soil and structure. The primary drivers of the impact forces are the wave-induced vessel motions that lead to horizontal and vertical spudcan velocities, which generate axial and lateral forces in the leg. The factors that contribute to the amount of energy contained in the system include the wave height, wave period, hull characteristics, vessel's inertia, jacking velocity, and the leg length below the hull, which is determined by the water depth.

Additionally, the energy absorbed by the soil and structure depends on their stiffness characteristics and behaviour. This insight led to the conclusion that it is relevant to obtain the stress waves within the leg and the small elastic deformations of the soil, assuming that no plastic deformations occur. This simplified the complex soil-structure interaction process, which is not extensively covered in existing standards, and allowed the soil behaviour to be modeled as a spring-damper system. Furthermore, it was concluded that the minimal soil-penetration depth results in a small contact area, yielding a smaller lateral resistance and thus a diminished horizontal force. This led to the primary conclusion that axial forces dominate over lateral forces during impacts. Based on these insights, the simplification of the system to a one-dimensional model was justified, as this approach yields the largest impact forces instead of distributing the energy over multiple DOF. Therefore, a one-dimensional rod model was developed to consider the governing forces in a jack-up leg during installation on a stiff seabed.

However, this study makes the assumption that the seabed comprises a uniform soil layer with perfectly horizontal bathymetry. This implies that the lateral forces depend on the soil-spudcan contact area and the corresponding lateral resistance. It is important to note that this assumption may not always hold true in reality, especially in cases of stiff or rocky seabeds where protruding rocks can be expected. Such conditions could result in side impacts on the jack-up legs, potentially causing significant bending

moments on the lower guide of the jacking system. Moreover, the risk is amplified when the jack-up vessel operates in deeper water, as the longer force arm magnifies the influence of the lateral forces, whether they arise from lateral resistances or side impacts on the jack-up legs. In conclusion, it is of importance to take into account the potential for lateral forces when operating in deeper water depths or in areas where seabed protrusions are anticipated.

Building upon the discussion of lateral forces, it is important to remember the environmental loads that the jack-up vessel is subjected to. Drawn from previous literature, it has been established that wave loads primarily induce vessel motions, while wind and current loads mainly cause the vessel drift. This drift is counteracted by the DP system, maintaining the vessel's position effectively. However, when incorporating lateral forces into the analysis, it becomes advisable to consider the effect of current loads on the jack-up leg, especially in the presence of severe currents. Although it is anticipated that the lateral forces from impacts are predominant, the influence of currents on the overall lateral forces and potential corresponding deflections should not be instantly neglected. Including these wind and current loads into the analysis contributes to a more realistic representation, however, introduces additional computational demand and complexity. Therefore, an engineering assessment on balance between desired accuracy and computational effort must be made.

Additionally, soil load-deformation behaviour is inherently nonlinear, which is excluded by the assumption that only small elastic deformations occur. This assumption is justified by the high bearing capacity of stiff seabeds. Although, this may not be entirely aligned with reality, it can still provide a sufficient estimate of the soil behaviour leading to the highest forces in the jack-up legs. This has been confirmed by previous research indicating that simplified linear methodologies can yield conservative yet reasonable results, particularly when considering stiff seabeds. Moreover, employing a conservative approach can be an informed decision when using impact forces to determine the operational limits. However, for a more realistic approach, despite the increase in computational demand and complexity, it would be necessary to incorporate the nonlinear characteristics of the soil.

Furthermore, insights from previous research suggest that the beam and rod theory provides reliable estimates on the leg's structural capacity, making it a suitable choice for a simplified representation of a jack-up leg. However, previous studies mostly use FE models to perform the structural analysis, as these models are able to capture any nonlinearities and more complex geometries. For instance, these models can accommodate the holes in the legs where the jacking frames are locked into. Although, using FE models is beneficial, it does increase the computational demand and complexity of the calculations. Therefore, the choice of method should be considered based on the desired level of complexity and accuracy required for the analysis.

Importantly, when applying existing methodologies, it is essential to be well-acquainted with the assumptions made and to consider the method most appropriate for the problem being analysed. A common employed method in the industry for determining the impact force is the classical DNV approach. This approach restricts the analysis by ignoring the contribution of heave, assumes that the seabed is indefinitely rigid, and that all energy prior to impact is absorbed by one single leg. However, both the heave direction and soil behaviour have been identified as significant factors when determining the impact force during installation on a stiff seabed. Recognising these insights, an enhanced method known as the 'improved energy method' has been developed by the JIP. Furthermore, when the inclusion of plastic deformations and nonlinear properties is necessary, previous research recommends employing advanced software or numerical solutions.

6.2. Influence of Identified Factors on the Governing Forces

The influence of the identified factors on the governing forces was analysed through a sensitivity study. The sensitivity study was conducted using the developed rod model, which had been validated using data from the Aeolus collected by Van Oord. The key stages of this process included data collection, impact identification, and model validation. Despite conservative assumptions, it was found that the model underestimated the forces. Additionally, minor alterations in initial velocity resulted in significant differences in the calculated impact force, leading to potential discrepancies with reality. Furthermore, the calculated impact duration diverged from the measured values. This divergence can be attributed to the exclusions of waves and related wave periods, model limitations, variations in vessel mass and soil

properties, and difficulties in incorporating nonlinear behaviour associated with the leg modifications. These conclusions, while drawn from a single jacking location, should be further validated with data from additional jacking up locations as they become available.

Upon focusing on the model's limitations, it is noteworthy that several simplifications were made. Firstly, the vessel's weight is represented as a point mass, effectively excluding its moment of inertia. Essentially, the wave-induced vessel motions can not be accurately captured by considering only an initial velocity. During impact, the vessel continues to be subjected to waves, potentially influencing both the impact force and duration. Similarly, the spudcan is simplified to a point mass in the model, despite its specific geometry that could affect the soil-spudcan interaction and the angle of impact.

Secondly, the presence of water is not accounted for in the model, which may contribute to the system's damping. However, it is anticipated that the influence of water is less significant then that of material damping, and its inclusion would add to the model's complexity and computational demands. Furthermore, the leg-hull connection is assumed to be rigid, while in reality it is a complex interaction mechanism influenced by the relative stiffness of the components and the leg-hull clearance. Although the leg-hull connection can be modelled more realistically, it may not necessarily yield higher impact forces, which is important for this study. A detailed evaluation of the load distribution on the jacking pins could be performed using a nonlinear FE model, as suggested by previous research.

Additionally, it is assumed that impact only occurs on one leg at a time and that no plastic deformations occur. These are considered reasonable; the first assumption yields the highest impact forces, and the second supports the vessel's durability across numerous jacking operations. Despite the assumption of uniformity, minor variations in axial stiffness exist along the leg length in reality. Although their influence on the impact force is assumed negligible, these variations can be incorporated by refining the discretised numerical model for a more accurate representation. It even holds potential to simulate various lateral forces along the leg length when desired to expand to a beam model, effectively accounting for the system's nonuniform properties. However, the model is unable to include any nonlinearities unless it is solved in the time domain. Despite this, it can generate a final solution without iterations, incorporating all contributions from external excitation, nonzero initial conditions, and inhomogeneous boundary conditions.

Importantly, the sensitivity analysis performed identified the vessel mass, initial velocity, and normal soil stiffness as the most influential factors on the impact force. It also highlights that the impact force and duration, the key outputs, are interconnected rather than separate occurrences: shorter impact durations lead to higher peak loads, while longer durations result in lower peak loads. Furthermore, the initial velocity predominantly influences the impact force, whereas the overall system stiffness, particularly the normal soil stiffness in the absence of the leg modifications, dictates the impact duration. Consequently, the sea state present primarily determines the magnitude of the impact force. The overall stiffness of the system can either shorten the impact duration and increase the force or lengthen the duration and reduce the force. Therefore, in the absence of considering the leg modifications, the sea state present and the soil stiffness predominantly influence the impact force. The vessel mass has relatively minor but noticeable influence on the overall impact force, which suggests that changes in vessel mass during jacking operation do not represent the most significant factor. Moreover, the damping ratio and the leg length were not identified as highly influential factors. However, if the lateral forces were taken into account, it is expected that the leg length could greatly influence the results by amplifying the force arm and generating high bending moments.

6.3. Performance of Specific Leg Modification

The specific leg modification is incorporated into the model to assess its performance. Despite the model's inability to capture its nonlinear characteristics, the modification is incorporated by a maximum and minimum equivalent stiffness. This approach acknowledges potential deviations from reality, but still allows for an assessment of the leg modification's overall performance. The obtained data revealed that for small initial velocities the model's estimate of the influence of the leg modification can further deviate from reality. As a result, these smaller velocities were excluded from the sensitivity study. Additionally, this might highlight the necessity of considering the nonlinear behaviour of the leg modifications for more realistic results. However, it is anticipated that when concerning higher impact forces,

the nonlinearity becomes less important. Notably, the performance of the specific leg modifications might decrease at extremely high and low initial velocities. In conclusion, to account for the nonlinear behaviour of the leg modification, the model must be solved in the time domain.

The sensitivity analysis conducted indicated that the system's overall stiffness influences the impact duration, and consequently, the impact force. Incorporating the leg modification leads to a lower overall stiffness, an increased impact duration, and thereby a decreased impact force. Specifically, an increase in impact duration of approximately 320-370% and a reduction in impact force of approximately 70-75%. Although it may be debated whether these exact percentages hold in reality, they undeniably signal a significant reduction in the impact force and provide an approximate indication of the leg modification's performance. Additionally, the inclusion of the leg modification significantly reduced the influence of the soil stiffness, making the vessel mass and damping ratio relatively more important.

From a broader perspective, implementing the leg modifications on the jack-up vessel not only reduces the overall impact forces but also mitigates the sensitivity to soil stiffness variability. This reduction in sensitivity enhances the operational versatility of the vessel, enabling it to operate in a wider range of soil conditions. Moreover, the modifications can expand the operational limits, and thereby potentially prevent any installation delays. Especially in scenarios where the operational advantages of using the specific leg modifications outweigh the potential costs of delays, they can prove to be a convenient and efficient solution. However, it is important to recognize that a comprehensive evaluation of the leg modifications would need to consider their limitations and the logistical complications associated with their installation and disassembly.

7

Conclusions

This chapter presents conclusions derived from the results and discussions of previous chapters. Additionally, it provides recommendations for future research in Section 7.1, which are based on the identified limitations of the current study and emerging questions that warrant additional investigation. The objective of this research was to identify the main physical phenomena that govern the forces in jack-up legs during installation on a stiff seabed, and to understand how these physical factors and a specific leg modification could influence them.

The key findings suggest that the governing forces mainly depend on the energy contained within the system prior to impact and how this energy is absorbed by the soil and structure. The primary drivers of the impact forces are the wave-induced vessel motions that lead to horizontal and vertical spudcan velocities, which generate axial and lateral forces in the leg. The factors that contribute to the amount of energy contained in the system include the wave height, wave period, hull characteristics, vessel's inertia, jacking velocity, and the leg length below the hull, which is determined by the water depth.

Additionally, the energy absorbed by the soil and structure depends on their stiffness characteristics and behaviour. This led to the primary conclusion that axial forces dominate over lateral forces during impacts on a stiff seabed. However, a uniform seabed with a perfectly horizontal bathymetry is assumed, which not always hold in true in reality. Protruding rocks may be expected which results in side impacts, potentially causing significant bending moments on the lower guide of the jacking system. Therefore, it is of importance to include the lateral forces when operating in deeper water depths or in areas where seabed protrusions are anticipated.

The sensitivity study indicated that the vessel mass, initial velocity, and normal soil stiffness significantly influence the impact force. Despite the simplifications, it was established that the initial velocity predominantly influences the impact force, whereas the overall system stiffness dictates the impact duration. The specific leg modification reduces the overall stiffness of the system, and thereby increases the impact duration. As a result, the impact force was reduced by approximately 70-75%, simultaneously with an increased impact duration of 320-370%. Moreover, it was found that the impact force and duration are interconnected rather than separate occurrences. Furthermore, the inclusion of the leg modification reduces the influence of soil stiffness variability. While the vessel mass has relatively minor influence, the damping ratio and leg length exert even less influence on the overall impact force. However, if the lateral forces were taken into account, it is expected that the leg length could greatly influence the results by amplifying the force arm and generating high bending moments.

The model developed in this study did not take into account the nonlinear behaviour of soil load-deformation and leg modification characteristics. Despite this simplification, literature suggests that the model can still provide a sufficient estimate of the stiff soil behaviour. However, a more realistic representation involves incorporating these nonlinear characteristics, which inevitably elevates the computational demand and complexity. When the inclusion of nonlinear properties becomes necessary, previous research recommends utilising advanced software or numerical solutions. Consequently, it

is crucial to perform an engineering assessment to balance desired accuracy against computational demand.

7.1. Recommendations

This section provides recommendations for future research, based on findings and limitations identified in this study. These recommendations are intended to guide the direction of subsequent research and to maximise the scientific and practical contributions of such investigations.

- Incorporation of nonlinear characteristics of the soil: While this study assumed only small elastic deformations, future research could consider the nonlinear characteristics of the soil for a more realistic estimation of the forces.
- Consideration of potential seabed protrusions: This study is based on the assumption of a perfectly horizontal seabed bathymetry. However, the potential existence of protrusions on the seabed, which might prevent perfect axial impacts, could be taken into account in future research.
- Incorporation of lateral forces: This study concluded that the axial forces dominate over lateral forces during impacts on a stiff seabed. However, in the context of deeper water operations or the potential presence of seabed protrusions, the importance of lateral forces could increase, warranting further investigation. Furthermore, including current loads in the analysis would contribute to a more realistic approach and could be considered in future research.
- Incorporation of nonlinear characteristics of the leg modifications: While the modification was incorporated by a maximum and minimum equivalent stiffness, future research should consider the nonlinearity of the leg modifications for a more accurate estimation of their performance.
- Utilisation of advanced software for nonlinear properties: If the incorporation of nonlinear properties becomes necessary in future research, previous studies recommend the use of advanced software or numerical solutions.
- Utilisation of FE models for detailed analysis: If future research necessitates detailed structural analysis, including nonlinearities, complex leg geometry, or leg-hull interactions, utilising FE models is recommended despite the increased computational complexity.
- Incorporation of wave-induced vessel motions during impact: This study only accounted for an initial velocity, but during impact, the vessel is subjected to wave loads. Future research should consider these wave-induced vessel motions, it would be advisable to start with regular waves.
- Incorporation of specific vessel and spudcan geometries: This study simplified the vessel's weight and the spudcan to point masses, effectively neglecting their moment of inertia and specific geometries. Future research should consider these factors for a more realistic representation of the system and its interaction, which would also enable a accurate inclusion of wave-induced vessel motions.
- Exploration of multiple jacking up locations: The analysis in this study mainly focused on a single jacking up location. For a comprehensive understanding of the impact behaviour, future research should consider studying multiple jacking up locations. This would not only enhance the validation of the developed model but also provide deeper insights into real-life impacts.

References

[1] International Renewable Energy Agency. “INNOVATION OUTLOOK OFFSHORE WIND About IRENA”. In: (2016).

[2] Global Wind Energy Concil GWEC. “Global offshore wind report 2022”. In: *URL https://gwec.net/gwecs-global-offshore-wind-report/* (2022).

[3] Casper van Lynden et al. “Offshore Wind Installation Vessels: Generating insight about the driving factors behind the future design”. In: *International Journal of Maritime Engineering* 164.A2 (2022), pp. 221–236.

[4] ULSTEIN. *Securing Your Future in Offshore Wind*. 2019. URL: `https://ulstein.com/news/securing-your-future-in-offshore-wind` (visited on 03/03/2023).

[5] Van Oord | Marine Ingenuity. *Offshore wind installation vessel | Van Oord*. URL: `https://www.vanoord.com/en/equipment/offshore-wind-installation-vessel/` (visited on 10/27/2022).

[6] Van Oord | Marine Ingenuity. *Aeolus - MPI*. URL: `https://www.mpi-offshore.com/equipment/aeolus` (visited on 05/12/2023).

[7] Van Oord | Marine Ingenuity. *Investing in the future: Major crane upgrade for offshore installation vessel Aeolus | Van Oord*. 2022. URL: `https://www.vanoord.com/en/updates/investing-future-major-crane-upgrade-offshore-installation-vessel-aeolus` (visited on 05/12/2023).

[8] Van Oord. *Internal document*. 2022.

[9] Van Oord | Marine Ingenuity. *Ailes Marines selects Van Oord for Saint-Brieuc Offshore Wind Farm | Van Oord*. 2020. URL: `https://www.vanoord.com/en/updates/ailes-marines-selects-van-oord-saint-brieuc-offshore-wind-farm/` (visited on 05/12/2023).

[10] *Saint-Brieuc Offshore Wind Farm - Under Construction - France | 4C Offshore*. URL: `https://www.4coffshore.com/vessels/france/saint-brieuc-france-fr36.html` (visited on 05/12/2023).

[11] Det Norske Veritas. *Self-elevating Units, Recommended Practice*. Tech. rep. DNV-RP-C104. On the WWW, at http://www. dnv. com, January. PDF file, 2012.

[12] Jacobus Dingeman Stroo, Sjaak Jan Jiskoot, and Erik Jacobus Bernardus Snijders. *Self-propelled jack-up vessel*. US Patent 11,142,290. Oct. 2021.

[13] W Tarełko. “Installation vessels of offshore wind farms and their take+ off systems”. In: *Journal of Polish CIMAC* 7.1 (2012), pp. 245–256.

[14] Van Oord. *Internal document*. Mar. 2021.

[15] Philip H Augener and Hannes Hatecke. “Sea-keeping analysis of an offshore wind farm installation vessel during the jack-up process”. In: *International Conference on Offshore Mechanics and Arctic Engineering*. Vol. 45370. American Society of Mechanical Engineers. 2014, V01AT01A031.

[16] Michiel AJ uit het Broek et al. “Evaluating resource sharing for offshore wind farm maintenance: the case of jack-up vessels”. In: *Renewable and Sustainable Energy Reviews* 109 (2019), pp. 619–632.

[17] Det Norske Veritas. *Wind Turbine Installation Units DNV-OS-J301*. Tech. rep. 2013.

[18] C. Wolfs. “The Leg Impact Forces of a Jack-up Vessel on a Rocky Seabed while Going on Location”. In: *Norwegian University of Science and Technology* (2022).

[19] Det Norske Veritas. “DNV-RP-C205 Environmental conditions and environmental loads”. In: *Det Norske Veritas: Oslo, Norway* (2010).

[20] GL Dnv. “Joint industry project (JIP) on: Bottom impact and partially submerged conditions, Main Technical Report, Offshore Wind Turbine Installations”. In: *Norway: DetNorskeVeritas* (2022).

[21] Van Oord. *Internal document*.

[22] IAA Smith et al. “Limiting motions for jack-ups moving onto location”. In: *Marine structures* 9.1 (1996), pp. 25–51.

[23] Wilson Guachamin Acero et al. “Methodology for assessment of the operational limits and operability of marine operations”. In: *Ocean Engineering* 125 (2016), pp. 308–327.

[24] Van Oord. *Internal document*. June 2020.

[25] Fredrik Olsson. “Impact loads on a self-elevating unit during jacking operation A methodology incorporating site-specific parameters for weather window assessment”. In: (2014).
[26] Partha Chakrabarti. “Going on Location Study for a Jack-Up Rig”. In: International Conference on Offshore Mechanics and Arctic Engineering Volume 1: Offshore Technology (July 2012), pp. 21–34. DOI: 10.1115/OMAE2012-83034. eprint: https://asmedigitalcollection.asme.org/OMAE/proceedings-pdf/OMAE2012/44885/21/4427926/21_1.pdf. URL: https://doi.org/10.1115/OMAE2012-83034.
[27] C Lakshmana Rao, Vijayabaskar Narayanamurthy, and KRY Simha. *Applied impact mechanics*. John Wiley & Sons, 2016.
[28] Herbert Goldstein, Charles Poole, and John Safko. *Classical mechanics*. 2002.
[29] B Yang. “THEORY OF VIBRATION| Fundamentals”. In: (2001).
[30] Bingen Yang. *Stress, strain, and structural dynamics: an interactive handbook of formulas, solutions, and MATLAB toolboxes*. Academic Press, 2005.
[31] Jonas W Ringsberg, Viktor Daun, and Fredrik Olsson. “Analysis of impact loads on a self-elevating unit during jacking operation”. In: *Journal of Offshore Mechanics and Arctic Engineering* 139.3 (2017).
[32] Jan Rychlewski. “On Hooke’s law”. In: *Journal of Applied Mathematics and Mechanics* 48.3 (1984), pp. 303–314.
[33] Karl F Graff. *Wave motion in elastic solids*. Courier Corporation, 2012.
[34] Alvar M Kabe and Brian Sako. *Structural Dynamics Fundamentals and Advanced Applications, Volume II: Volume II*. Academic Press, 2020.
[35] Singiresu S Rao. *Vibration of continuous systems*. John Wiley & Sons, 2007.
[36] Andrei Metrikine. *Personal communication*. 2023.
[37] Junbo Jia and Jia. *Soil dynamics and foundation modeling*. Springer, 2018.
[38] Van Oord. *Internal document*. 2020.
[39] P Gjerde, SJ Parsons, and SC Igbenabor. “Assessment of jack-up boat impact analysis methodology”. In: *Marine Structures* 12.4-5 (1999), pp. 371–401.
[40] Jose H Vazquez et al. “Jackups Going on Location-Understanding Energy Principles on Leg Impact Loads”. In: *SNAME 21st Offshore Symposium*. OnePetro. 2016.
[41] IAA Smith et al. “Evaluation of Leg Damage Risk for Jackups Going on Location”. In: *Offshore Technology Conference*. OnePetro. 1994.
[42] Partha Chakrabarti, Byron Halbleib, and John Laird. “Analysis of jack-up units during transit with legs lowered”. In: *Offshore Technology Conference*. OnePetro. 1995.
[43] Partha Chakrabarti, Sanjay P Joshi, and Manoj K Maiti. “Pull-Down Analysis Of Jack-Up Rigs”. In: *International Conference on Offshore Mechanics and Arctic Engineering*. Vol. 42673. 2007, pp. 77–83.
[44] Edwin Kreuzer et al. “Leg-seabed interactions of jack-up vessels due to motions in irregular waves”. In: *International Conference on Offshore Mechanics and Arctic Engineering*. Vol. 45387. American Society of Mechanical Engineers. 2014, V01BT01A025.
[45] JH Vazquez et al. “Using CEL to Account for Seabed Deformation Effects for Jack-ups Going of Location”. In: *Proceedings of the 22nd Offshore Symposium. Houston, Texas*. 2017.
[46] Yi-kan Zheng, Shi-lian Zhang, and Lei Lai. “Load distribution on the hull-leg connection components of a jack-up”. In: *Journal of Shanghai Jiaotong University (Science)* 20 (2015), pp. 721–728.
[47] N Spidsøe and D Karunakaran. “Nonlinear dynamic behaviour of jack-up platforms”. In: *Marine Structures* 9.1 (1996), pp. 71–100.
[48] Martin S Williams, Richard SG Thompson, and Guy T Houlsby. “Non-linear dynamic analysis of offshore jack-up units”. In: *Computers & structures* 69.2 (1998), pp. 171–180.
[49] Singiresu S Rao. *Mechanical vibrations*. 2019.
[50] Pau Trubat and Climent Molins. “Rheological damping of slender rods”. In: *Marine Structures* 67 (2019), p. 102639. ISSN: 0951-8339. DOI: https://doi.org/10.1016/j.marstruc.2019.102639. URL: https://www.sciencedirect.com/science/article/pii/S0951833918305045.
[51] Ke Yang. “A unified solution for longitudinal wave propagation in an elastic rod”. In: *Journal of Sound and Vibration* 314.1-2 (2008), pp. 307–329.
[52] Jeroen S Hoving Andrei V Metrikine. “A mixed time-frequency domain method to describe the dynamic behaviour of a discrete medium bounded by a linear continuum”. In: ().

[53] Joel L Schiff. *The Laplace transform: theory and applications*. Springer Science & Business Media, 1999.
[54] Hans Petter Langtangen. *Finite Difference Computing with Exponential Decay Models*. Springer Nature, 2016.
[55] Hans Petter Langtangen and Svein Linge. *Finite difference computing with PDEs: a modern software approach*. Springer Nature, 2017.
[56] Jinping Ou et al. "Vibration control of steel jacket offshore platform structures with damping isolation systems". In: *Engineering Structures* 29.7 (2007), pp. 1525–1538. ISSN: 0141-0296. DOI: https://doi.org/10.1016/j.engstruct.2006.08.026. URL: https://www.sciencedirect.com/science/article/pii/S0141029606003853.
[57] Jian Zhang et al. "Identification of jack-up spudcan fixity by an output-only substructural strategy". In: *Marine Structures* 29.1 (2012), pp. 71–88.
[58] *Global Offshore Renewable Map | 4C Offshore*. URL: https://map.4coffshore.com/offshorewind/ (visited on 07/13/2023).
[59] SEAMAFOR - ACTIMAR. 2022. URL: https://www.seamafor.actimar.fr/ams_stb/map/page?view=global (visited on 07/20/2023).
[60] O.M. Faltinsen. *Sea loads on ships and offshore structures*. Vol. 1. Cambridge university press, 1993.
[61] Andrea Saltelli et al. *Global sensitivity analysis: the primer*. John Wiley & Sons, 2008.
[62] Van Oord. *Internal document*. 2018.
[63] IM Sobol'. "Sensitivity estimates for nonlinear mathematical models". In: *Math. Model. Comput. Exp.* 1 (1993), p. 407.
[64] Jiri Nossent, Pieter Elsen, and Willy Bauwens. "Sobol'sensitivity analysis of a complex environmental model". In: *Environmental Modelling & Software* 26.12 (2011), pp. 1515–1525.
[65] J. Herman and W. Usher. "SALib: An open-source Python library for Sensitivity Analysis". In: *Journal of Open Source Software* 2.9 (2017), p. 97. DOI: 10.21105/joss.00097.
[66] Van Oord. *Internal document*. Dec. 2018.

A

Jacking Up Process of Hydraulic Jacking System

The jacking up process of the hydraulic jacking system undergoes multiple operation cycles, which can be described through various stages. These stages are outlined in Table A.1 and visually represented in Figure A.1.

Table A.1: Outline of the different stages of the jacking up process [66].

State	Upper Jacking Frame	Lower Jacking Frame	Action for Next State
Start	Top position; pins locked	Bottom position; pins unlocked	Upper frame travels down; Lower frame travels up
2	Near to bottom position	Topmost position	Upper frame travels down and slows down; Lower frame travels down with higher speed
3	Near to bottom position	Near to a hole to lock in	Lower frame slows down and extends pins; Load is transferred to lower frame
4	Pins locked	Pins locked	Upper frame retracts pins;
5	Bottom position; pins unlocked	Top position; pins locked	Upper frame travels up; Lower frame travels down
6	Topmost position	Near to bottom position	Upper frame travels down with higher speed; Lower frame travels down and slows down
7	Near to a hole to lock in	Near to bottom position	Upper frame slows down and extends pins; Load is transferred to upper frame
8	Pins Locked	Pins Locked	Lower frame retracts pins
9	Top position; pins locked	Bottom position; pins unlocked	

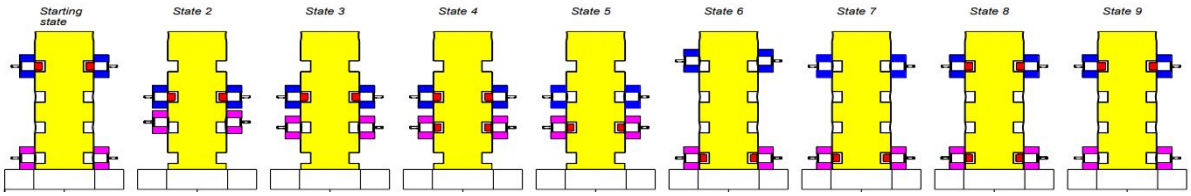

Figure A.1: The different stages of the jacking up process [66].

B

Calculations of the Rod Model

The analytical calculations of the rod model are presented here in detail. The equation of motion of the defined system in the form of the wave equation is given as follows:

$$\rho A \frac{\partial^2 u(z,t)}{\partial t^2} - \hat{E} A \frac{\partial^2 u(z,t)}{\partial z^2} = 0 \tag{B.1}$$

Further elaboration of the equation of motion gives the following:

$$\frac{\partial^2 u(z,t)}{\partial t^2} - c^2 \frac{\partial^2 u(z,t)}{\partial z^2} - c^2 \xi_c \frac{\partial^3 u(z,t)}{\partial z^2 \partial t} = 0 \tag{B.2}$$

The boundary conditions are defined as:

$$EA \frac{\partial u(0,t)}{\partial z} + EA\xi_c \frac{\partial^2 u(0,t)}{\partial z \partial t} = M_v \frac{\partial^2 u(0,t)}{\partial t^2} \tag{B.3}$$

$$EA \frac{\partial u(L,t)}{\partial z} + EA\xi_c \frac{\partial^2 u(L,t)}{\partial z \partial t} = -M_{sp} \frac{\partial^2 u(L,t)}{\partial t^2} - c_s \frac{\partial u(L,t)}{\partial t} - k_s u(L,t) \tag{B.4}$$

And the initial conditions:

$$u(z,0) = 0 \tag{B.5}$$

$$\frac{\partial u(z,0)}{dt} = v_i \tag{B.6}$$

B.1. Laplace Domain

The equation of motion in the Laplace domain is represented as:

$$s^2 \tilde{u}(z,s) - c^2 \left(1 + \xi_c s\right) \tilde{u}''(z,s) = -c^2 \xi_c u_0''(z) + s u_0(z) + v_0(z) \tag{B.7}$$

Subsequently, the boundary condition at $z = 0$ gives:

$$EA \left(1 + \xi_c s\right) \tilde{u}'(0,s) - M_v s^2 \tilde{u}(0,s) = EA\xi_c u_0' - M_v s u_0 - M_v v_0 \tag{B.8}$$

While the boundary condition at $z = L$ yields:

$$EA \left(1 + \xi_c s\right) \tilde{u}'(L,s) + \left(M_{sp} s^2 + c_s s + k_s\right) \tilde{u}(L,s) = EA\xi_c u_0' + M_{sp} s u_0 + M_{sp} v_0 \tag{B.9}$$

Satisfying the initial conditions simplifies the problem to the following expressions:

$$s^2\tilde{u}(z,s) - c^2\left(1+\xi_c s\right)\tilde{u}''(z,s) = v_i \tag{B.10}$$

$$EA\left(1+\xi_c s\right)\tilde{u}'(0,s) - M_v s^2\tilde{u}(0,s) = -M_v v_i \tag{B.11}$$

$$EA\left(1+\xi_c s\right)\tilde{u}'(L,s) + \left(M_{sp}s^2 + c_s s + k_s\right)\tilde{u}(L,s) = M_{sp}v_i \tag{B.12}$$

The initial problem is now defined as an ODE in the Laplace domain and still depends on the $z-$position along the rod. An expression for $\tilde{u}(z,s)$ must be found which can later be numerically converted to the time domain by the inverse Laplace transform. The solution for $\tilde{u}(z,s)$ can be obtained either analytically or numerically.

B.1.1. Analytical Solution

Since the equation of motion is nonhomogeneous, its general solution $\tilde{u}_g(z,s)$ consists of the sum of the homogeneous solution $\tilde{u}_h(z,s)$ and the particular solution $\tilde{u}_p(z,s)$ [49].

$$\tilde{u}_g(z,s) = \tilde{u}_h(z,s) + \tilde{u}_p(z,s) \tag{B.13}$$

The homogeneous equation can be given by

$$\tilde{u}_h''(z,s) - \frac{s^2}{c^2\left(1+\xi_c s\right)}\tilde{u}_h(z,s) = 0 \tag{B.14}$$

which represents the free vibration of the system in the absence of external forces. In other words, it describes the subsequent vibrations that occur after an initial disturbance. The solution of the homogeneous equation is given as follows:

$$\tilde{u}_h(z,s) = C_1 e^{-\beta z} + C_2 e^{\beta z} \tag{B.15}$$

The first and second derivative are given in Equation B.16 and B.17, respectively.

$$\tilde{u}_h'(z,s) = -C_1\beta e^{-\beta z} + C_2\beta e^{\beta z} \tag{B.16}$$

$$\tilde{u}_h''(z,s) = C_1\beta^2 e^{-\beta z} + C_2\beta^2 e^{\beta z} \tag{B.17}$$

Substituting the above equations into the homogeneous equation results into an expression for β:

$$\beta = \frac{s}{c\sqrt{1+\xi_c s}} \tag{B.18}$$

The particular solution exists as long as the forcing function is present [49]. Therefore, the general solution can be expressed as follows:

$$\tilde{u}_g(z,s) = C_1 e^{-\beta z} + C_2 e^{\beta z} + \frac{v_i}{s^2} \tag{B.19}$$

The constants C_1 and C_2 can be found by substituting the solution of the homogeneous equation into the boundary conditions.

B.1.2. Numerical Solution by the Finite Difference Method

Solving an ODE using the central FDM consists of the following steps [54, 55]:

1. Discretise the spatial domain into N+1 points
2. Fulfilling the equation at a finite set of discrete points
3. Substituting derivatives with finite differences
4. Formulate a recursive algorithm

Step 1: The spatial domain $[0, N]$ is represented by a finite number of $N + 1$ points along the rod, denoted as z_n:

$$z^n = n\Delta z \quad \text{where} \quad n = 0, 1, 2, ..., N \tag{B.20}$$

Here, $\Delta z = L/N$ represents the spacing between consecutive points.

Step 2: The equation of motion is discretised for a finite set of discrete points:

$$s^2\tilde{u}\left(z^n, s\right) - c^2\left(1 + \xi_c s\right)\tilde{u}''\left(z^n, s\right) = v_i \tag{B.21}$$

Step 3: The first order derivative of central differences is given by

$$u'(z^n) = \frac{u^{n+1} - u^{n-1}}{2\Delta z}, \tag{B.22}$$

and the second order derivative by

$$u''(z^n) = \frac{u^{n+1} - 2u^n + u^{n-1}}{\Delta z^2}. \tag{B.23}$$

Substituting these expressions into the equation of motion gives the following discrete system:

$$s^2\tilde{u}^n - c^2\left(1 + \xi_c s\right)\frac{\tilde{u}^{n+1} - 2\tilde{u}^n + \tilde{u}^{n-1}}{\Delta z^2} = v_i \tag{B.24}$$

Applying the central finite differences to the boundary condition at $z = 0$ generates the following equation:

$$EA\left(1 + \xi_c s\right)\frac{\tilde{u}^1 - \tilde{u}^{-1}}{2\Delta z} - M_v s^2\tilde{u}^0 = -M_v v_i, \tag{B.25}$$

For the boundary condition at $z = L$, the resultant equation is as follows:

$$EA\left(1 + \xi_c s\right)\frac{\tilde{u}^{N+1} - \tilde{u}^{N-1}}{2\Delta z} + \left(M_{sp}s^2 + c_s s + k_s\right)\tilde{u}^N = M_{sp}v_i \tag{B.26}$$

The ghost points can be derived by using the boundary conditions:

$$\tilde{u}^{-1} = \frac{2\Delta z}{EA\left(1 + \xi_c s\right)}\left(M_v v_i - M_v s^2\tilde{u}^0\right) + \tilde{u}^1 \tag{B.27}$$

$$\tilde{u}^{N+1} = \frac{2\Delta z}{EA\left(1 + \xi_c s\right)}\left(M_{sp}v_i - \left(M_{sp}s^2 + c_s s + k_s\right)\tilde{u}^N\right) + \tilde{u}^{N-1} \tag{B.28}$$

Step 4: Formulate recursive algorithm for $n = 0$:

$$s^2\tilde{u}^0 - c^2\left(1 + \xi_c s\right)\frac{2\tilde{u}^1 - 2\tilde{u}^0}{\Delta z^2} + \frac{2c^2}{EA\Delta z}M_v s^2\tilde{u}^0 = v_i\left(1 + \frac{2c^2}{EA\Delta z}M_v\right) \tag{B.29}$$

For $n = 1, \ldots, N - 1$:

$$s^2\tilde{u}^n - c^2\left(1 + \xi_c s\right)\frac{\tilde{u}^{n+1} - 2\tilde{u}^n + \tilde{u}^{n-1}}{\Delta z^2} = v_i \tag{B.30}$$

For $n = N$:

$$s^2\tilde{u}^N - c^2\left(1 + \xi_c s\right)\frac{2\tilde{u}^{N-1} - 2\tilde{u}^N}{\Delta z^2} + \frac{2c^2}{EA\Delta z}\left(M_{sp}s^2 + c_s s + k_s\right)\tilde{u}^N = v_i\left(1 + \frac{2c^2}{EA\Delta z}M_{sp}\right) \tag{B.31}$$

In matrix form, this gives the result shown on the next page:

$$\boldsymbol{Au} = \boldsymbol{B} \tag{B.32}$$

$$\begin{bmatrix} s^2 + \frac{2c^2(1+\xi_c s)}{\Delta z^2} + \frac{2c^2}{EA\Delta z} M_v s^2 & \frac{-2c^2(1+\xi_c s)}{\Delta z^2} & 0 & & 0 & 0 & 0 \\ \frac{-c^2(1+\xi_c s)}{\Delta z^2} & s^2 + \frac{2c^2(1+\xi_c s)}{\Delta z^2} & \frac{-c^2(1+\xi_c s)}{\Delta z^2} & \cdots & 0 & 0 & 0 \\ \vdots & & \ddots & & \vdots & & \\ 0 & 0 & 0 & \cdots & \frac{-c^2(1+\xi_c s)}{\Delta z^2} & s^2 + \frac{2c^2(1+\xi_c s)}{\Delta z^2} & \frac{-c^2(1+\xi_c s)}{\Delta z^2} \\ 0 & 0 & 0 & & 0 & \frac{-2c^2(1+\xi_c s)}{\Delta z^2} & s^2 + \frac{2c^2(1+\xi_c s)}{\Delta z^2} + \frac{2c^2}{EA\Delta z}(M_{sp} s^2 + c_s s + k_s) \end{bmatrix} \begin{bmatrix} u_0 \\ u_1 \\ \vdots \\ u_{N-1} \\ u_N \end{bmatrix}$$

$$= \begin{bmatrix} v_i \left(1 + \frac{2c^2}{EA\Delta z} M_v\right) \\ v_i \\ \vdots \\ v_i \\ v_i \left(1 + \frac{2c^2}{EA\Delta z} M_{sp}\right) \end{bmatrix} \tag{B.33}$$

B.2. Verification of Rod Model

The observed problem, defined as an ODE in the Laplace domain, is solved for $\tilde{u}(z, s)$ analytically and numerically. This is done with the aim of verifying the numerical solution derived by the FDM against a simpler calculation. The system is solved for various frequencies, with a small chosen value of σ to ensure the convergence of the Laplace integral. Displacements determined from both the analytical and numerical solution are plotted against these frequencies, as depicted in Figure B.1.

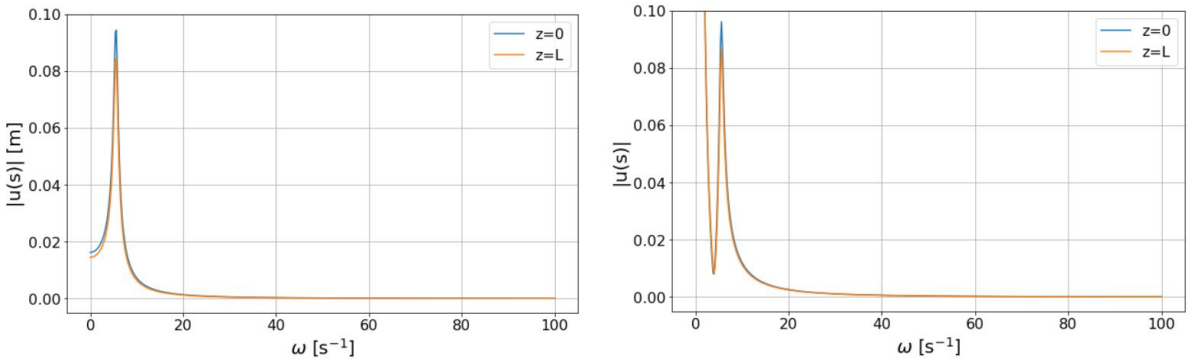

(a) (b)

Figure B.1: The absolute value of $\tilde{u}(z, s)$ at $z = 0$ and $z = L$: Comparison of results from the FDM (a) and the analytical solution (b).

Comparing the graphs, it becomes noticeable that both solutions yield similar results, with the exception of lower frequencies in the analytical solution. This can be explained by observing the general solution in Equation B.19, which becomes increasingly high for lower frequencies. Especially, when the problem is observed for a small value of σ, the particular solution increases significantly for small frequencies, and consequently s. To analyse the effect of this event on the stress distribution in the time domain, the stress is determined and shown in Figure B.2.

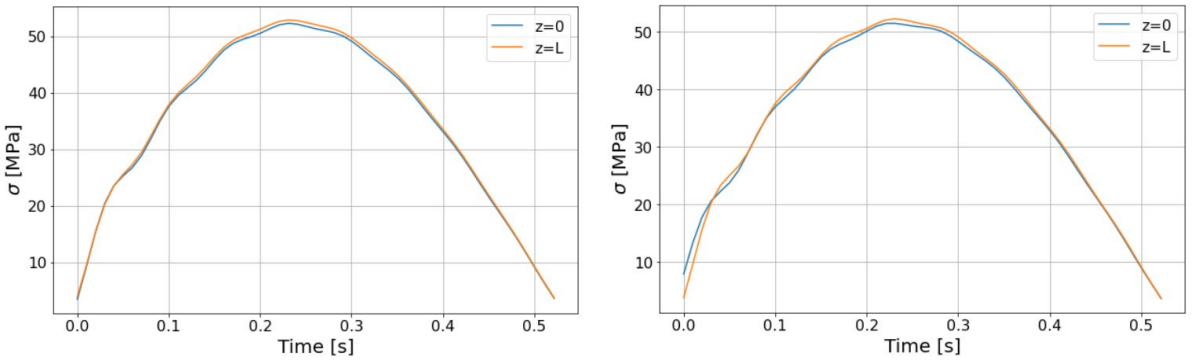

(a) (b)

Figure B.2: The stress distribution σ at $z = 0$ and $z = L$: Comparison of results from the FDM (a) and the analytical solution (b).

The figures demonstrate similar results, with minor differences primarily observed in the initial part of the simulation. The simulation starts at the first contact moment, where the rod's kinetic energy is at its maximum. Due to contact, the kinetic energy is gradually converted to potential energy, leading to an increase in stresses until the kinetic energy is fully transformed. At this point, the rod stops and the stresses within the rod reach their maximum. Subsequently, the kinetic energy begins to rise again until the stresses diminish and reach zero, signifying the disconnection of the rod from the seabed and the end of the simulation.

C

Sensitivity Analysis

C.1. Plots One-at-a-Time Sensitivity Analysis

C.1.1. OAT Analysis for Individual Comparison

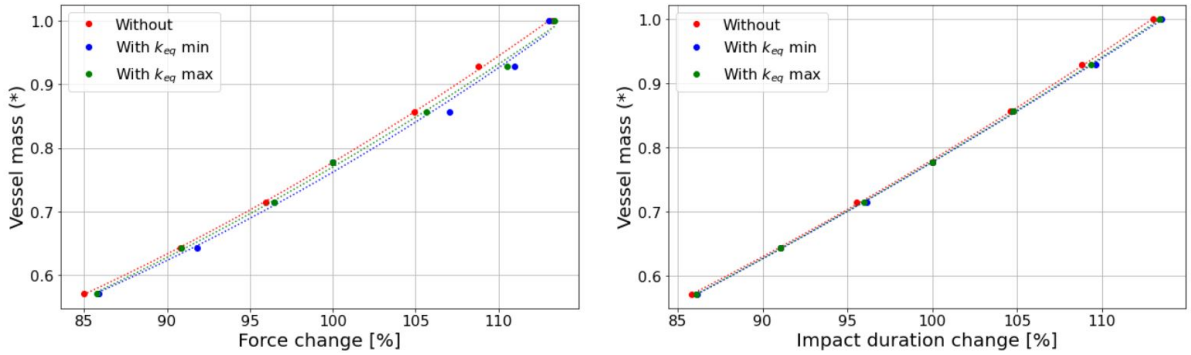

Figure C.1: Change in impact force (a) and impact duration (b) resulting from vessel mass variation: Comparison of three conditions - without leg modification, and with leg modification for minimum and maximum k_{eq}.

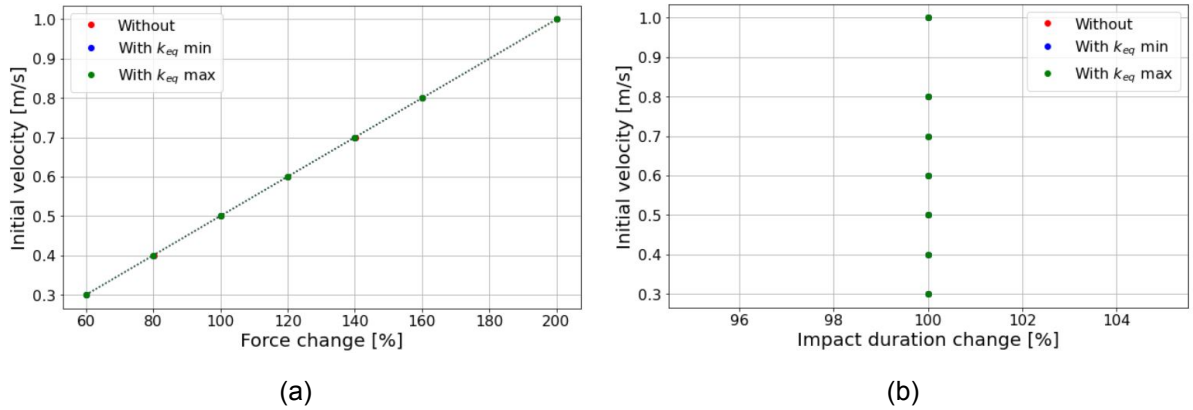

Figure C.2: Change in impact force (a) and impact duration (b) resulting from initial velocity variation: Comparison of three conditions - without leg modification, and with leg modification for minimum and maximum k_{eq}.

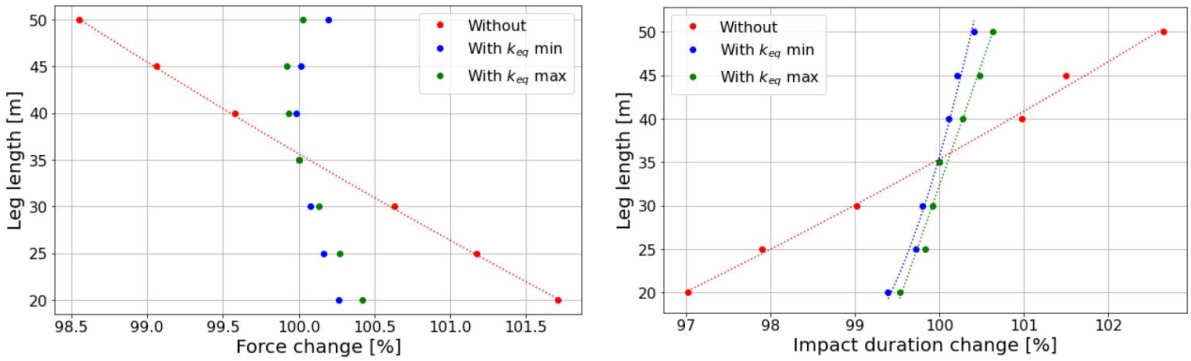

Figure C.3: Change in impact force (a) and impact duration (b) resulting from leg length variation: Comparison of three conditions - without leg modification, and with leg modification for minimum and maximum k_{eq}.

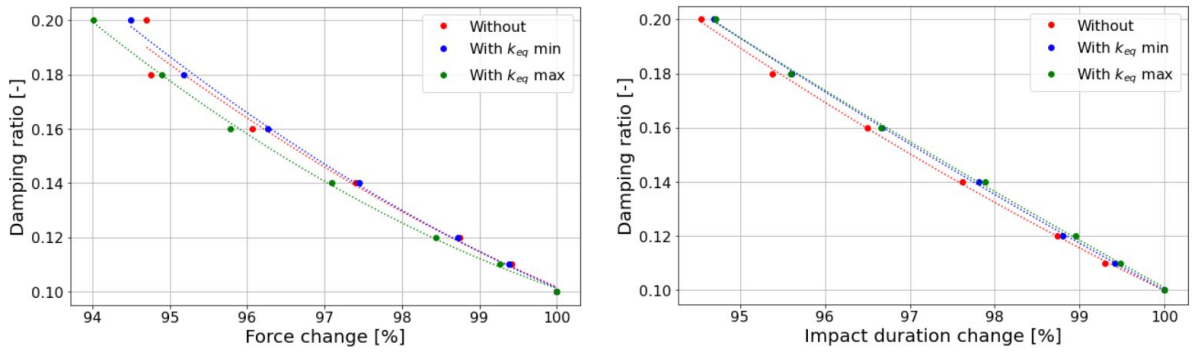

Figure C.4: Change in impact force (a) and impact duration (b) resulting from damping ratio variation: Comparison of three conditions - without leg modification, and with leg modification for minimum and maximum k_{eq}.

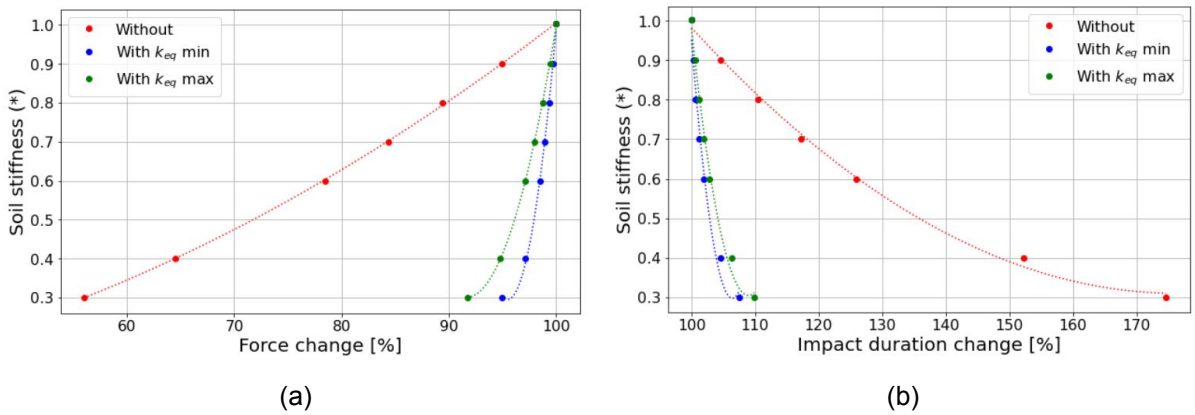

Figure C.5: Change in impact force (a) and impact duration (b) resulting from soil normal stiffness variation: Comparison of three conditions - without leg modification, and with leg modification for minimum and maximum k_{eq}.

C.1.2. OAT Analysis for Global Comparison

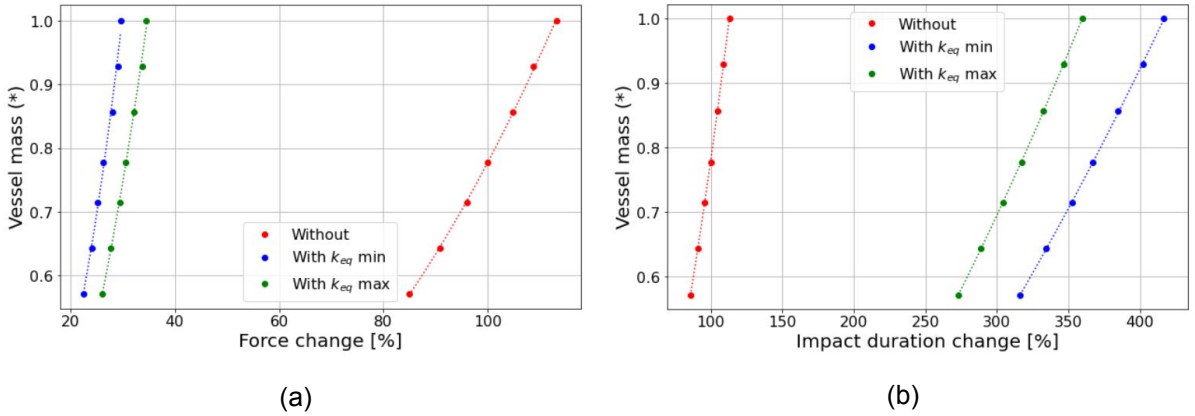

Figure C.6: Change in impact force (a) and impact duration (b) resulting from vessel mass variation: Comparison of three conditions - without leg modification, and with leg modification for minimum and maximum k_{eq}.

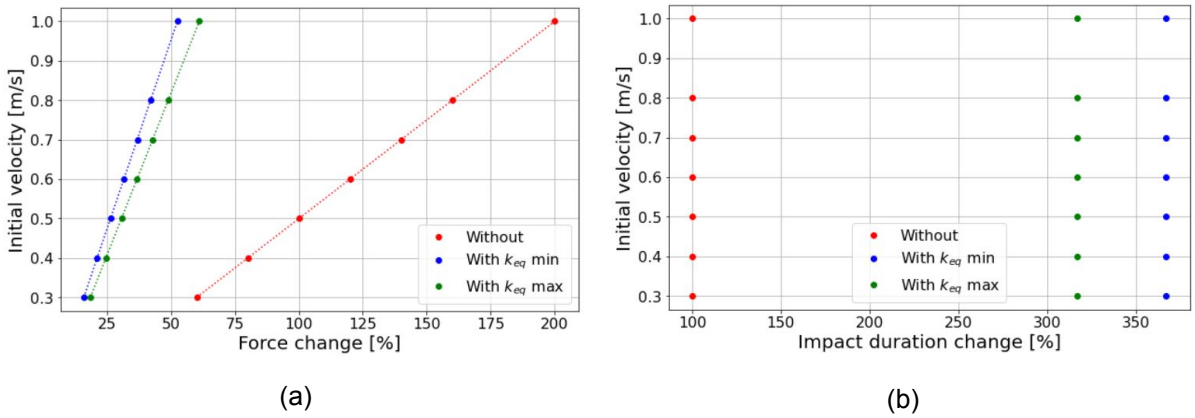

Figure C.7: Change in impact force (a) and impact duration (b) resulting from initial velocity variation: Comparison of three conditions - without leg modification, and with leg modification for minimum and maximum k_{eq}.

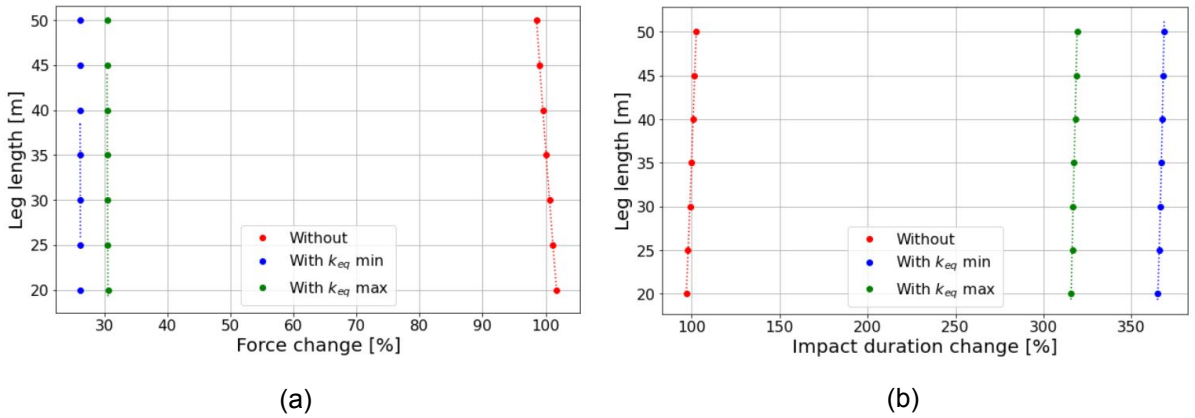

Figure C.8: Change in impact force (a) and impact duration (b) resulting from leg length variation: Comparison of three conditions - without leg modification, and with leg modification for minimum and maximum k_{eq}.

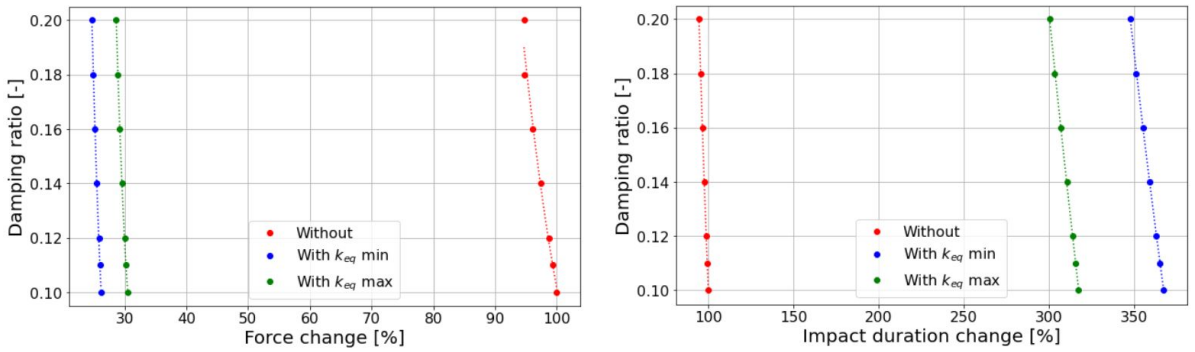

Figure C.9: Change in impact force (a) and impact duration (b) resulting from damping ratio variation: Comparison of three conditions - without leg modification, and with leg modification for minimum and maximum k_{eq}.

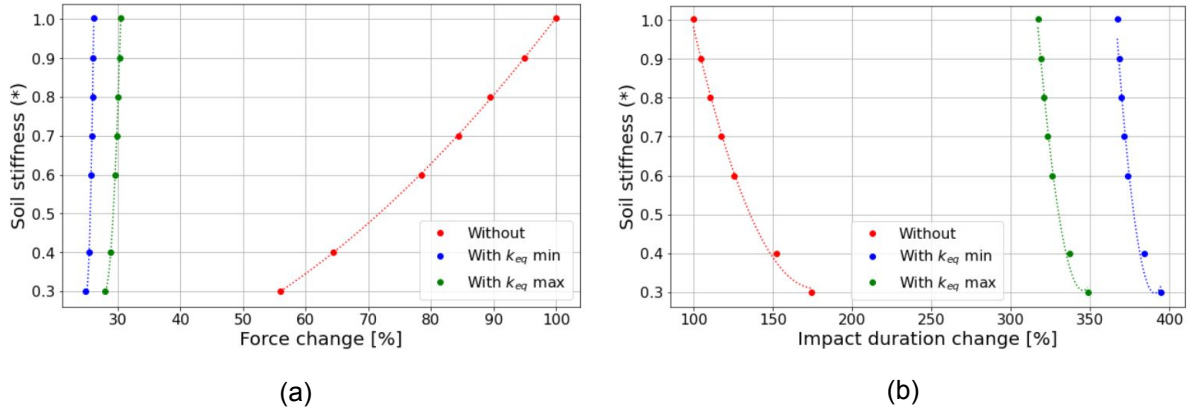

Figure C.10: Change in impact force (a) and impact duration (b) resulting from soil normal stiffness variation: Comparison of three conditions - without leg modification, and with leg modification for minimum and maximum k_{eq}.

C.2. Plots Global Sensitivity Analysis

C.2.1. Analysis 1: Most Influential Parameters

Impact Force

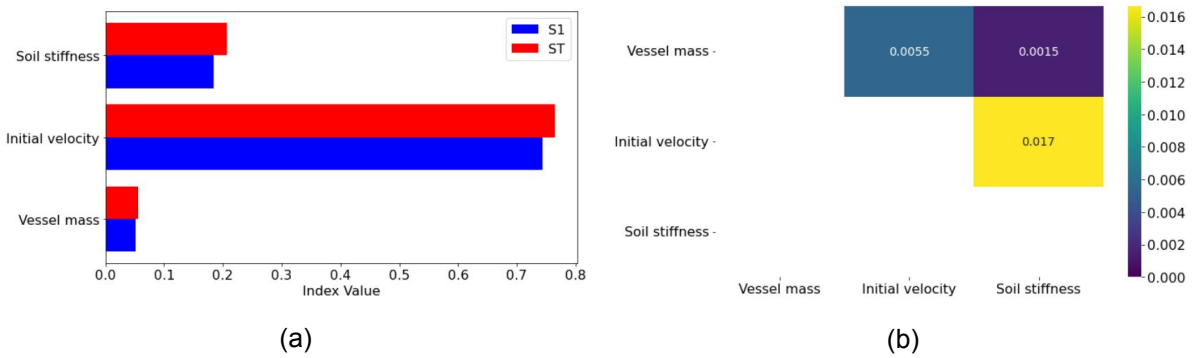

Figure C.11: S1 and ST sobol sensitivity analysis (a), and S2 sobol sensitivity analysis (b) for impact force without leg modification.

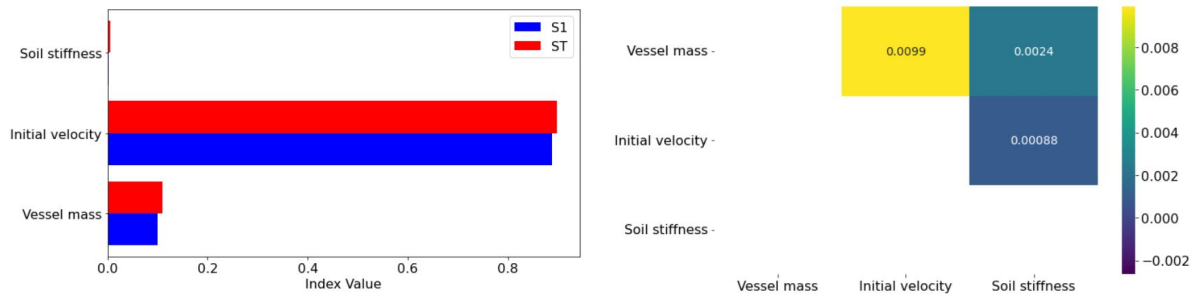

(a) (b)

Figure C.12: S1 and ST sobol sensitivity analysis (a), and S2 sobol sensitivity analysis (b) for impact force with leg modification, maximum k_{eq}.

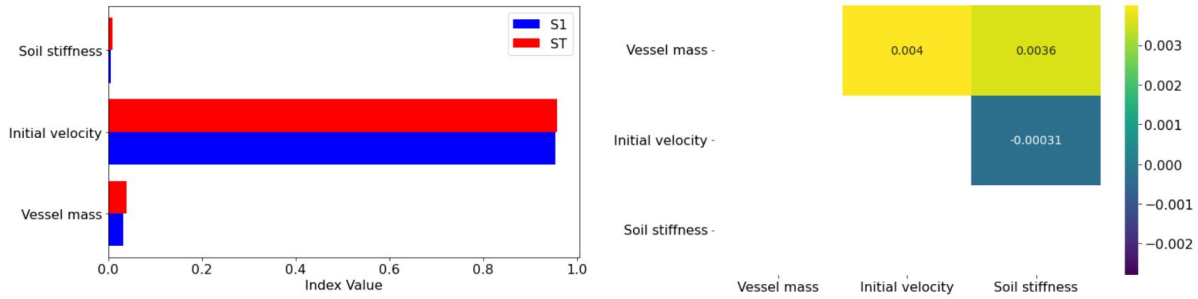

(a) (b)

Figure C.13: S1 and ST sobol sensitivity analysis (a), and S2 sobol sensitivity analysis (b) for impact force with leg modification, minimum k_{eq}.

Impact Duration

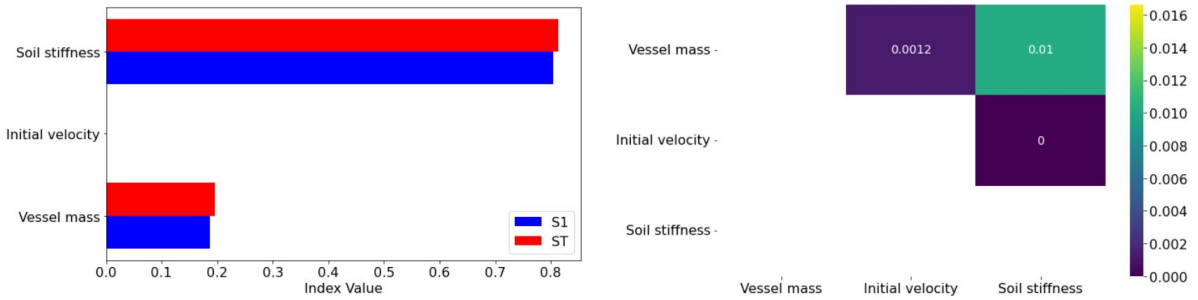

(a) (b)

Figure C.14: S1 and ST sobol sensitivity analysis (a), and S2 sobol sensitivity analysis (b) for impact duration without leg modification.

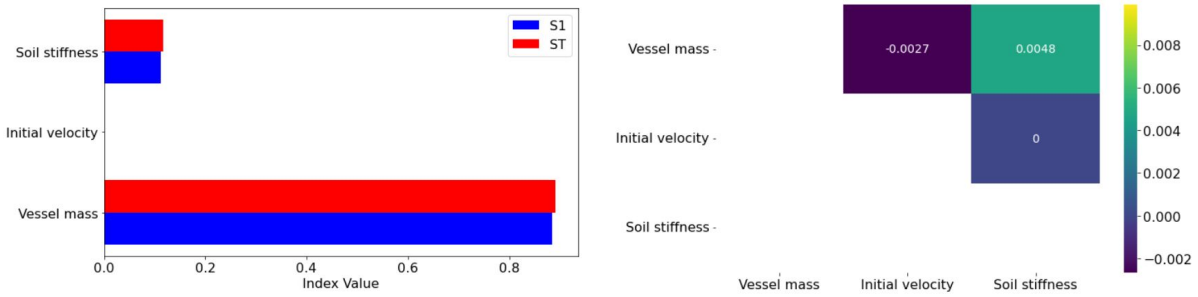

(a) (b)

Figure C.15: S1 and ST sobol sensitivity analysis (a), and S2 sobol sensitivity analysis (b) for impact duration with leg modification, maximum k_{eq}.

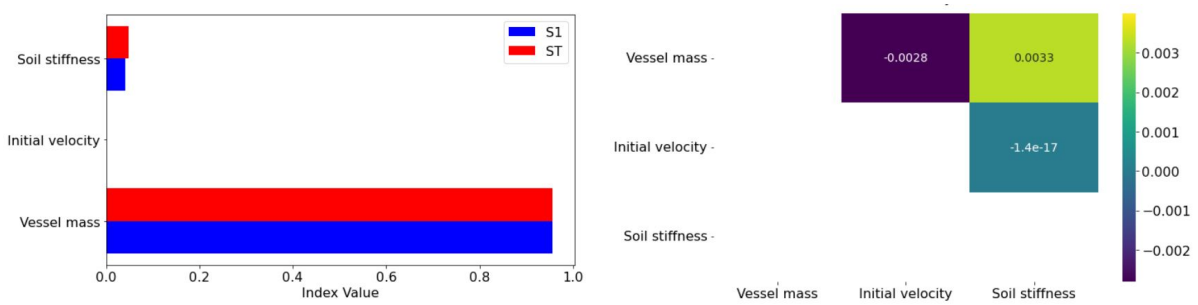

(a) (b)

Figure C.16: S1 and ST sobol sensitivity analysis (a), and S2 sobol sensitivity analysis (b) for impact duration with leg modification, minimum k_{eq}.

C.2.2. Analysis 2: Parameters with the Most Uncertainty

Impact Force

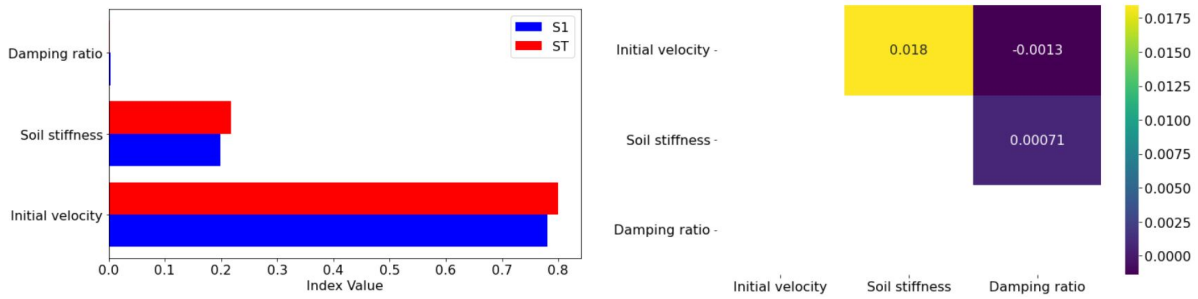

(a) (b)

Figure C.17: S1 and ST sobol sensitivity analysis (a), and S2 sobol sensitivity analysis (b) for impact force without leg modification.

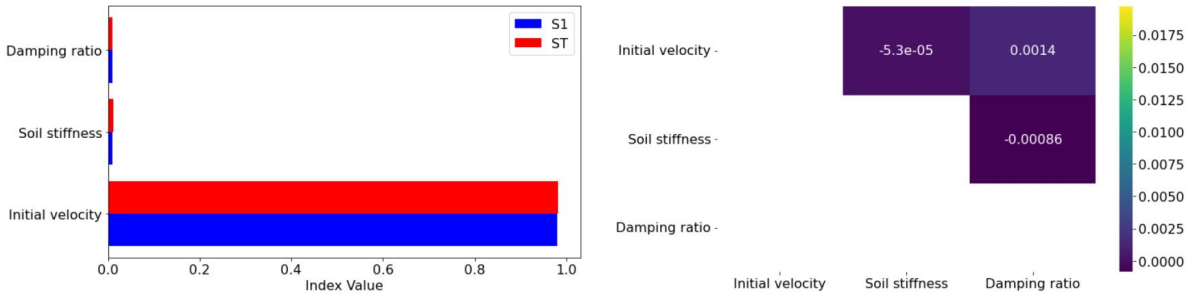

(a) (b)

Figure C.18: S1 and ST sobol sensitivity analysis (a), and S2 sobol sensitivity analysis (b) for impact force with leg modification, maximum k_{eq}.

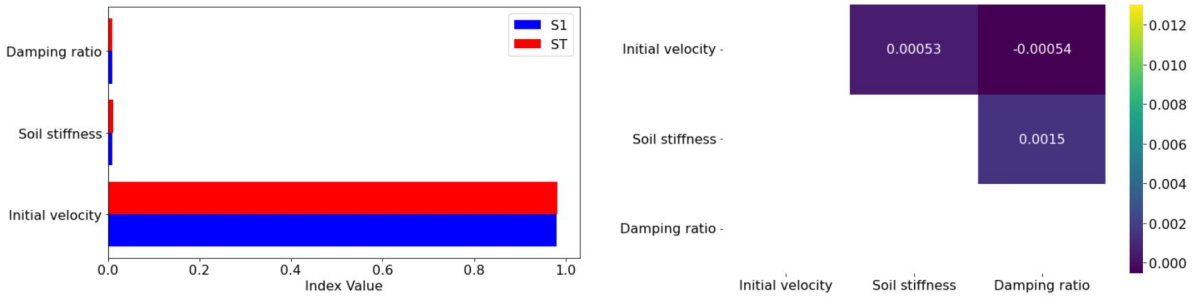

(a) (b)

Figure C.19: S1 and ST sobol sensitivity analysis (a), and S2 sobol sensitivity analysis (b) for impact force with leg modification, minimum k_{eq}.

Impact Duration

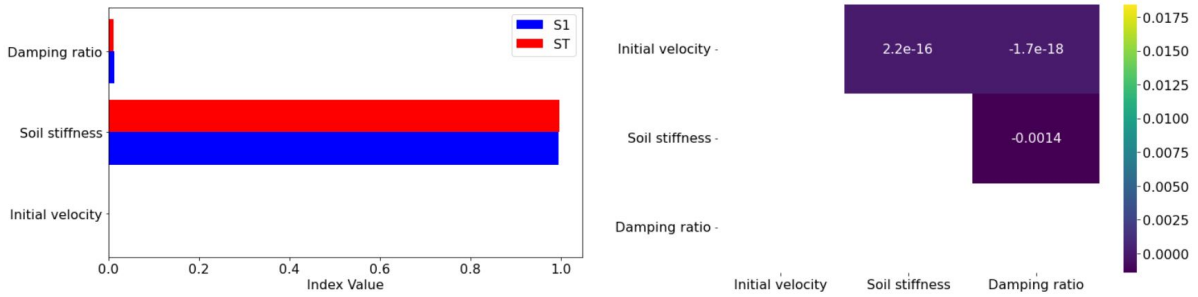

(a) (b)

Figure C.20: S1 and ST sobol sensitivity analysis (a), and S2 sobol sensitivity analysis (b) for impact duration without leg modification.

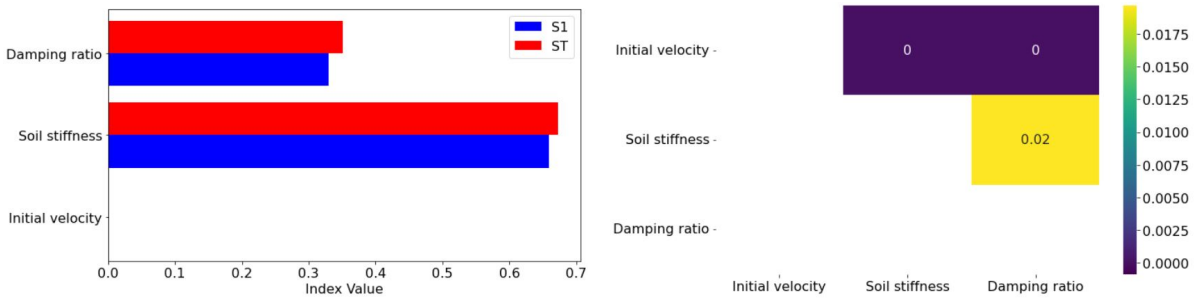

(a) (b)

Figure C.21: S1 and ST sobol sensitivity analysis (a), and S2 sobol sensitivity analysis (b) for impact duration with leg modification, maximum k_{eq}.

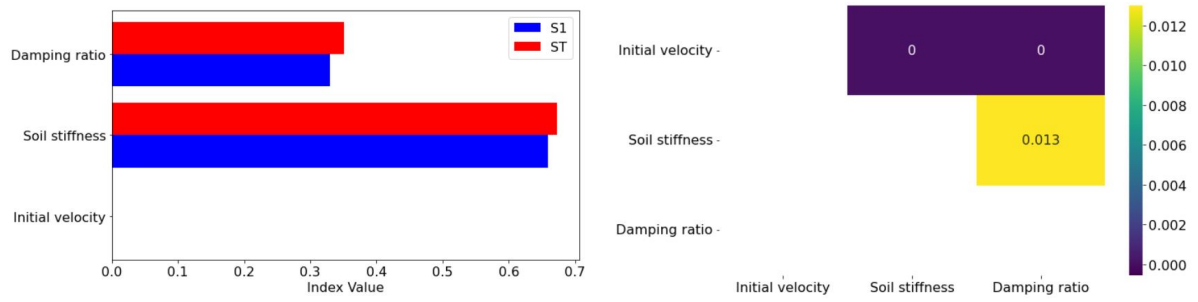

(a) (b)

Figure C.22: S1 and ST sobol sensitivity analysis (a), and S2 sobol sensitivity analysis (b) for impact duration with leg modification, minimum k_{eq}.

C.2.3. Analysis 3: Vessel-Related Parameters

Impact Force

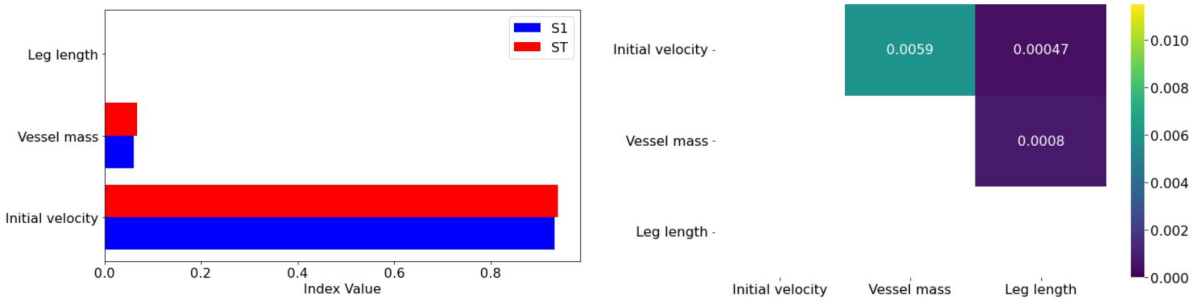

(a) (b)

Figure C.23: S1 and ST sobol sensitivity analysis (a), and S2 sobol sensitivity analysis (b) for impact force without leg modification.

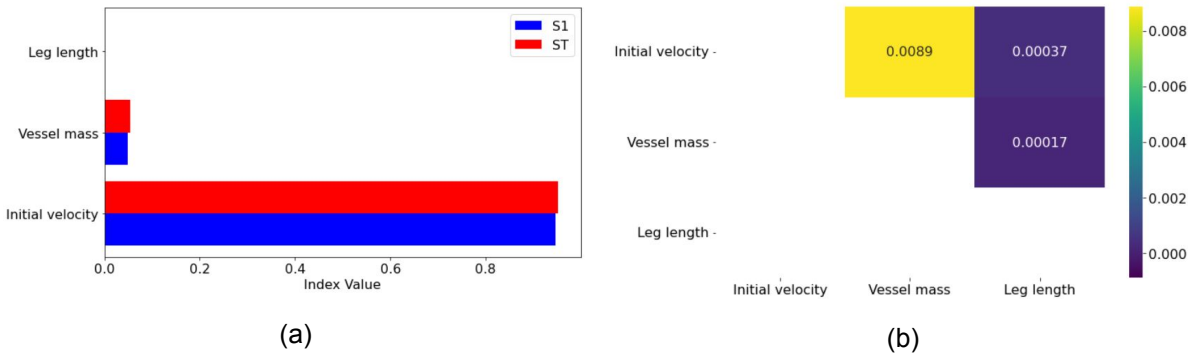

Figure C.24: S1 and ST sobol sensitivity analysis (a), and S2 sobol sensitivity analysis (b) for impact force with leg modification, maximum k_{eq}.

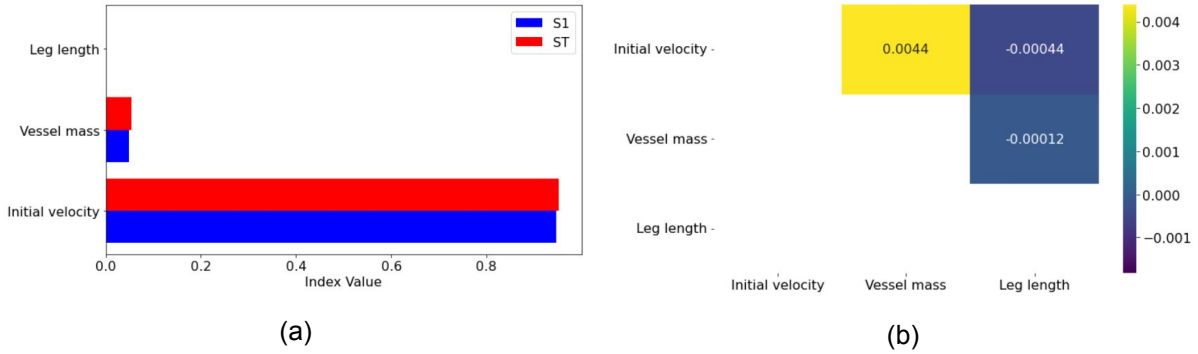

Figure C.25: S1 and ST sobol sensitivity analysis (a), and S2 sobol sensitivity analysis (b) for impact force with leg modification, minimum k_{eq}.

Impact Duration

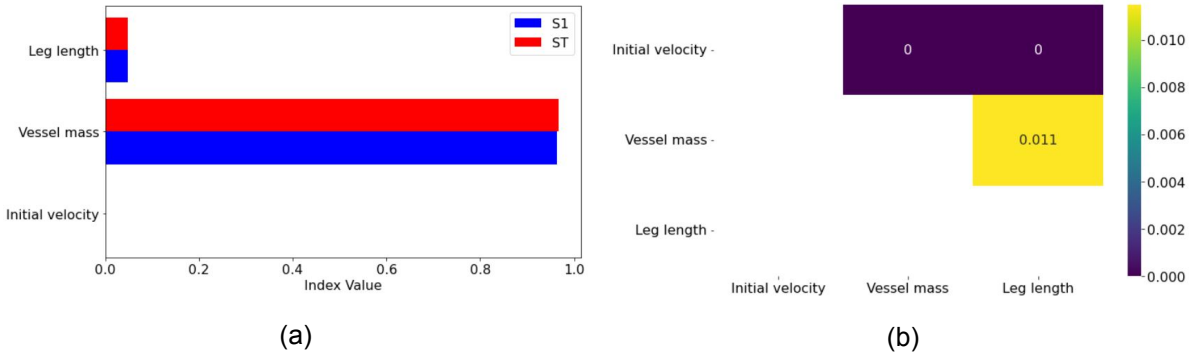

Figure C.26: S1 and ST sobol sensitivity analysis (a), and S2 sobol sensitivity analysis (b) for impact duration without leg modification.

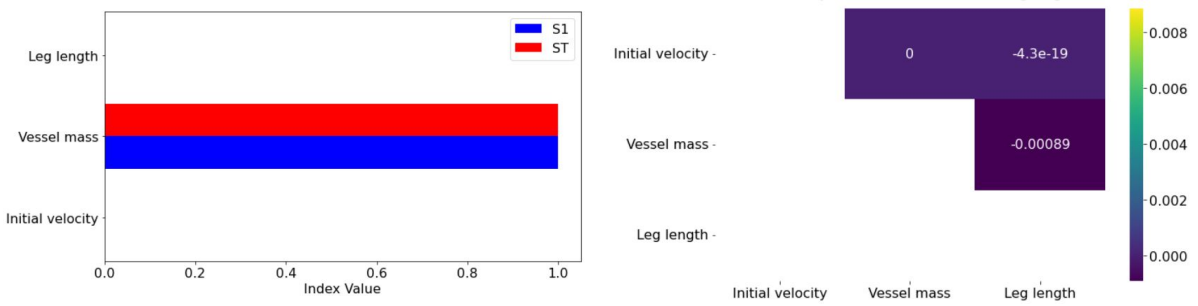

(a) (b)

Figure C.27: S1 and ST sobol sensitivity analysis (a), and S2 sobol sensitivity analysis (b) for impact duration with leg modification, maximum k_{eq}.

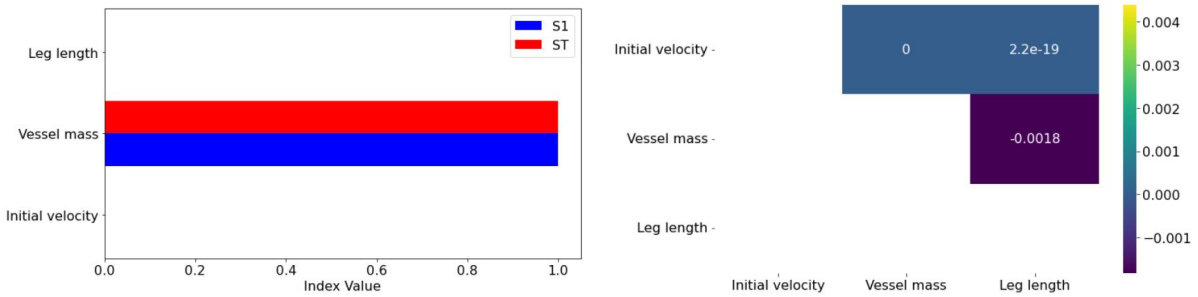

(a) (b)

Figure C.28: S1 and ST sobol sensitivity analysis (a), and S2 sobol sensitivity analysis (b) for impact duration with leg modification, minimum k_{eq}.